Order Number 9207087

# Switching-, logic-, memory-, and symbolic substitution-oriented optical signal processing

Kim, Dai Hyun, Ph.D.

City University of New York, 1991



U·M·I
300 N. Zeeb Rd.
Ann Arbor, MI 48106

# SWITCHING-, LOGIC-, MEMORY-, AND SYMBOLIC SUBSTITUTION-ORIENTED OPTICAL SIGNAL PROCESSING

A

by

DAI HYUN KIM

A dissertation submitted to the Graduate Faculty in Engineering in partial fulfillment of the requirements for the degree of Doctor of Philosophy, The City University of New York.

1991

This manuscript has been read and accepted for the Graduate Faculty in Engineering in satisfaction of the dissertation requirement for the degree of Doctor of Philosophy.

Date 6/14/1991

Chairman of Examining Committee

Date 6/14/1991

Executive Officer

Prof. Samir Ahmed

Prof. Joseph Barba

Prof. Sanghamitra Basu

Prof. Ping-Pei Ho

Dr. Ming H. Wu
Hamamatsu Corporation

Supervisory Committee

**The City University of New York**

ABSTRACT

SWITCHING-, LOGIC-, MEMORY-, AND SYMBOLIC
SUBSTITUTION-ORIENTD OPTICAL SIGNAL PROCESSING

by

Dai Hyun Kim

Mentor Dr. George Eichmann (Deceased, June 1990)
Herbert G. Kayser Professor of Electrical Engineering
Co-Mentor Dr. Yao Li
Final Mentor Professor Yao Li

In this thesis, switching-, logic-, memory-, and symbolic substitution- oriented optical signal processing is studied. In order to maximize the major advantages of optical signal processing, various, such as binary, residue, and modified signed-digit number systems, are studied. Utilizing these number systems together with various optically passive and active elements, nine different optical signal processors are implemented.

A new method to realize a medium-scale, free-space optical programmable logic array is proposed. This device, together with a multiple-variable OR matrix, can be used to implement Boolean combinatorial logic operations. For an optical binary combinatorial logic computation, the proposed method efficiently uses three-dimensional space and optical elements. Experimental results obtained using an inexpensive liquid-crystal television are included.

A new optical morphological image processor is presented and experimentally implemented. The morphological CLOSING operation is performed via a combination of two optical DILATION and an INVERSION operations, instead of a DILATION followed by an EROSION operation. The DILATION is optically performed by a lenslet array, while the inversion is performed by an optically

addressable spatial light modulator.

Using two inexpensive LCTVs and an image subtraction technique, a new optical pyramidal tracking novelty filter is suggested and the experimental demonstrations are presented. This optical processor, unlike electronic processors which require both a mesh-type cellular array and a pixel by pixel image subtraction leading to a time-consuming processing, performs real-time parallel image tracking.

A new scheme for digital optical computing utilizing a non-holographic content addressable memory is discussed. Designs of optical modified signed-digit arithmetic processor is presented. This non-holographic content addressable memory-based MSD processor offers a number of practical advantages, such as fast processing speed and ease of implementation. Also, using logic reductions, stored information is minimized.

Optical register transfer microoperations based on an associative memory are proposed. A hybrid optical word-parallel, bit serial register transfer processor architecture based on an optical holographic associative symbolic substitution is described and experimental results are presented.

Several new higher-order spatial symbol recognition methods for symbolic substitution-based calculations are presented. Three different higher-order optical symbolic recognition architectures are suggested. An optical cavity-based scheme is experimentally implemented. By superimposing replicas of input image generated by a lenslet array, a content addressable memory-based optical symbolic recognition processor is presented. Finally, a lenslet-based optical symbolic recognition processor is also proposed. Either a dual-rail or a triple-rail optical spatial intensity encoding is employed. Some experimental results are also presented.

## ACKNOWLEDGEMENT

All of the tasks in this thesis were accomplished by the guidance and support of Late Dr. George Eichmann who was a Herbert G. Kayser Professor of Electrical Engineering at The City College and at The Graduate School of the City University of New York. Professor Eichmann suddenly passed away in June 1990 when parts of the dissertation were completed. I would like to deeply appreciate Dr. Eichmann's warm, responsible, and valuable advices. Also, I believe that the lessons and experiences from him will influence and help me through my future professional career.

During my entire academic work I have also received numerous valuable guidance from Professor Yao Li who was my co-mentor and became my final mentor after Professor Eichmann's death. For his thoughtful and considerable academic guidance during the past several years, I appreciate him with full of sincere.

To my daughter Patricia,

my wife Young Jae,

and my Guadian Angel Brown Elf.

## Table of Contents

## Table of Figures

## Table of Tables

# I INTRODUCTION

## 1.1 Why Optics?

It is undoubtable that information science plays a major role in modern life. Some of the most important roles in information science have been played out by computers. For the past 40 years, computer engineering has depended on advances in electronics, mainly semiconductor-based electronics. Computers of the next century may require advanced technologies that could seem as radical as what semiconductors were in 1964. The understanding of the limitations of conventional (electronic) computers has given rise to various research efforts that attempt to create machines of new types. One idea revolves around the fifth-generation computers that will incorporate ideas from artificial intelligence and logic programming. Another is concerned with parallel computers. The parallel computers may utilize a totally different concept, one that departs from conventional computers: the concept of optical processing.

Like electricity, light is one of the quantum phenomena. It is convenient, sometimes, to think that light is a stream of particles called photons (particles for electricity are called electrons or holes). In the universe, there are two types of particles; boson and fermion. Since the former (boson), unlike the later (fermion), does not have charges, it does not interact while crisscrossing with each other in linear media. This property of light provides great advantages to optics compared to electronics, such as massive parallelism, high temporal and spatial bandwidth, interconnectivity, and noninterference propagation.

Since optics has been used as a powerful means in information science, to utilize its advantages, special devices are demanded. As a result of the demand, some optically active devices, such as liquid crystal spatial light modulators (SLMs), self-electrooptic effect devices (SEEDs), nonlinear Fabry-Perot etalons (NLFPEs), and acoustooptic cells, have been invented and developed. These

optically active devices, providing one-dimensional (1-D) as well as two-dimensional (2-D) modulation of light, widely and adequately let us utilize the inherent parallelism and high spatial-bandwidth product (SBP) by spatially and temporally modulating the optical signals. Moreover, these optically active together with optically passive devices provide optical switching, threshold, inversion and amplification capabilities which further broaden the scope of optical information processing, computing and interconnect operations.

## 1.2 A Brief history of Optical Information Processing

The ancient history of optical information processing is linked, to a large extent, to that of a solar clock, communications based on sun-light reflection using mirrors. The early modern optical signal processing application stems from radar systems [1]. The need to process the vast amount of data supplied by radar was one of the motivating forces behind early optical signal processing research efforts. Conversely, many ideas developed by the radar community were later found useful in optical processing. Early optical processing systems were described by K. Preston, Jr. [2] in his book "Coherent Optical Computer".

Optical computing has received a great attention after the invention of laser in 1960. The characteristics of this coherent light source allow numerous new operations to be realized by optical means. These operations were analog in nature, and are best described by the term signal processing. Unlike conventional electronic signal processing systems, which have only one degree of freedom (temporal), typical optical processing systems have two degrees of freedom (both temporal and spatial). In other words, in the case of optical processing systems, the data are normally represented as 2-D images. One of the best signal processing examples that can be performed on images under the laser illumination is the Fourier transform which leads to numerous applications.

## 1.3 Thesis Statement and Organization

The research goal in this thesis was to utilize presently existing optical elements and techniques to implement various optical information processors and/or to improve their performance. The optical information processing schemes to be studied in this thesis include switching-, logic-, memory-, and symbolic substitution-oriented data and image processors. Efficient optical architectures, software algorithms, effective number systems, and new optical spatial encoding schemes were investigated. Based on these techniques, various optical image, data (arithmetic and symbolic) processors were proposed and implemented. In the case of dedicated image processors, capable of performing morphological processing and optical novelty filtering, twice of SHIFT-OR-THRESHOLD-INVERSION and EXCLUSIVE-OR (based on a image subtraction technique) optical logic operations were drafted, respectively. For arithmetic processors, various number systems such as binary, residue, and modified-signed digit number systems as well as content-addressable memory (CAM) and associative memory (AM) were applied. In the case of symbolic processors, three different optical information processing schemes were presented using switching-, logic-, and memory-based techniques.

The organization of this thesis is stated as follows. After this introduction chapter, brief descriptions of both optically active and passive elements as well as selected number systems are addressed in chapter II. In chapter III, switching-oriented optical information processors, an optical compact programmable logic array processor and a liquid-crystal television (LCTV)-based optical position coded residue (PCRN) processor are implemented. Using an optical cavity and a transmissive SLM, an optical programmable logic array processor will be implemented. For the PCRN processor, a single laser source together with two identical LCTVs are engaged to implement crossbar switch. In chapter IV, logic-oriented optical information processors will be addressed.

Based on EXCLUSIVE-OR logic operation a white light optical pyramidal tracking novelty filter was designed and experimental results were also presented. Next, based on optical AND (performed via cascaded SHIFT-OR-THRESHOLD optical logic operations) followed by an INVERSION logic operations, an optical programmable real-time morphological image processor is studied. In chapter V, memory-oriented processor such as a CAM-based single-stage optical MSD processor and an optical holographic associative memory-based parallel register transfer processor, will be discussed. Finally, in chapter VI, new optical spatial encoding schemes for optical higher-order symbolic processing are introduced first. Followed this section, three new optical symbolic processors: an optical cavity-based, a lenslet array-based, and a CAM-based higher-order symbolic processors are presented.

### 1.4 References


[1] E. N. Leith, "Complex spatial filters for image deconvolution", Proceedings of the IEEE 65 (1), 18-28, (1977)

[2] K. Preston,Jr., *Coherent optical computers*, McGraw-Hill, 1972

# II BACKGROUND

## 2.1 Optical Elements and Devices

In this section, basic optical elements and devices are briefly introduced. Most of optical information processing systems are built on a variety of basic components, grouped together in various ways. These basic optical components can be classified into two groups, e.g. optically passive and optically active elements. The main difference between a passive and an active elements is its switching capability and its programmability.

### 2.1.1 Optically Passive elements

#### 2.1.1.1 Mirrors and Prisms

Mirrors and prisms are used to guide the directions of beams in an optical system. The major difference between a mirror and a prism is the ways of changing beam directions. The beam direction is changed by reflection via mirrors, while by reflection and/or refraction via prisms. A mirror, depending on its formation material, can affect the polarization state of the reflected light. The polarization state tends to be parallel to the plane of the mirror. This phenomenon is at the base of polaloid sunglasses, which avoid bright reflections by blocking out horizontally polarized light. In prisms, the angle of refraction depends on the formation material and on wavelength. Thus, a prism can be used to perform spectral analysis of polychromatic signals.

#### 2.1.1.2 Beam Splitters

The information in an optical processing system is carried by beams of light. Therefore, it is often necessary to split a beam of light into two or more beams, or to join two or more beams into one. Both functions can be achieved by beam splitters. A beam splitter is actually just a semi-transparent mirror. Part of the light that hits the semitransparent mirror is reflected, as in an ordinary mirror; the rest goes through the semitransparent mirror without changing direction. To join beams, the two input beams are directed in such a way that the reflected part of the beams and the passing part of the other beam come out together.

The problem with this conventional configuration is that part of the energy is always lost, because both beams are split and we only use one part of each. This can be avoided by using polarization beam splitters, which reflect all the light in one polarization state and transmit all the light in its orthogonal polarization direction. With proper control of the polarization, lossless operation may be achieved.

#### 2.1.1.3 Lenses

Lenses are well known to everyone from daily experience. However, their full power does not come into play in everyday conditions. In an optical information processing system, in particular, lenses have three main uses: to create collimated beams of light, to cast images onto another, and to perform Fourier transformation.

A collimated beam is a plane wave of limited extent; this is a straight, parallel beam of light that does not change its diameter over a reasonably long distance. Convex lenses may convert a diverging beam from a point source into a less converging, or into a collimated one or even into a

converging one. Concave lenses do the opposite: they convert a converging beam into a collimated beam or into a diverging one. Combinations of convex and concave lenses are used to change the diameter of a collimated beam within an optical information processing system.

The Fourier transform is extremely important in information analysis, and as we shall see it also has many usefulness in optical data computation. In short, it generates the spectrum of the input signal, which is a feature representation of the signal in its frequency domain.

#### 2.1.1.4 Polarizers and Analyzers

Polarizers and analyzers are actually the identical optically passive elements. They are filters that only allow light in one polarization to pass. Light in the orthogonal polarization is blocked. The name polarizer is used when the objective is to create a beam of polarized light. The name analyzer is used when the objective is to analyze whether the beam of incident light is in a certain polarization, or to deliberately block light of a certain polarization.

#### 2.1.1.5 Gratings

A transmissive (reflective) grating is a set of fine, straight parallel rulings on a transparency (reflector). Like mirrors, gratings may be used to change the direction of a light beam based on diffraction. However, with a grating the beam can also be split into a number of beams that propagate in different directions. The exact change in direction depends on the wavelength of the light, the angle of incidence and the period of the grating. Thus, a grating may also be used to perform the spectral analysis of polychromatic light.

When a coherent beam of light impinges upon a grating, it can be considered equivalent to a set of coherent, long, linear sources. The light from these sources interfaces each other. In certain directions where the path difference for light coming from adjacent coherent sources are integral multiples of the wavelength, constructive interference occurs. These are the directions in which we get beams of light. In other directions destructive interference occurs, and the waves tend to cancel out. More generally, the directions in which constructive interference takes place must satisfy (see Fig.2.1)

$$d\sin\theta = n\lambda \qquad (2-1)$$

where d, $\lambda$, and n are the grating spacing, the wavelength, and an integer called the diffraction order, respectively.

### 2.1.2 Optically Active Elements

#### 2.1.2.1 Spatial Light Modulators (SLMs)

A SLM is an optically active device that creates some sort of modulation on the cross section of a light beam. SLM spatially modifies the phase, polarization, amplitude, and/or intensity of either one or two dimensional light distribution (optical information).

There are several classification ways for a SLM. In this thesis, two essential classifications are used. One classification is based on the addressing mechanism. In this category a SLM is classified as either an electrically addressed SLM (E-SLM) or an optically addressed SLM (O-SLM). For the E-SLM, the control or write signal is an electrical signal, while the intensity distribution of light beam is used as an optically

control or a write signal.

In case of E-SLM, the control signal changes a variable associated with the readout optical beam such as amplitude, intensity, phase, polarization and spatial frequency through the modulation part of the resolution element. In O-SLM the mechanism of the detection is isolated from the readout optical beam because of the operation of the SLM analogous to a transistor by which the small control signal modulates a large output signal.

The other classification method is based on the SLM geometry, i.e. either a transmissive or a reflective type. This classification will be discussed in detail.

#### 2.1.2.1.1 Basic structure of LCSLM

There are several types of SLMs, such as photodichroic SLMs, deformable mirror SLMs, electrooptic crystal SLMs, magnetooptic matrix SLMs, and liquid crystal SLMs. In this thesis, since mainly liquid crystal SLMs (LCSLMs) were used during research, main focus will be placed on its description. From now on, both SLMs and LCSLMs mean liquid crystal SLMs.

A common every-day type SLM is the LCSLM. Liquid crystals are liquids in which an ordered arrangement of molecules exists. Generally, most LCSLM structures consist of a charge-generation element and a light-modulation element. The modulation element is a layer of LC thin film deposited between two meshed transparent conductive electrodes which are sandwiched between two cross polarizers. O-SLMs tend to employ either photoconductors or photocathodes as the

charge-generation element, while E-SLMs generally employs electron beams, a matrix of electrodes, or an array of active devices such as charge-coupled devices (CCD) or transistors.

#### 2.1.2.1.2 Reflective Type LCSLM

Hughes' reflective type SLM is the most well-known LCSLM. In Fig.2.2, the schematic diagram is shown. It is one of the O-SLM and basically acts like a controlled birefringent mirror. It has a sandwich-type construction. Both outside elements consist of transparent conducting electrodes. A polarizer and an analyzer are placed in the incident and reflected beam planes, respectively. During an off-stage (in the absence of an applied electric field), incident input beam first passes through the LC layer which rotates its polarization by $45^0$ to the fast and slow axis. The $45^0$ rotated input beam is reflected from the dielectric mirror, then passes through the LC second time with an additional rotation of its polarization to the direction of the incident input beam where it is blocked by the analyzer.

During an on-stage (in the presence of an applicable electric field), since the input beam is elliptically polarized after reflecting from the mirror; beam transmission occurs. The applied voltage destroies the twist spiral of the molecules. With the applied voltage, half of the molecules in the layer adopt the preferred alignment direction associated with one electrode, while the other half adopt the alignment direction associated with the other electrode. With the preferred directions of the electrodes at an angle of $45^0$ with respect to each other, the polarization of the input beam will make an angle of $45^0$ with respect to the extraordinary axis of the layer.

#### 2.1.2.1.3 Transmissive Type LCSLM

A commercially available flat screen liquid crystal television (LCTV) is one of the frequently used transmission type LCSLMs in optical information processing. LCTV has been slightly modified to be a SLM in a VanderLugt-type coherent optical correlator. The small and inexpensive LCTV has been used as a replacement for extremely expensive SLMs such as the Hughes LCLV and the Litton magnetooptic device.

The basic operation principle of the LCTV is similar to that of the Hughes LCLV. The $90^0$ twisted nematic liquid crystal structure is common to both the LCTV and transmission type LCLV. A major difference between two devices is the addressing method. The LCLV is optically addressed with either coherent or incoherent light, while the LCTV is only addressed electrically.

### 2.1.2.2 Self-Electrooptic Effect Device (SEED)

SEED, like an etalon, is an optically bistable device. SEEDs, because of its bistability, small size, low power requirement, quick responding time, and ease of adjustment resonators, are very useful for implementing optical logic gates, optical switching, threshold, and amplification devices. In a SEED, low power inputs are transmitted while high power inputs are blocked.

In Fig.2.3, the schematic diagram of the SEED is shown. The SEED is based on a multiple quantum well (MQW) structure placed inside a PIN photodiode detector [1-3]. The MQW structure is a stack of a very thin (less than 10 nm) alternating layers of GaAs and GaAlAs. The GaAs layers have a smaller band gap than the GaAlAs layers, so electrons in the

conduction band of the GaAs are trapped and are not allowed to pass the GaAlAs barriers. These traps are quantum mechanical energy wells; hence it is named "multiple quantum well".

A PIN photodiode detects light by absorbing photons and creating electron-hole pairs. With an applied voltage, the electron-hole pairs are turned into a photocurrent. The point is that in the absence of light (and hence the absence of a photocurrent), the applied voltage creates an electric field across the diode. This field affects the MQW structure, and induces low absorption. As the incident light intensity starts to rise, some of the light is absorbed. As a result, a small photocurrent is generated. This current pass through a resister, and cause some of the voltage to fall on it. Therefore less voltage is left for the diode, and the electric field on the MQW is weakened. However, most of the incident light is not absorbed; it is transmitted. Thus when the incident intensity is increased, the transmitted intensity that follows it, is increased too. Only when the incident light intensity is high enough to cause an appreciable decrease in the electric field, the MQW starts to absorb strongly. In fact, it absorbs practically all the incident light. At this stage the transmitted light intensity suddenly drops to zero. This is the switching from the transmitting state to the blocking state. When the input intensity is subsequently lowered, the switch back occurs at a somewhat lower level.

#### 2.1.2.3 Nonlinear Fabry-Perot Etalon

The nonlinear Fabry-Perot etalon (NLFPE) is one of the optically active devices based on optical bistability [4-5]. The schematic diagram of the NLFPE is shown in Fig.2.4. This device exploits transmission and reflection instead of absorption to control or to modulate a bias beam. Without a signal beam, the bias beam either passes through or reflected

by NLFPE.

With an incident light, the NLFPE changes states which forces the bias beam to be reflected or transmitted. In the stable state of low transmission, the illuminating beam is somewhat off resonance. When its intensity is increased, the characteristic resonant frequency of the cavity changes, and becomes nearer to the frequency of the illuminated light. At a certain stage it is close enough for the interference between the beams to become constructive mode, and an intensity buildup occurs inside the resonator. This causes a condition of positive feedback, and very rapidly the intensity increases and the resonance of the cavity comes to fit the input illumination frequency. The positive feedback causes the system to overshoot, and to enter into a condition with negative feedback, just above resonance. If the intensity rises, the resonance moves away so that the intensity falls again. If the intensity drops, the device again approaches the resonance condition, so the intensity goes up. This is, therefore, a stable state called the high transmission stable state.

When the input intensity is subsequently lowered, it does not immediately affect the intensity buildup in the resonator because of the self maintenance of the buildup. Therefore the input intensity may be lowered to below its initial value while the system stays in the high transmission state. However, the intensity buildup in the resonator depends on the input illumination. When the input intensity is lowered far enough, the intensity in the resonator will not suffice in order to keep the resonator in tune with the input frequency. As soon as the tuning is lost, there is no more constructive interference, the intensity in the resonator decreases sharply, and the system switches back to the low transmission stable state.

This device, like the previously described SEED, can perform NOR operations. The NLFPE can also be designed such that it can operate as an AND, OR, NAND, or XOR gate. This device can also be integrated

into large arrays. At present, there are different types of NLFPE structures being studied. The first is based on a thermal nonlinearity which makes it relatively slow, on the order of microseconds. The promiss for this device is that large arrays can be fabricated to exploit the strength of parallelism. The other type of this device, referred to as an optical logic etalon, is a pulsed device that requires two separate wavelengths; one for the bias and one for the signal. In case of the pulsed device, the two inputs (data and clock) are separated in both time and wavelength.

#### 2.1.2.4 Acoustooptic Cell

The acoustooptic Bragg's effect is due to diffraction of light by ultrasonic waves. An acoustooptic device consists of a piezoelectric transducer bonded to a transparent medium capable of supporting sound propagation. An electrical signal input to the transducer is converted into an ultrasonic wave that carries both the amplitude and the phase of the electrical signal. The traveling ultrasonic wave manifests itself as a density wave, which through the photoelastic effect results in an index of refraction variation in the acoustooptic material. This index variation, or grating, carries the amplitude and phase information of the ultrasonic wave (and thus of the original electrical input). The amplitude and phase of the resulting light diffracted by the grating is thus proportional to that of the original electrical input.

## 2.2 Selected Number Systems

In this section, a review of selected number systems that find applications in optical information processing is presented. Among many, the binary number (BN), the modified signed-digit (MSD) number, the residue number (RN) and recently the sign/logarithm number (SLN) systems are studied for uses in optical computations. The BN system, widely used in electronic applications, can be used in general purpose processors. Due to the carry propagation, the sequential computation algorithms limit the processing speed, although parallel algorithms (e.g. carry-look ahead addition) can be applied to improve the processing speed [6-7]. Applying other number systems, processing speed improvement can also be achieved. The SLN system can provide high dynamic range and fast computational speed. The major advantage of this number system is that multiplication/division is calculated via logarithm addition/subtraction [8-9]. The MSD number system with its inherent weak carry dependence is suitable for both parallel addition and subtraction operations [10-11]. Using a tree structure fast multiplication operation can be implemented. For RN representation, an arithmetic operation can also be decomposed into a set of independent suboperations, the RNs represent an effective parallel code. The high dynamic range and fast processing for addition, subtraction and multiplication operations are attractive features of this number system [12].

### 2.2.1 Binary Number (BN) System

In general, a number in base $r$ is expressed with a power series in $r$

$$A_n r^n + A_{n-1} r^{n-1} + \ldots A_0 r^0 + A_{-1} r^{-1} + A_{-2} r^{-2} + \ldots \quad (2.2)$$

where $A_i$ = 0, 1, 2, 3, .....,r-1. When the number is expressed in positional notation, only the coefficients and the decimal point are written down:

$$A_n A_{n-1} \ldots A_0 \quad . \quad A_{-1} A_{-2} \ldots \tag{2.3}$$

The BN system, although widely employed in electronic computational devices, is suitable for a sequential type of processing. For all arithmetic operations, the carry propagation from digit to digit slows down the computational speed which is inversely proportional to the length of a represented BN. Some calculations such as a carry look-ahead addition (CLA), where the carry propagation is precalculated and the resulting output can be represented as a set of Boolean functions, can be executed using parallel algorithms. The hardware complexity increases rapidly with the representation length and only moderate dynamic range calculations can be implemented. On the other hand, the major advantage of the BN system is its compatibility with existing electronic devices based also on BN systems.

### 2.2.2 Modified Signed-Digit (MSD) Number System

In this section, some basic properties of the MSD number system are reviewed. The MSD number representation [10-11] is a redundant radix 2 trinary number system whose weights are 1, 0, and -1 ($\bar{1}$). Using the MSD representation, a decimal number $N_{10}$, where the subscript denotes base ten, is written as

$$N_{10} = (1,0,\bar{1})2^{p-1} + \ldots + (1,0,\bar{1})2^1 + (1,0,\bar{1})2^0$$

$$N_{10} = \sum_i a_i 2^i \tag{2.4}$$

where $\alpha_i \in [-1, 0, 1]$. Positive as well as negative numbers can be represented in a MSD number system. With this representation, decimal numbers A=14 and B=-14 can be expressed as

$$A = 10\bar{1}10 \qquad (2.5a)$$

$$B = \bar{1}01\bar{1}0. \qquad (2.5b)$$

It can be seen that by a parallel bit-wise logic inversion of nonzero digits, the sign of a number can be negated. One advantage of the MSD number system is its parallel addition and subtraction capability. The addition and subtraction operation can be performed using an array of four 2-bit MSD logic gates, e.g. W, T, $W^1$ and $T^1$ gates. The truth tables for these gates are shown in Table 2.1. In Fig.2.5, a typical 5-bit MSD addition logic flow diagram is shown. Using this architecture, the carries generated from the first processing stage can only propagate 2-bits to the left. The addition result is independent of the number of bits to be added. A parallel subtraction of two MSD numbers, X - Y, can be achieved by negating Y followed by a MSD addition [10-11]. Multiplication and division operations can be decomposed into a set of MSD additions and subtractions, together with parallel shifts.

### 2.2.3 Sign/Logarithm Number (SLN) System

SLN system is especially suitable for both multiplication and/or division operations. The addition (subtraction) operations can be also implemented using a SLN system [13]. To multiply (divide) two binary numbers (BNs) a

and b, first the numbers are converted into a SLN system. The multiplication (division) is then obtained by adding (subtracting) appropriate logarithms. As a final multiplication step,

$$ab = antilog_2(\log_2 a + \log_2 b), \qquad (2.6)$$

a conversion from SLN to BN system is needed. The major advantage of an SLN system is that the product/quotient calculation is performed via fixed-point binary addition/subtraction. Because BN addition can be performed in a considerably shorter time than multiplication/division, the SLN system can achieve a multiplication speed that is higher than with any other equivalent length fixed-point number system [14].

Since a logarithm of a BN may contain an infinite number of digits, a binary approximation of the logarithm mantissa is required. The multiplication accuracy depends mainly on the binary logarithm approximation. Using a linear approximation [8], the logarithm of a variable a between points $a=2^n$ and $2^{n+1}$ (where n is an integer) is approximated by a linear function of a. From [15], the absolute value of the logarithm approximation error E is

$$0 \le E \le 0.08639. \qquad (2.7)$$

The linear approximation for a logarithm can be implemented using shift operations performed by an n-bit BN. Shifting the BN until the most significant "one" is shifted to the left-most (to the most significant bit (MSB)) position, both the characteristic and the mantissa of the logarithm are obtained. If the number of shifts is equal to m, its characteristic is equal to n-m-1. The mantissa is represented by a BN that lies to the right (after the

shift) of the MSB.

By truncating the mantissa at different bit positions, better multiplication accuracy is achievable. In Table 2.2, multiplication error as a function of the mantissa length is shown. For each additional representation bit the accuracy increases by a factor of two.

### 2.2.4 Residue Number (RN) System

To represent a number in a RN system, a representation base must be chosen. A k-tuple of integers (set of relative prime integers $m_1, m_2, \ldots m_k$ called moduli) can be employed. To represent a number X, a set of integers $r_1, r_2, \ldots r_k$ that satisfy following condition

$$r_i = x / m_i, \; for \quad i = 1, 2, \ldots k \tag{2.8}$$

where $r_i$ denotes the least positive integer remainder of the division of x by $m_i$, is satisfied. As an example, consider using' five moduli 3, 4, 5, 7 and 11. Two decimal numbers 23 and 15 are represented by a 5-tuple set of integers: $23_{10} = 1_{11}\, 2_7\, 3_5\, 3_4\, 2_3 = 12332_R$ and $15_{10} = 4_{11}\, 1_7\, 0_5\, 3_4\, 0_3 = 41030_R$, where R stands for RN representation.

To obtain a unique number representation, the represented numbers should not exceed RN's dynamic range. The residue representation dynamic range $D_m$ satisfies the following condition

$$0 \le D_m \le \left[ \prod_{i=1}^{k-1} (m_i) \right] - 1 \tag{2.9}$$

The RNs can be represented using multilevel representation or can be encoded

using BN system. In the later case, each residue digit is encoded using its binary equivalent. In Table 2.3, the RN dynamic range as a function of bit number of binary encoded RNs is shown.

The major advantage that RN system offers is its carry free arithmetic operations capability. Operations, such as addition, subtraction, and multiplication of two numbers A and B are performed according to

$$[A \odot B]_{m_i} = [[A]_{m_i} \odot [B]_{m_i}]_{m_i} \qquad (2.10)$$

where $\odot$ denotes one of the above mentioned arithmetic operations. In this case, an operation is decomposed into a set of k-suboperations, each performed independently and in parallel. To perform an arithmetic operation, a set of residue processors, each corresponding to a different modulus should be employed. By suitably combining the partial results generated by each processor, the final result can be obtained. As an example consider addition and multiplication operations performed on two RN $12332_R$ (decimal 23) and $41030_R$ (decimal 15)

$$\begin{array}{r} 12332 \\ +41030 \\ \hline 53322 \end{array} \qquad (2.11a)$$

$$\begin{array}{r} 12332 \\ \times 41030 \\ \hline 42010 \end{array} \qquad (2.11b)$$

Regardless of the RN major advantages, the disadvantages such as comparison

problems, overflow detection and difficulties with division operation prevents the use of the RN system in a general type computational processor. In applications where for simple arithmetic operations high processing speed and high dynamic range are essential, the RN system can prove to be advantages.

## 2.3 References


[1] D. A. B. Miller, D. S. Chemla, T. C. Damen, A. C. Gossard, W. Wiegmann, T. H. Wood, and C. A. Burrus, "Novel Hybrid Optically Bistable Switch: The Quantum Well Self Electro-optic Effect Device," Appl. Phys. Lett. 45, 13-15 (1984).

[2] D. A. B. Miller, D. S. Chemla, T. C. Damen, T. H. Wood, C. A. Burrus, A. C. Gossard, and W. Wiegmann, "The Quantum Well Self Electro-optic Effect Device: Optoelectronic bistablility and Oscilation, and Self-lineared Modulation," IEEE J. Quantum Electronic QE-21, 1462-1476 (1985).

[3] D. A. B. Miller, "Quantum Wells for Optical Information Processing," Opt. Eng. 26, 2059-2069 (1987).

[4] S. D. Smith, A. C. Walker, B. S. Wherrett, F. A. P. Tooley, J. G. H. Mathew, M.R. Taghizadeh, and I. Janossy, "Cascadable Digital Optical Logic Circuit Elements in the Visible and Infrared: Demonstration of Some First All-optiical Circuits," Appl. Opt. 25, 1586-1564 (986).

[5] N. Peyghambarian and H. M. Gibbs, "Optical Bistability for Optical Signal Processing and Computing," Opt. Eng. 24, 68-73 (1985).

[6] J. J. Cavanagh, *Digital Computer Arithmetic.* New York: McGraw-hill, 1984.

[7] I. Flores, *The Logic of Computer Arithmetic.* New York: Van Nostrsand, 1955.

[8] J. N. Michell, IRE Trans. Electron. Comput., pp 512-517, Aug. (1962).

[9] M. Combet, H. Van Zonneveld, and L. Verbeek, "Computation of the base two logarithm of binary numbers," IEEE Trans, Electronic Computers, vol. EC-14, 863, (1965).

[10] A. Avizienis, "Signed-digit number representations for fast parallel arithmetic," IRE Trans, Electronic Computers, EC-10,389 (1961).

[11] Y. Harata, Y. Nakamura, H. Nagase, M. Takigawa and N. Takagi, Proc. ICCD'84, Oct. 1984.

[12] N. S. Szabo and R. Tanada, *Residue Arithmetic and Its Application to Computer Technology*. New York: McGraw-Hill, 1967.

[13] H. Henkel, "Improved Addition for the Logarithmic Number System," IEEE Trans. ASSP, 37, 301 (1989).

[14] G. L. Sicuranza, "On Efficient Implementations of 2-D Digital Filters using Logarithmic Number Systems," IEEE Trans. ASSP, 31, 877 (1983).

[15] T. A. Brubaker and J. C. Becker, "Multiplication using Logarithms Implemented with Read-Only Memory," IEEE Trans. Comput.,24, 761, (1974).

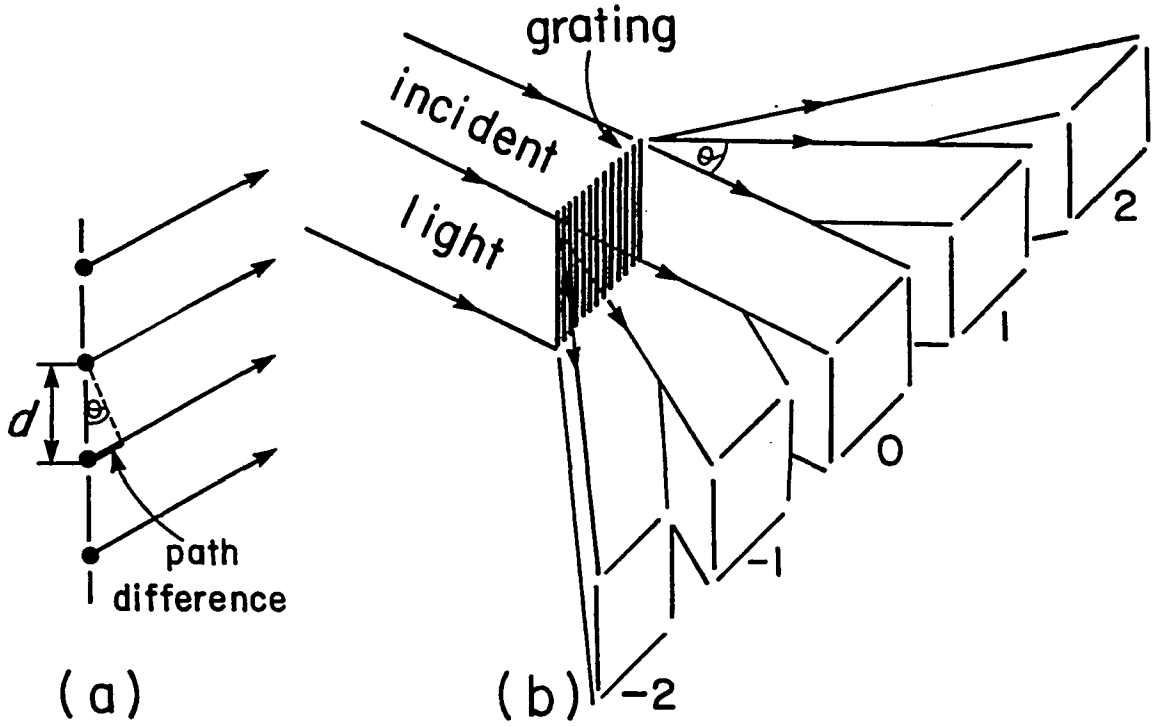


Fig.2.1 Bragg diffraction: (a) Constructive interference depends on a path difference which is an integral number of wavelengths. (b) Many diffraction orders may be produced.

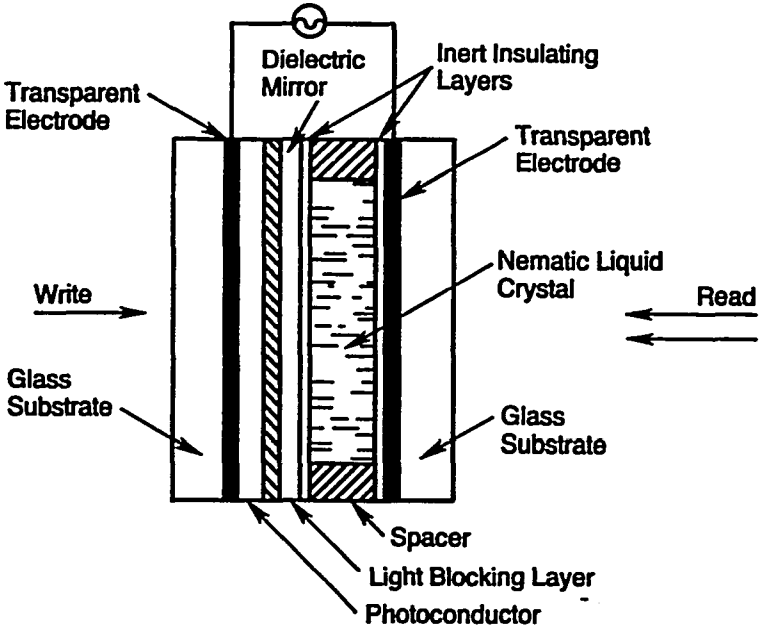


Fig.2.2 Schematic liquid crystal SLM.

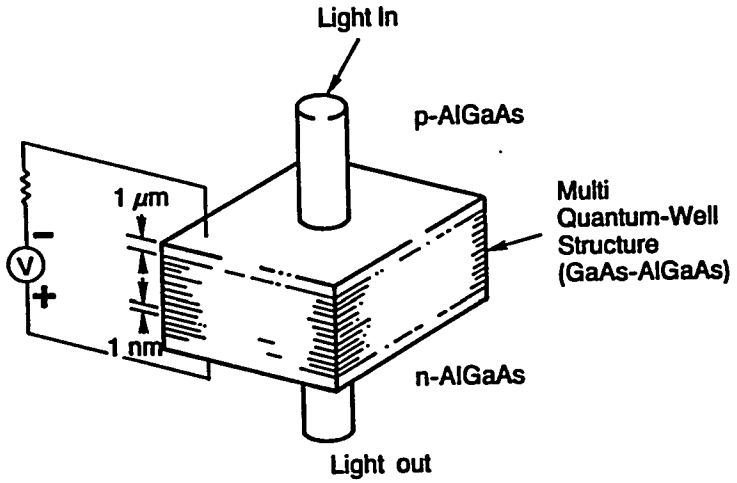


Fig.2.3 Schematic self-electrooptic effect bistable device.

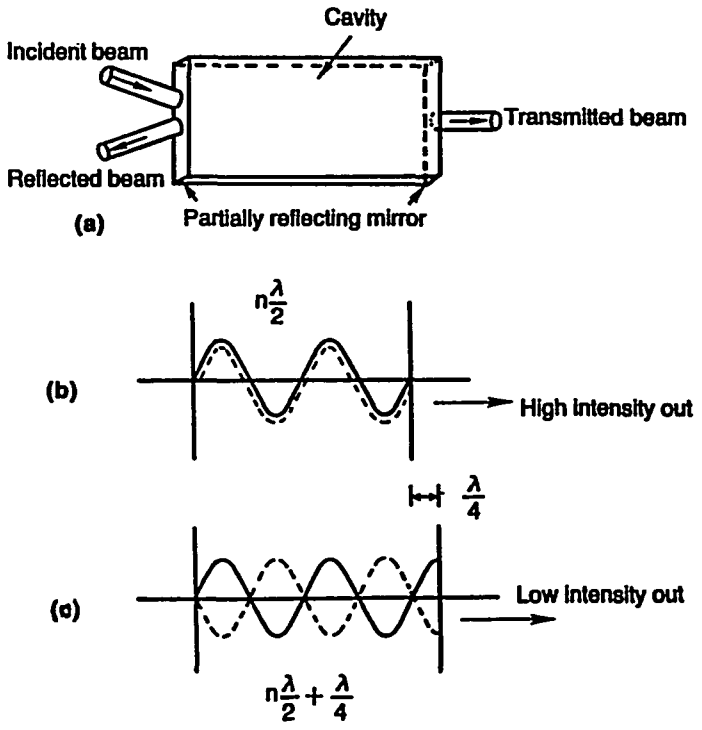


Fig.2.4 Schematic nonliear Fabry-Perot bistable device.

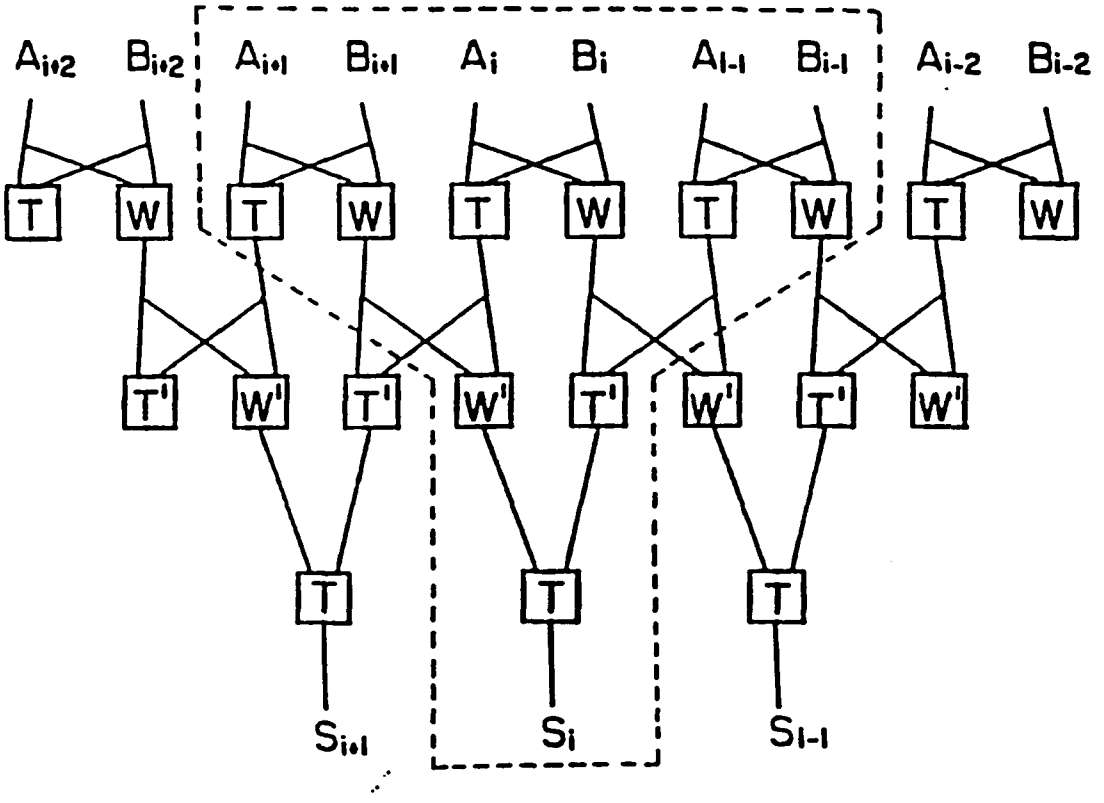


Fig.2.5 5-bit MSD addition logic flow diagram

**T**

| | 1 | 0 | $\bar{1}$ |
|---|---|---|---|
| 1 | 1 | 1 | 0 |
| 0 | 1 | 0 | $\bar{1}$ |
| $\bar{1}$ | 0 | $\bar{1}$ | $\bar{1}$ |

(a)

**W**

| | 1 | 0 | $\bar{1}$ |
|---|---|---|---|
| 1 | 0 | $\bar{1}$ | 0 |
| 0 | $\bar{1}$ | 0 | 1 |
| $\bar{1}$ | 0 | 1 | 0 |

(b)

**$T^1$**

| | 1 | 0 | $\bar{1}$ |
|---|---|---|---|
| 1 | 1 | 0 | 0 |
| 0 | 0 | 0 | 0 |
| $\bar{1}$ | 0 | 0 | $\bar{1}$ |

(c)

**$W^1$**

| | 1 | 0 | $\bar{1}$ |
|---|---|---|---|
| 1 | 0 | 1 | 0 |
| 0 | 1 | 0 | $\bar{1}$ |
| $\bar{1}$ | 0 | $\bar{1}$ | 0 |

(d)

Table 2.1 Truth tables for MSD logic gates

| Mantissa length | Truncation error % |
|---|---|
| 4-bit | 8.1 |
| 5-bit | 4.1 |
| 6-bit | 2.02 |
| 7-bit | 1.07 |
| 8-bit | 0.53 |
| 9-bit | 0.28 |
| 10-bit | 0.13 |
| 11-bit | 6.7 X 10-2 |
| 12-bit | 3.3 X 10-2 |
| 13-bit | 1.6 X 10-2 |
| 14-bit | 8.4 X 10-3 |
| 15-bit | 4.1 X 10-3 |
| 16-bit | 2.1 X 10-3 |

Table 2.2 Multiplication accuracy for SLNs

| NUMBER OF BITS | MODULI | RANGE (DECIMAL) | BINARY |
|---|---|---|---|
| 3-BIT | 5,6,7 | 210 | $2^7$ |
| 4-BIT | 11,13,14,15 | 30,030 | $2^{14}$ |
| 5-BIT | 17,19,23,29,30,31 | 200,360,130 | $2^{27}$ |

Table 2.3 Binary-coded RN dynamic range

# III SWITCHING-ORIENTED OPTICAL SIGNAL PROCESSORS

In this chapter, two switching-oriented optical signal processors, an optical compact programmable logic array (OPLA) and a LCTV-based optical position coded residue number (PCRN) processor, are presented. In case of the OPLA, using either a 2-D optical spatial light modulator (SLM) or an array of 1-D SLMs inside a lens-based multiple-beam-path cavity, an array of optical multiple-variable logic product terms are generated. In this case the 2-D SLM or the array of 1-D SLMs provide optical spatial switching and programmable capability. This device together with a programmable multiple-variable OR matrix can be used to implement any Boolean combinatorial logic operations. For an optical binary combinatorial logic computation, the proposed method efficiently uses 3-D space and optical elements.

For the PCRN processor, the use of a single laser source together with two commercial LCTVs eliminates the complexity of the switching device which is the major drawback in LED arrangement based system. On the two cascaded LCTVs, the operands are represented as two mutually orthogonal light bars. Their intersection at a LCTV output plane represents a particular arithmetic result. For a specific arithmetic operation, the collection of light output constitute a PCRN look-up table. A hologram together with a projection lens maps each truth-table point to a proper PCRN results plane position.

## 3.1 An Optical Compact Programmable Logic Array Processor

### 3.1.1 Preliminary

Programmable logic array (PLA) is a device that is finding increasing usage in logic operations. This structure handles combinatorial sequential logic functions. System designs in Boolean functions and state diagrams can be readily implemented into hardware.

A PLA is similar to a read-only memory (ROM) in concept except that it does not provide full decoding of the input lines. A ROM is implemented by a fixed array of AND gate array and an array of OR gates, with programmable interconnections between the outputs of the AND gate array and the OR gate array inputs. In case of a PLA, it is configured with an AND gate array and OR gate array cascaded to perform a sum-of-products realization of the Boolean functions, with not only programmable interconnections between the inputs and the AND gate array but also the OR gate array with programmable interconnections from the outputs of the AND gate array.

Thus, in a PLA, the decorder is replaced by a group of AND gates each of which can be programmed to produce an AND term of the input variables. Outputs from the OR gate array are delivered either off-chip or to a feedback latch located on the chip. Therefore, the desired specific logic functions are implemented in the last processing step together with a interconnection for linking the inputs to the AND gate array and the outputs of the AND gates to the inputs of the OR gate array.

### 3.1.2 Optical Implementation

In this section, a new compact folded-path OPLA is presented. A two-stage multiple-variable programmable logic array (PLA) is usually implemented as a cascade of two logic matrices (see Fig.3.1). In the first (an AND) matrix, the input signals and their complements (the negations) are selectively ANDed such that a certain input combination generates, on one or more of its output lines, a logic "1" [3]. Using a second (an OR) matrix, the first matrix outputs are selectively ORed to form the final logic outputs. To implement switching capability, a 2-D transmissive SLM (LCTV) is inserted in the cavity. According to input, the LCTV either let the beam pass through or block it,

so that the switching operation (programmability) can be achieved. Using this scheme a large number of logic variable can be easily processed [1-2]. Using an optical cavity, multiple-beam pathes are obtained. Through the use of a multiple-variable AND operation, the required logic product terms are directly generated.

Because of the compact geometry and simple optical elements, i.e. three lenses, two mirrors, and a SLM, this OPLA is suitable for practical implementation. Here, the two logic levels are on/off signal states. For an array of multiple-variable optical AND operations, the optical beam must traverse a sequence of optical SLM planes. Since each SLM's pixel diffracts light, between every two consecutive SLMs an imaging lens is needed [4-6]. Furthermore, since a direct N-stage cascade of SLMs is impractical, To save on both the number of SLMs and the overall processing space, the following steps are suggested. First, instead of using N SLMs to represent N logic variables, a single SLM is reused N times. Second, to drive the SLM with N consecutive normally incident beams, a compact, lens-based, multiple-beam-path cavity is employed. In Fig.3.2, with a transmissive SLM, a schematic of an optical multiple-variable binary-logic product generator is depicted. The system uses, in a folded 4F geometry, two end mirrors and two identical focal-length (F) Fourier lenses. The two lenses are laterally displaced by a distance

$$\Delta = \frac{D}{N-2} \tag{3.1}$$

where D is the lens aperture size, and N denotes the number of equally-spaced parallel beam paths. This cavity has been proposed for either laser Doppler or heterodyne interferometry [7-9]. For a transmissive SLM based OPLA, programmed to either pass or block an input, the SLM is placed at the cavity

center-plane. When all the N SLM points are activated, an output is detected. This optical cascade implies an N-variable AND operation. Since for logic product term generation both the logic variables and their complements are needed [1], for each product term, all N SLM pixels (activated to be either the variable $x_i$ or its complement $x_i$ but not both) should be independently accessible. This access can be achieved by either preprogramming the SLM's video signal or modifying it with an external INVERTER circuit.

In Fig.3.3, a compact, reflective SLM based optical logic product generator is shown. Note that here the front polarizer of the LCTV used as SLM is removed and, instead, mutually-perpendicular polarizers are placed in the two separate arms.

To implement an N-variable Boolean combinatorial logic operation, in general, a canonical sum of up to $2^N$ N-variable logic product terms may be required [1-3]. Since for each logic product term N linearly distributed SLM points are needed, for $2^N$ optical logic product terms, $2^N$ parallel 1-D stripes should be used. Based on a transmissive SLM, in Fig.3.4 a schematic cylindrical lens-based, multiple-beam-path, OPLA system is illustrated. Using $2^N$ vertical slices, the $2^N$ logic product terms are generated. Using content-addressable memory [9] based preprogramming, and with the help of logic don't care terms, the reduction from a canonical to a minimum sum of product logic expression can be performed leading to an efficient processing scheme. In this case, regardless of its input, the "don't care" pixels are always activated. At the output, to perform a matrix of multiple-variable (up to $2^N$) binary logic OR operation, an additional SLM, together with beam splitters and a cylindrical lens is employed. With the SLM selecting the desired OR output for a particular channel, the cylindrical lens performs the final OR operations.

### 3.1.3 Experimental Results

To demonstrate the proposed concept, the following preliminary experiments were performed. The source was a 2 mm waist Ar ($\lambda$ = 514 nm) laser beam. To form the multiple-beam-path cavity, a pair of antireflectively coated Fourier lenses (F = 40 cm and D = 9 cm) and two end-mirrors were employed. For 10 mw input power and a $\delta$ = 3 mm, 32 visible beam paths were observed. To generate the optical multiple-variable product terms, a 200 mw beam was first expanded and then masked into five parallel beams, each with an approximate 10 mw power. Using a pair of F = 21 cm and D = 2.5 cm cylindrical lenses, a four beam-path cavity was designed. To test the system switching ability, a commercial CITIZEN liquid-crystal TV (LCTV) was employed. The operational principle of this device is similar to other LCTV's described in the literature [4-6, 10-12]. The LCTV was programmed to pass beams corresponding to the following five product terms:

$$f_1 = \bar{x}_1 \bar{x}_2 \bar{x}_3 \bar{x}_4, \qquad (3.2a)$$

$$f_2 = \bar{x}_1 x_2 \bar{x}_3 x_4, \qquad (3.2b)$$

$$f_3 = x_1 \bar{x}_2 x_3 \bar{x}_4, \qquad (3.2c)$$

$$f_4 = \bar{x}_1 x_2 x_3 \bar{x}_4, \qquad (3.2d)$$

$$f_5 = x_1 x_2 x_3 x_4, \qquad (3.2d)$$

During the operation only the $f_1$, $f_2$, and $f_5$ were activated, while in the third and fourth channels other input combinations were used. Correspondingly, at the AND array output, the first, second and last channel outputs were detected (see Fig.3.5a). These outputs were then split into three channels and

guided into the OR array (see Fig.3.5b). In front of the output cylindrical lens, a preprogrammed mask that selects for each of the three OR array channels was inserted. In Figs.3.5c and 5d, the selected signals as well as the final OPLA results (at a slightly defocused plane) were shown: $O_1 = f_1 + f_2$, $O_2 = f_1 + f_5$, and $O_3 = f_2 + f_5$. Since with most LCTVs, a maximum transmission of 50 % [10] can be achieved, to process more logic variables, extensive improvements must be made. First, the present polarizer should be replaced with a high optical-quality, low-absorption polarizer with an antireflective coating. Second, because of the cascading geometry, the back analyzer should be removed. This removal can lead to an additional transmission increase [6]. Third, because the low-cost LCTV's dynamic contrast is limited [11-12], additional electronics should be attached to obtain a larger switchable bias voltage difference.

Besides the transmission loss ($t_s$) caused by the switching array, other loss factors, such as the beam propagation loss ($t_p$) caused by diffraction and lens surface reflection, and mirror reflection loss ($t_r$), should also be considered. In general, for a given fanout K, input power $P_{in}$, and detectable output power $P_{out}$, in each product term, the maximum number of variables (N) that can be processed is

$$N = \frac{\log((1-t_r)KP_{out}/P_{input})}{\log((1-t_s)(1-t_p)(1-t_r))} \qquad (3.3)$$

Assume that K = 100, $P_{input}$ = 10 mw, $P_{out}$ = 10 nw, $t_s$ = 0.15 (achievable with a high quality front polarizer LCTV), $t_p$ = 0.1 and $t_r$ = 0.02, for each product term, N = 32 logic variables can be included. Now, suppose that each logic channel extends 50 $\mu m$, and a pair of f/3.0 lenses are used. Simple calculation shows that for a 32-variable product term the propagation delay is about 2 ns. To process more logic variables, additional efficient modulation/switching

schemes need to be incorporated. For example, to compensate for cavity losses, a high gain microchannel SLM [12] ($G \approx 10^3$) may be helpful. In addition, since each multiple-variable logic product term uses only a 1D slice, it is also possible to use a parallel array of 1D SLM's, such as acoustooptic (A-O) Bragg cells. Using a fast A-O device can increase both the signal output and the switching rate from a low KHz rate to 100 MHz range leading to a higher throughput ($10^7$ operations per second) medium fan-in/out OPLA. On the other hand, it is also possible to serially decompose a large size input array into many smaller sized arrays [1].

## 3.2 A LCTV-based Optical Position Coded Residue Processor

### 3.2.1 Preliminary

During the past few years, an increased interest in applying optical parallel processing techniques to digital computation has been noted. Methods that are based on optical 2-D spatial light modulators (SLMs), due to their parallel data processing capability, can achieve a high throughput. For different optical logic and arithmetic operations, using either binary or multiple-valued logic, a number of optical truth-table processing schemes have been proposed [13-21]. By applying different optical encoding (i.e. position, density, polarization, etc.) techniques, either location- or content-addressable truth-tables can be implemented. The residue number (RN) system is well suited for both content-addressable (CAM) and location-addressable memory (LAM) look-up processors. In the RN system, a number of relative prime moduli are employed. Its dynamic range is equal to the product of all the moduli. For example, using the relative prime moduli 9, 10, 11, 13, the dynamic range is equal to 12,870. Because with RNs arithmetic operations can be decomposed into a set of independently performed suboperations [13], RNs represent an effective parallel code. The present position-coded RN (PCRN) look-up table processors utilize a 2-D LED (or laser diode) array [17-20]. The major disadvantage of this method is that, for a large modulus, a large number of LEDs is required (e.g. for a modulus m, $m^2$ LEDs are required). Although LAM processors that use smaller number (for a modulus m, 2m or $4\sqrt{m}$) LEDs have been proposed, they require a real-time optical thresholding element not readily available at the present time [20].

In this section, a new real-time optical PCRN processor is proposed. By using a single laser source together with two commercial liquid-crystal TVs (LCTVs), crossbar switching capability can be achieved easily. This crossbar

switching scheme offers following advantages. First, this scheme reduces the number of input source. It requires only one laser source instead of $m^2$, 2m or $4\sqrt{m}$. Second, it provides the less architecture complexity compared to the LED arrangement. On the two cascaded LCTVs, the operands are represented as two mutually orthogonal light bars. Their intersection at a LCTV output plane represents a particular arithmetic result. For a specific arithmetic operation, the collection of light output points constitute a PCRN look-up table. A hologram, placed at the LCTV's output plane, maps each truth-table point to a proper PCRN result plane position. For each result plane position, using a different reference angle beams, a subhologram is generated. After presenting the details of this PCRN processor, an experimental PCRN optical multiplier will be described.

### 3.2.2 Optical Implementation

Optical PCRN look-up table evaluation is a two stage process. First, a look-up table is generated and stored. Next, during a read-out stage, based on operands $x_i$ and $y_i$ indices, the operation result is accessed. The optical PCRN look-up table processor requires that, for each $x_i$ column and $y_i$ row intersection pair, a light pulse be produced. In this approach, for each operand an inexpensive LCTV device is employed. The operation of a LCTV is based on the use of a twisted nematic liquid crystal cell [22-25]. The input light first passes through a polarizer, next through a glass-LC-glass cell, and finally, through an analyzer. Because at each LCTV's pixel, in the absence of an applied electric field, the incoming beam's polarization plane rotates by 90°, a parallel analyzer blocks the light at the output. In the presence of an appreciable dc electric field, there is a net polarization change resulting in an analyzer light output. By cascading two LCTVs, (see Fig.3.6) a logical AND of the two displayed images is performed. On $LCTV_1$, the first operand

$x_i$ is a vertical light bar whose position depends on the value of $x_i$. When $x_i$ increases, its position shifts to the right. On $LCTV_2$, the second operand $y_i$ is a horizontal light bar whose position, for increasing $y_i$, shifts downward. When the two LCTVs are transilluminated with a collimated beam, the output light represents the desired arithmetic result. To produce the two LCTV images, two separate computer graphics imaging boards are utilized. At the LCTV's output plane, in a second stage, a hologram-lens combination maps all the output (truth-table) plane points into position-coded result points. By utilizing different reference beam angles, for each result position, a hologram that consists of a 2-D array of subholograms where each subhologram represents a particular arithmetic result is produced. During the hologram's read process, the light passing through the cascaded LCTVs illuminates each subhologram. It is then deflected by the hologram-lens combination to one of the PCRN result positions (e.g. for a mod m multiplication there are m, from 0 to m-1, positions).

For a PCRN look-up table processor, the arithmetic operation result is mapped to a given truth-table position. The present commercially available LCTV is limited to 1000 X 1000 pixels. The size of this display limits the dynamic range of an RN processor. By increasing the number of neighboring LCTVs, e.g. using a set of four LCTVs, this limit can be increased to say 2000 X 2000 pixels. In this configuration, each LCTV displays a fourth of the look-up table. In addition, for k different residue numbers, each LCTV screen can be sub-divided into k parts or k neighboring LCTVs, representing a particular modulus PCRN look-up table. For each modulus, a separate deflecting hologram (each consisting of a set of subholograms) must be generated.

### 3.2.3 Experimental Results

In our experiment, two CASIO (TV 400) 2" diagonal LCTVs were used. To illuminate the entire LCTV screen, the 632.8 nm He-Ne laser beam was expanded and collimated. The set of four relative prime moduli were 3, 4, 5, and 7. For a RN multiplication, the LCTV screens were divided into four parts, with each part representing a different modulus LAM look-up table. In Fig.3.7, this LCTV's screen partition is depicted. Each multiplication operand was either a horizontal or a vertical light bar (see Fig.3.8a and 8b). With the light passing through the common image points, particular multiplication results (the bright points in Fig.3.8c) were generated. For example, the upper-left hand corner point (3,0) represents a multiplication in mod 4, the upper-right hand corner point (2,2) a multiplication in mod 3, the lower-left hand corner point (3,4) a in mod 5 and the lower-right hand corner point (4,4) a multiplication in mod 7. To assure the proper display intensity, the LCTV's brightness control was adjusted.

For each modulus, a lens-hologram combination deflects the beam to a result plane. The holograms were produced using Kodak 649F spectroscopic plates. The collimated input beam was first separated, by a beamsplitter, into a signal and reference arms. With the signal arm containing the LCTVs, the reference beam was directed to various angular directions. As an experimental example, a mod 3 multiplication was considered. The signal and reference beam intensity ratio was 1:3. The angular spacings between the signal and the first object beam was 20° while the angular separation between two consecutive reference beams was 5°. For a mod 3 multiplication, to fabricate a nine element composite hologram, three different exposures with the three angular object beams were taken. To generate a set of subholograms, for each angular object beam, a particular mask was used. After a chemical processing, the composite hologram was positioned at the correct reference

beam position. Since the nine subholograms diffract their input beams into three different output directions, to obtain the three position-coded results, a convex lens was employed. To collect the signal, in the lens back focal plane, either a photographic film or a photodetector can be used. As an example, in Fig.3.9c, the composite slightly defocused holographic outputs are shown. In each case, an over 10:1 contrast ratio was observed. For each modulus, a different subhologram array was generated and the four position-coded multiplication results were obtained.

For the existing LED/LD look-up processor, the light source complexity rapidly increases with the RN's dynamic range. On the other hand, the proposed LCTV-based processor requires, regardless of the RN's dynamic range, only a single light source. To increase the speed of this PCRN processor, a surface stabilized ferroelectric LC (SSFLC) plate may be used. It has been indicated [26] that a 1000 X 1000 SSFLC gate array (assuming 4 $\mu m^2$/gate) will operate at 1 MHz frame rate. Although this rate still does not approach the fastest laser diode speed, its fabrication is said to be relatively simple.

### 3.3 Summary and Conclusion

In this chapter, two switching-oriented optical signal processors were presented. Using an optical cavity and a single laser source together with two LCTVs, optical switching capabilities were achieved for an optical compact programmable logic array and an LCTV-based optical position coded residue processor were implemented, respectively.

In case of the RN processor, the use of two transmissive type LCTVs for a PCRN look-up table processor has been described. On the two cascaded identical LCTVs, the two inputs were represented as two mutually orthogonal light bars. Finally, at the output plane, the intersection of the two orthogonal bars represented the result. During the experiment, a slightly modified (e.g. the analyzer was removed) inexpensive LCTV, (CASIO TV 400) was used. The proposed processor's dynamic range is limited by the number of available LCTV pixels. By combining a number of separate LCTVs, a high dynamic range optical multiplication can be achieved. To map the look-up truth-table results into PCRN output channels, holographic beam directors were used

A new method to implement switching capability for a medium scale, compact, free-space OPLA, using a LCTV located inside of optical cavity, was implemented for a large number of logic variable. The main feature of the proposed device is that it efficiently uses 3-D space and optical elements to perform general-purpose combinatorial logic computation. Additional features include: (1) unlike other proposed SLM-based multiple beam path signal processing schemes that use oblique incidence angles which can degrade the SLM performance, the new approach always uses the normal incidence for best SLM performance, (2) the folded 4F imaging system [5-6] limits the accumulative diffraction noise caused by long optical paths, and (3) by inserting spatial filters

at two common focal planes, the SLM's switching contrast can be improved [5-6, 11]. Using an inexpensive SLM, some preliminary experimental results were described. Further processor improvements are under investigation.

### 3.4 References


[1] R. Arrathoon and S. Kozaitis, Proc. SPIE, 752, 34 (1987).

[2] R. Arrathoon and S. Kozaitis, "Architectural and Performance Consideration for $10^7$-Instruction/sec Optoelectronic Central Processing Units," Opt. Lett. 12, 956 (1987).

[3] M. Davio, J.-P. Deschamps, and A. Thayse, *Digital Systems with Algorithm Implementation*, (John Wiley, New York, 1983), ch.3.

[4] J. A. McEwan, A. D. Fisher, P. B. Rolsma, and J. N. Lee, J.Opt.Soc.Am. A2, 8 (1985).

[5] M. Young, "Low-Cost LCD Video Display for Optical Processing," Appl. Opt. 25, 1024 (1986).

[6] F. T. S. Yu, S. Jutamulia, and D. A. Gregory, "Optical Parallel Logic Gates using Inexpensive Liquid-Crystal Televisions," Opt. Lett. 12, 1050 (1987).

[7] J. S. Yoon and S. S. Lee, "Multiple-Reflection Laser Doppler Interferometer," Appl. Opt. 24, 3429 (1985).

[8] Y. Li and G. Eichmann, "Multipass Counterrotaing Wave-Plate Frequency Shifts for Hetrodyne Interferometry," Opt. Lett. 11, 718-720 (1986).

[9] M. M. Mirsalehi and T. K. Gaylord, "Truth-Table Look-Up Parallel Data Processing using an Optical Content-Addressable Memory," Appl. Opt. 25, 2277 (1986).

[10] H. K. Liu, J. A. Davis, and R. A. Lilly, "Optical-Data-Processing Properties of Liquid-Crystal Television Spatial Light Modulator," Opt. Lett. 10, 635 (1985).

[11] D. Casasent and S. F. Xia, "Phase Correlation of Spatial Light Modulator," Opt. Lett. 11, 398 (1986).

[12] Y. Suzuki, T. Hara, Y. Ooi, and M. H. Wu, "Optical Transfer Characteristics of Microchannel Spatial Light Modulator," Proc. SPIE, 881 (1988).

[13] N. S. Szabo and R. Tanada, Residue Arithmetic and Its Application to Computer Technology (McGraw-Hill, New York, 1967).

[14] A. Huang, Y. Tsunida, J. Goodman and S. Ishihara, "Optical computation using residue arithmetic," Appl. Opt. 18, 149 (1979).

[15] A. M. Tai, I. Cindrich, J. R. Fienup, and C. C. Alexsoff, "Optical residue arithmetic computer with programmable computation modules," Appl. Opt. 18, 2182 (1979).

[16] C. C. Guest, and T. K. Gaylord, "Truth-table look-up optical processing utilizing binary and residue arithmetic," Appl. Opt. 19, 1201 (1980).

[17] A. P. Goutzoulis, D. K. Davis and E. C. Malarkey, "Prototype position-coded look-up table using laser diodes," Opt. Comm. 61, 302 (1987).

[18] M. M. Mirsalehi, and T. K. Gaylord, "Truth-table look-up parallel data processing using content-addressable memory," Appl. Opt. 25, 2277 (1986).

[19] R. I. McDonald, "Optoelectronic switch matrix as look-up table for residue arithmetic," Opt. Lett. 12, 787 (1987).

[20] A. P. Goutzoulis, "Complexity of residue position-coded lookup table array processor," Appl. Opt. 26, 4823 (1987).

[21] Y. Li, G. Eichmann, R. Dorsinville and R. R. Alfano, "Demonstration of a picosecond optical residue computation," Opt. Lett. 13, 178 (1988).

[22] F. T. S. Yu, S. Jutamulia and D. A. Gregory, "Optical parallel logic gates using an inexpensive liquid-crystal TV," Opt. Lett. 12, 1050 (1987).

[23] F. T. S. Yu, S. Jutamulia, and D. A. Gregory, "Real-time liquid crystal TV XOR- and XNOR-gate binary image subtraction technique," Appl. Opt. 26, 2738 (1987).

[24] K. D. Hughes, S. K. Rogers, J. P. Mills, and M. Kabrisky, "Optical pre-processing using liquid crystal televisions," Appl. Opt. 26, 1042 (1987).

[25] H. K. Liu, J. A. Davis, and R. A. Lilly, "Optical data processing properties of a liquid-crystal TV spatial light modulator," Opt. Lett. 10, 635 (1985).

[26] K. M. Johnson, M. R. Surette, and T. Shamir, "Optical interconnection network using polarization-based ferroelectric liquid crystal gates," Appl. Opt. 27, 1727 (1988).

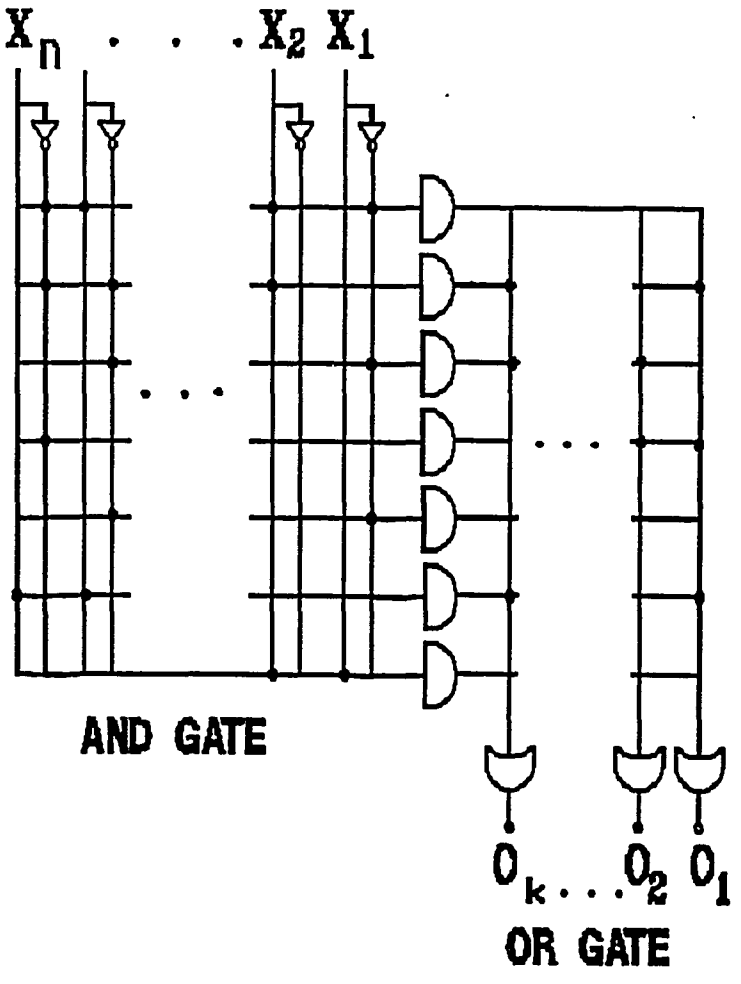


Fig.3.1 A block diagram of a two-step PLA. The N inputs are selected by N inverters to generate the required inputs to an AND matrix (a cross-bar). This cross-bar switching network can be programmed to connect the selected input and output channels to generate the multiple-variable product terms. These product term outputs are then guided into an OR matrix that selects, for each PLA output channel, the required multiple-variable OR result.

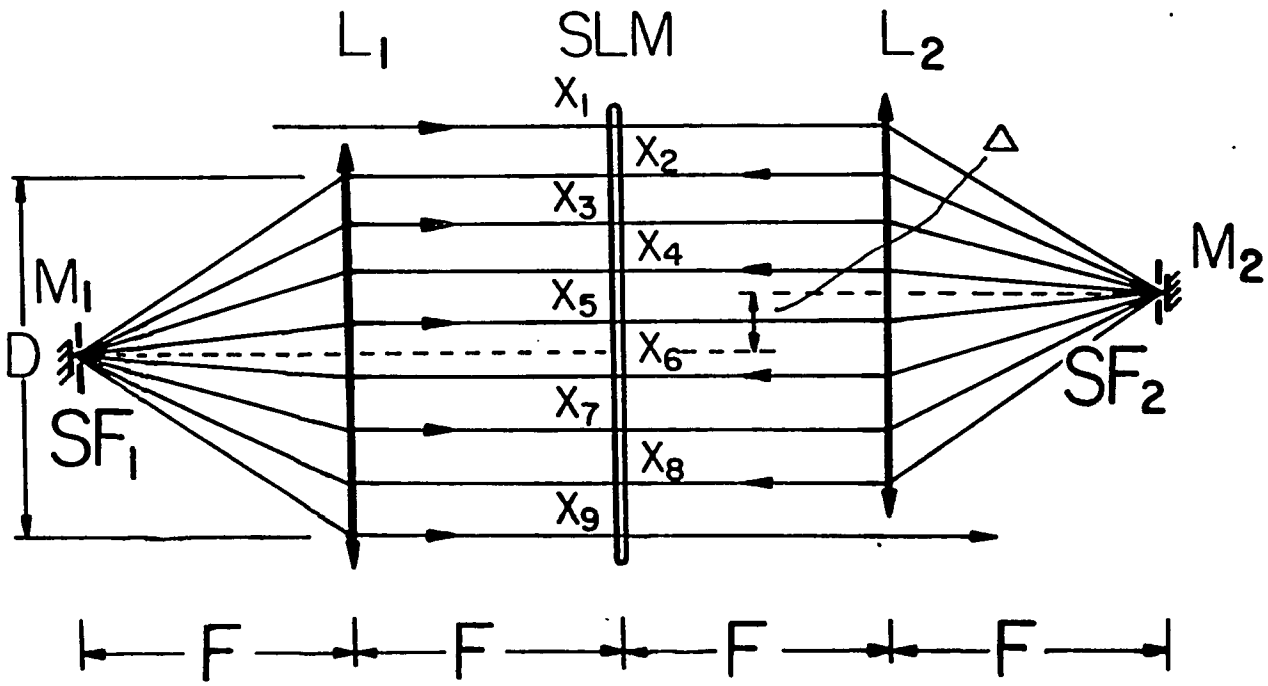


Fig.3.2 A transmissive SLM based, optical, multiple-variable logic, product-term generator. To form a multiple-beam-path cavity, a noncoaxial lens based 4F system is used. D (F), the lens aperture (focal length); Δ the lateral shift of the lens axes; $M_1$ and $M_2$, end-mirrors; $SF_1$ and $SF_2$, spatial filters; $L_1$ and $L_2$, Fourier lenses.

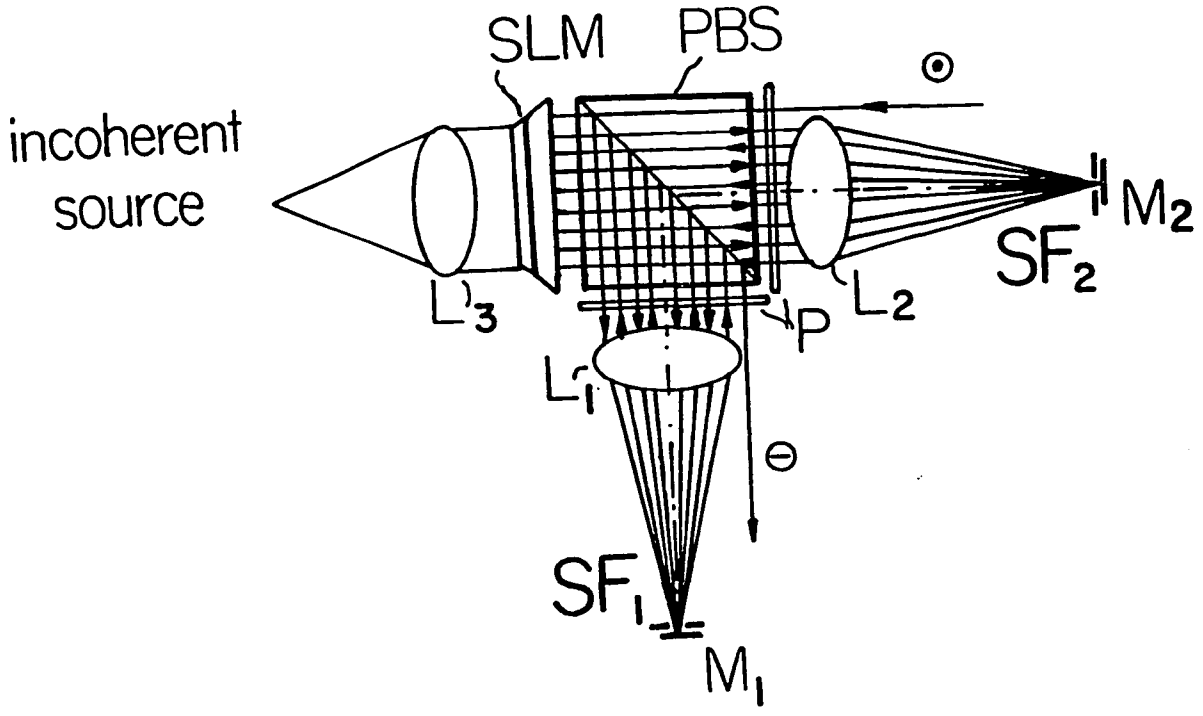


Fig.3.3 A reflective SLM based optical multiple-variable logic product term generator. PBS, polarizing beamsplitter; P, polarizers; $SF_1$ and $SF_2$, spatial filters; $M_1$ and $M_2$, end mirrors; $L_1$ - $L_3$, lenses. The input and output polarizations are mutually orthogonal.

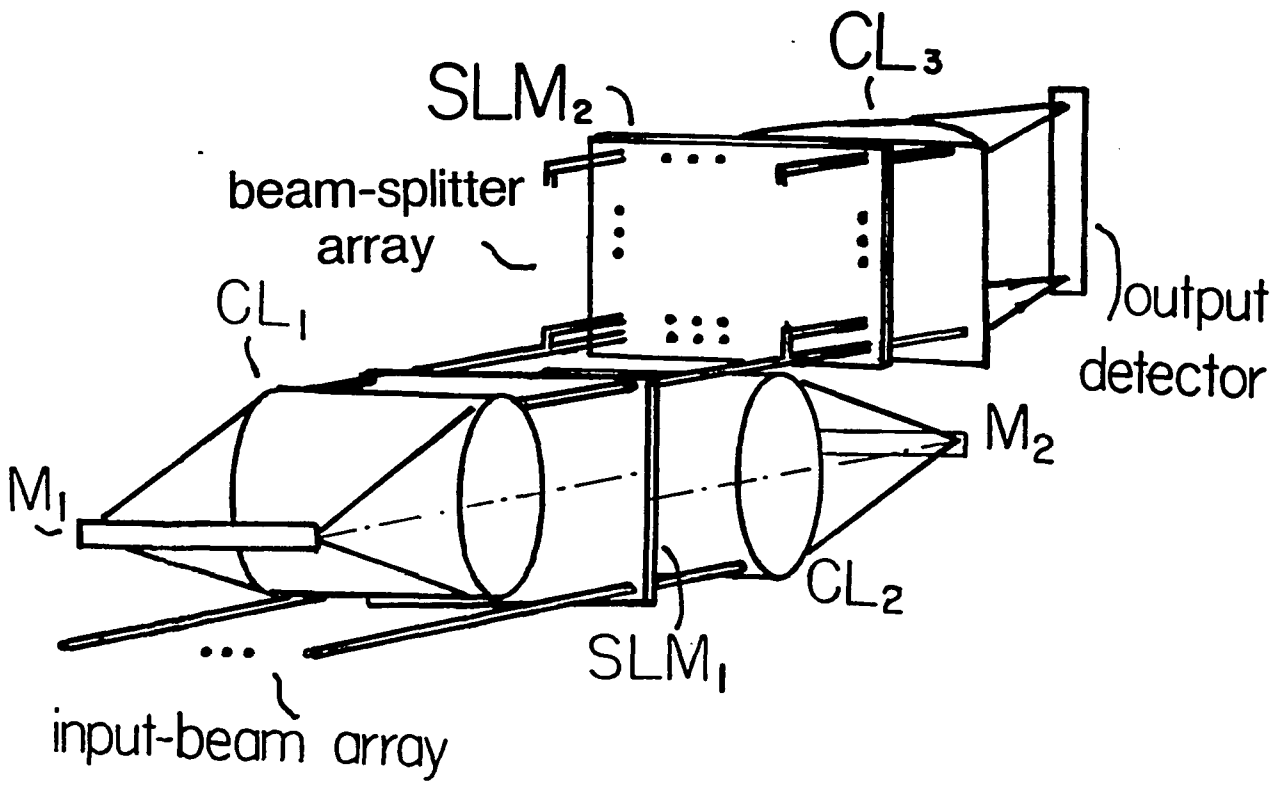


Fig.3.4 Schematic OPLA with optical programmable AND and OR matrices. For the AND matrix, $SLM_1$ is sandwiched between two cylindrical lenses $CL_1$, $CL_2$ and two end-mirrors $M_1$ and $M_2$. Using a beamsplitter array, the AND outputs are split, then switched by $SLM_2$. To form the final OPLA outputs, the switched outputs are collected by the cylindrical lens $CL_3$.

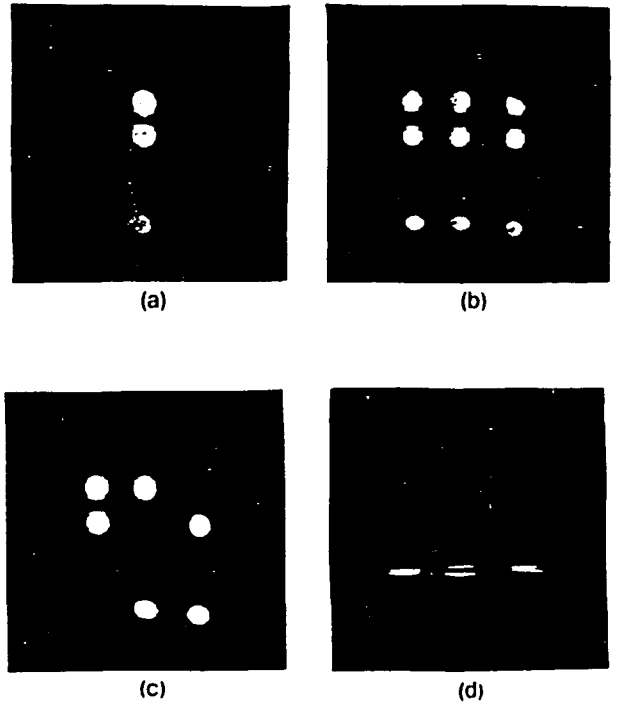


Fig.3.5 Results of the proposed OPLA obtained at different processing planes. (a) the three activated four-variable AND results at the AND array output, (b) duplicated results of (a) to be used for OR array processing, (c) the selected signals to be separately ORed, and (d) the three OR channel results at a slightly defocused OPLA output plane.

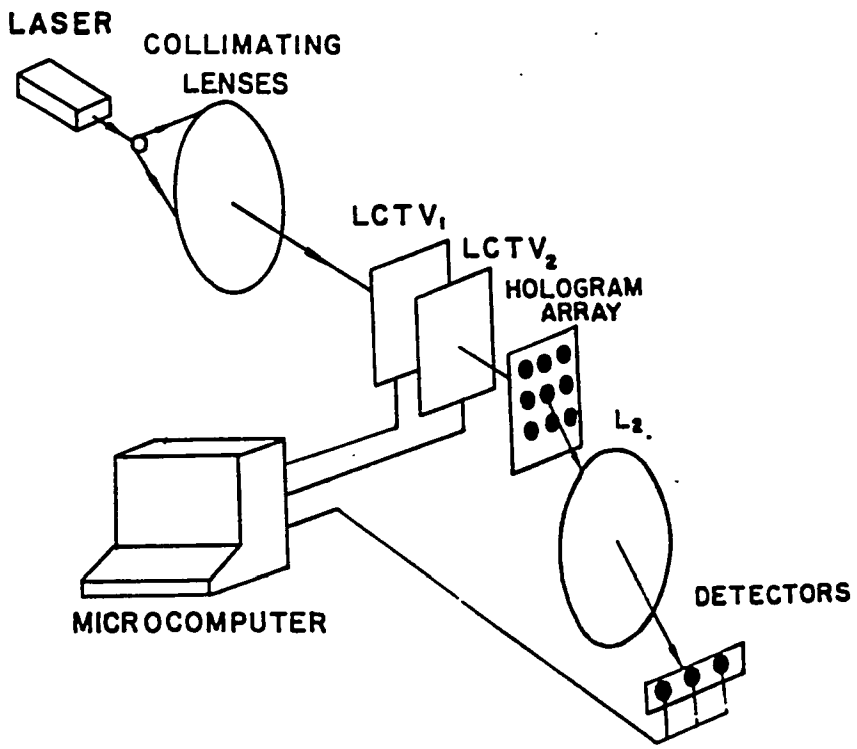


Fig.3.6 Experimental setup for a single laser source optical PCRN processor.

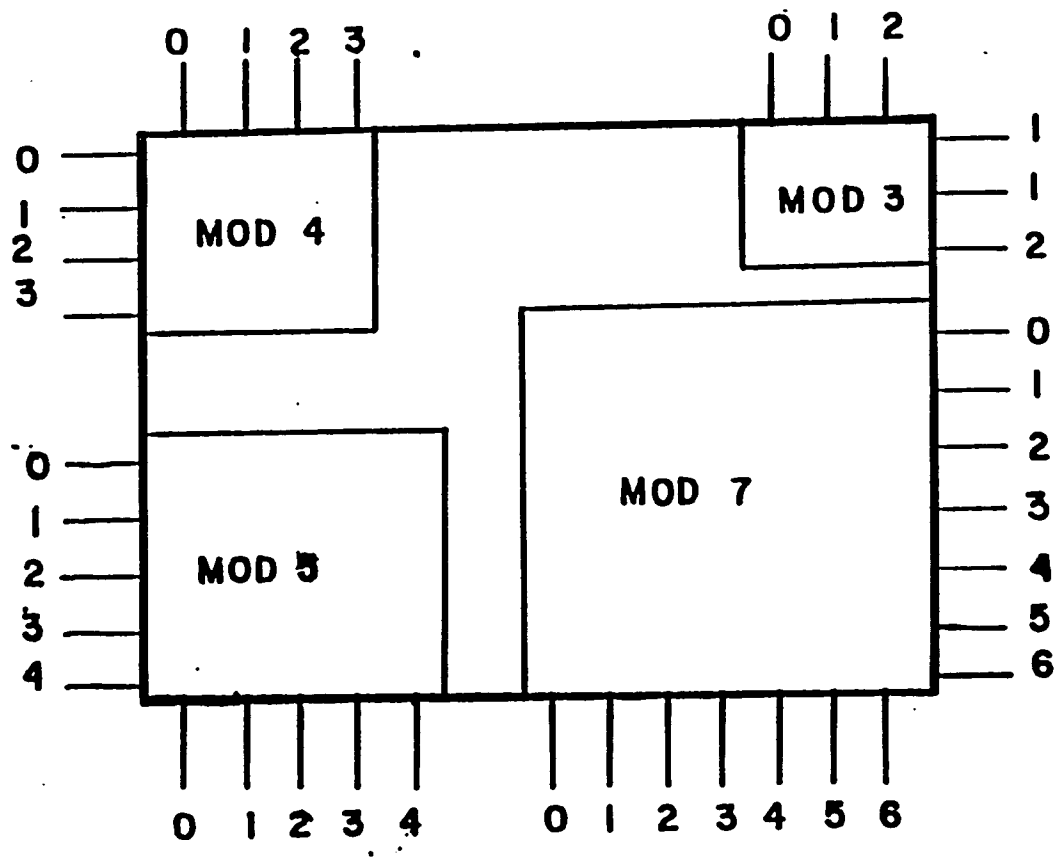


Fig.3.7 Four-part LCTV screen partition where each partition represents a different modulus multiplication result.

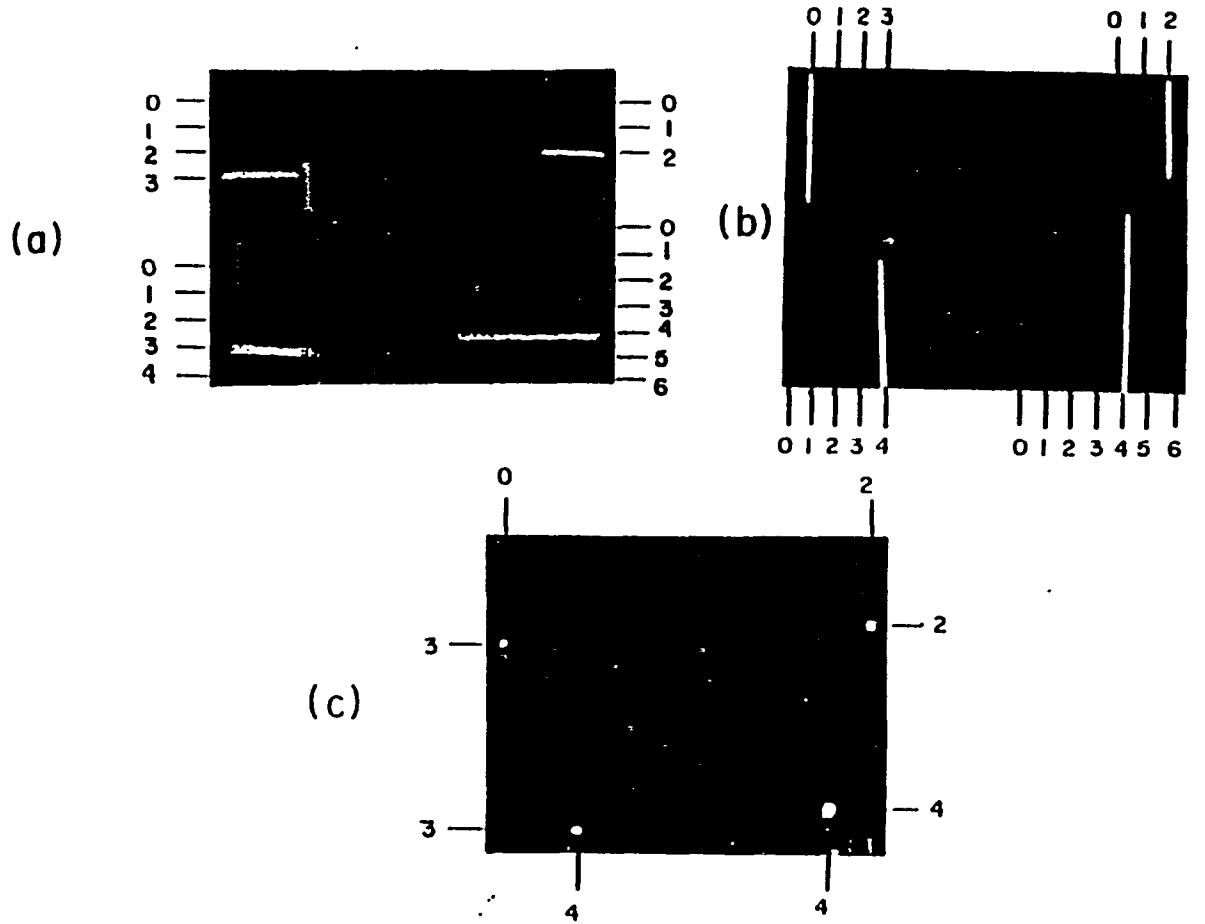


Fig.3.8 Addressing of an experimental PCRN processor: (a) the four horizontal light bars (the first operand) representing mod 4, 3, 5, 7 multiplication, (b) the four vertical light bars (the second operand) representing the moduli of (a), (c) the superposition of the results of (a) and (b).

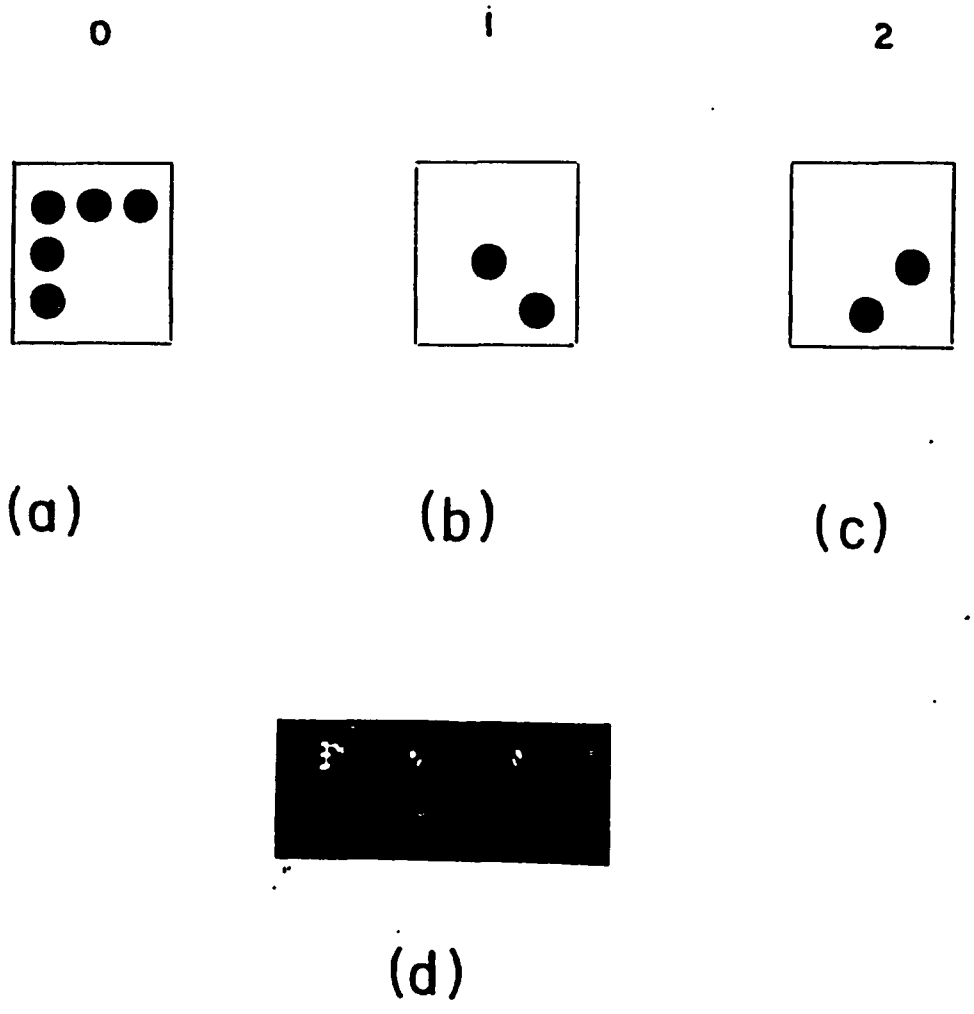


Fig.3.9 The 3 X 3 hologram used to map the PCRN mod 3 multiplication truth-table entries. In (a), (b), and (c), the hologram represents the PCRN level 0, 1 and 2, respectively, while in (d) the holographic mapping result at the processor's slightly defocused output plane is shown.

# IV LOGIC-ORIENTED OPTICAL SIGNAL PROCESSORS

In this chapter, two logic-oriented optical signal processors, a white-light optical pyramidal tracking novelty filter and an optical programmable real-time morphological image processor, are presented. The major advantage of logic-oriented optical signal processing compared to digital electronic image processing is the ease of real-timew implementation for relatively large amount of data. In case of the digital electronic image processing, to perform a parallel processing, mesh-type cellular array-based massively wired interconnections, which lead to hardware complexity and high energy consumption, are required.

For the white-light optical pyramidal tracking novelty filter, EXCLUSIVE-OR logic operation, based on an optical image subtraction technique using two identical inexpensive LCTVs, is employed. In this scheme there are three major advantages. First, the coherent source required by a coherent optical tracking novelty filter can be replaced by a more practical white-light source. Second, the nonlinear optical phase-conjugation crystal is replaced by two inexpensive and compact LCTV SLMs. Finally, an efficient real-time optical parallel processing architecture can be implemented easily.

In case of the optical programmable real-time morphological processor, optical AND followed by INVERSION logic operations are engaged. The optical AND logic operation is performed via twice of the cascaded optical SHIFT-OR-THRESHOLD logic operations. In this approach, two major advantages compared to existing schemes are acquired. First, based on this new architecture, any size and shape of structuring elements can be easily processed. Second, OPENING and CLOSING operations can be performed only using optical DILATION and INVERSION operations which lead to less hardware complexity.

## 4.1 A White Light Optical Pyramidal Tracking Novelty Filter

### 4.1.1 Preliminary

Pyramidal image processing (PIP) [1-3] is a form of multiresolution image analysis that has been suggested as a useful image representation for many real-time image and pattern processing applications. A primary image is decomposed into a set of different resolution image copies that carry significant features of the image appearing at different resolutions. Recently, using coherent optical illumination and spatial filtering, coherent optical linear PIP has been demonstrated [3]. Here, the significant features are at different spatial resolutions of the input image. Using a somewhat different concept, the nonlinear spatial PIP has also been proposed [4]. Instead of spatial resolutions, at different output channels, the sizes and shapes of an input image are identified. In this thesis, an extension of PIP to time domain image processing is proposed. As a simple example, the concept of tracking novelty filter (TNF) [5] is generalized as a means of realizing various temporal image pyramids. Instead of extracting the image's spatial features, its temporal features, such as the speed of a moving target, are extracted. As an optical implementation of the temporal pyramidal filter, inexpensive LCTVs with noncoherent illuminations are used. A combination of such a temporal and various new optical noncoherent spatial PIP techniques may enhance the performance and reliability of a real-time optical target tracking system.

A tracking novelty filter (TNF) compares a present and a stored reference image and displays the image changes [5]. Because a TNF updates the new information from a real-time video scene, its implementation is an active research area. A digital version of a TNF performs a pixel-by-pixel subtraction between a previously stored reference and a periodically updated image. Recently, using a phase-conjugation-based Michelson interferometer,

a coherent optical TNF (COTNF) was proposed [6-8]. With this device, two important features of the phase conjugation effect were used: first, because of the phase-front reversal, the Michelson interferometer performs an image subtraction resulting in a destructive interference [9] at the output, and second, due to the phase-conjugate crystal's finite response time, when the updated image undergoes a sudden change, this change will not immediately be compensated by the phase-conjugator leading to a non-destructive interference at the output. Using a LCTV as a real-time input polarization modulator, the phase-conjugation Michelson interferometer-based COTNF has been experimentally demonstrated [6-7]. It has been indicated that by modifying other existing coherent image subtraction schemes [10-13], various different versions of COTNFs can also be implemented. In the next section, as an alternative approach, a noncoherent optical TNF (NOTNF) implementation is studied and modified for an optical temporal PIP.

### 4.1.2 A LCTV-based Noncoherent TNF

For an ideal TNF operation, a time-domain differentiation of an image is performed. For a sharp time domain input image pixel change, the TNF produces an impulse at the same pixel location. On the other hand, for a stationary image, the TNF's output is a zero (dark) background. Because of the finite visual response and other physical device limitations, an ideal TNF is neither implementable nor useful. A practical TNF performs, instead of differentiation, a time differencing operation. To optically reproduce this time differencing operation, an optical device that performs an optical pixel-by-pixel difference operation on two successive image frames can be used. In this approach, an optical white-light polarization subtraction scheme is used. In order to accomplish a real-time white-light noncoherent image subtraction, two intensity-modulated LCTV SLMs are employed.

A LCTV is a hybrid device that acquires a RF signal from either a TV port or a video camera. A LCTV consists of a layer of LC thin film deposited between two meshed transparent conductive electrodes. The two electrodes are then sandwiched between two cross-polarizers. The LC thin film has the property that when no external voltage is applied, it simply acts as a polarization half-wave retardation plate, rotating its input beam's polarization by $90^0$. With an external voltage, and depending on its value, the induced LC birefringence either advances or retards the output beam's polarization. When a composite LC thin-film between the two cross-polarizers is used, the polarizer forces the input to be linearly polarized while the output polarizer acts as a polarization analyzer. Using this LCTV's SLM property, various coherent image processing and digital computations, such as image addition, subtraction, thresholding, edge enhancement, Fourier transforming, convolution, correlation, matched-filtering, logic and arithmetic operations have been proposed and demonstrated [14-17]. However, because of the poor optical quality of an inexpensive LCTV, the fidelity of an output image is not comparable to that obtainable from a high-resolution optical SLM. To enhance the inexpensive LCTV's image quality, various methods, such as the use of a holographic phase-corrector or a spatial-frequency domain filter etc., were suggested [18-19].

To construct a LCTV-based NOTNF, in this approach, an optical polarization modulation-based image differencing operation is used. Two cascaded but identical LCTVs are utilized. By rotating $90^0$ the second LCTV's analyzer and by removing the analyzer (polarizer) from the first (second) LCTV, in Fig.4.1, a schematic of a polarization-modulated optical image differencing device is sketched. The operational principle of the device is as follows. With a horizontal input polarization and when no signal is applied to either LCTV, the beam's polarization state at the output of the first (second) LCTV is horizontal (vertical). After the beam passes the final, the

vertically-polarized analyzer, the output is a zero. When an electronic signal is applied to both LCTVs, the two corresponding polarization states are both vertical, also leading to a dark output. On the other hand, when a signal is applied to either the first or second LCTV only, the two corresponding polarization states are either vertical-and-horizontal or horizontal-and-horizontal, respectively, leading to a bright output. Such a device has also been proposed as a way to implement a binary EXCLUSIVE-OR logic operation [17].

To modify this optical image differencing operator to a NOTNF, first, instead of a laser beam, a collimated noncoherent white-light beam is used. Since the LCTV's polarization modulation does not require a coherent source (e.g. wrist watch and calculator LCD displays operate with noncoherent light), the advantage of this change is, first, the use of noncoherent light source is more practical, and second, the use of noncoherent source can eliminate the additional coherent speckle noise leading to a better image quality.

For a NOTNF the video camera's output is split into two parts: with one output directly connected to the first LCTV while the there output connected, using a digital imaging board, to the second LCTV. The digital imaging board must possess a feature that, with a memory array, allows a frame of image to be stored and later retrieved. This feature can be realized with either a personal computer (e.g. inexpensive personal computer with a graphic imaging board, such as Commodore 64, is commercially available) or simply a clocked memory array. With a thus connected device, the two LCTVs can always perform an image differencing operation between its two consecutive input frames. Because the reference image is periodically updated, this novelty tracking operation is useful for both tracking moving objects and removing fixed targets that block the radar or video camera's view [6].

### 4.1.3 NOTNF-based Temporal PIP

Before a NOTNF-based temporal PIP is described, the key concept of conventional spatial PIP is reviewed. In a Gaussian PIP, an input image is decomposed into a series of images at different resolution levels. This decomposition can be achieved in two ways. First, using a coherent optical spatial filtering system with a set of spatial low-pass filters, a coherent optical Gaussian spatial PIP can be implemented. Here, each filter has a cut-off frequency $f_{ci}$ a factor of two smaller than its immediate predecessor, i.e. $f_{c_i} = f_{c_{i-1}}/2$. Second, using an incoherent illumination and a lenslet array, an incoherent Gaussian spatial PIP can be realized. Here, over certain neighboring pixels, the lenslet array performs an intensity average operation which is equivalent to the reduction of spatial resolutions.

In a similar way, a temporal image pyramid can be defined. Instead of reducing the spatial resolution, temporal resolution can be reduced. In Fig.4.2, a schematic of the experimental sut up for the temporal image pyramid is shown. The temporal pyramid is useful to identify moving but different speed targets. Specifically, each TNF can filter out objects moving with a particular speed. In this case, not only the background but also all the slower targets disappear. In order to tune the cut-off speed for each TNF, a simple calculation is presented. For an object moving with a speed $v$ and assuming that the TNF reference image is updated every $\Delta t$ seconds, then the object travels a distance $D = v \cdot \Delta t$. For a given demagnification factor $\alpha$ (the ratio between the real object size and its size appearing on LCTV screen), the corresponding traveled distance on LCTV is $d = \alpha D$. When the distance d is smaller than the LCTV's pixel size $d_p$, the moving object will not be shown on the TNF screen. The corresponding cutoff speed is $v_c = \frac{d_p}{\alpha}\Delta t$. To generate a speed pyramid of input image, a set of NOTNFs each of which is tuned

to a cut-off speed $\nu_{c_i} = \nu_{c_{i-1}}/2$, can be employed. The availability of such an inexpensive NOTNF-based temporal PIP device can help in the design of a real-time target tracking system.

### 4.1.4 Experimental Results

To demonstrate the proposed device concept, a real-time NOTNF experiment was first implemented. In Fig.4.3, a schematic of the experimental setup is shown. For the white-light source, a mercury arc lamp was used. After a preliminary focusing (by a parabolic reflector and lens combination), a spatial filtering was performed. The filtered beam was collimated via a 45 cm focal length collimating lens. A pair of commercial Radio Shack black and white LCTVs (Realistic Pocketvision) were used. Using a razor blade, both the front and back linear polarizers of the two LCTVs were carefully removed. To closely attach the two LCTV screens, one of the LCTV screens was turned by $180^0$. The thus attached two screens were then mounted on two x-y translational stages. To sandwich the LCTV screens, two x-y plane rotatable linear polarizers were used. The two polarizers' transmission axes were oriented $\pm 45^0$, respectively. To form a real image on an output ground glass screen, a second 45 cm focal length imaging lens was used. On the other side of the screen, for an output recording, either a still camera or a video camera was used. In the experiment, a video recorder with a prerecorded video tape served as the real-time signal source. To calibrate the device, the video output was split into two parts, with each output connected to a LCTV. Because of the use of a collimated white-light beam, misalignment caused Moire fringes was observed. By adjusting the x and y translation stages, the reduction of these fringes via a fine alignment of two LCTVs was performed. Because of the chromatism of the white-light source, the different temporal

frequency response of the polarizer and LC material results in an unsubtractable blurred image. To reduce the color dispersion, an ORIEL narrow frequency band filter (10 nm wavelength bandwidth at $\lambda = 540$ nm) was used. Finally, by adjusting (through a brightness control knob) the LCTV's electronic bias level, real-time image cancellation was achieved.

After this calibration step, for a real-time NOTNF operation, the connection between the $LCTV_2$ and the video recorder was changed. The recorder's output was first connected to a Video Technology imaging board that is capable to sample, store, and retrieve an image frame. By using different temporal sampling rate (such as storing and retrieving every tenth video frames) a delayed video frame was obtained. The delayed video signal was then connected to $LCTV_2$. With this change, a real-time input is compared to a periodically updated reference image. In other words, in this mode of operation, within each reference update period, the device performs a fixed reference real-time comparison. However, macroscopically, a pseudo-continuous real-time TNF operation is performed. In our experiment, as a reference, a moving airplane prerecorded on a video tape was used. For a clear TNF demonstration, the time interval for updating a reference image was set to ten video frames (330 ms). In Fig.4.4, the corresponding experimental results are shown. To display the NOTNF operation in a complete delay cycle, five images are shown. In the first image (see Fig.4.4a) the obtained result right after the reference image was updated is shown. Because of the use of an identical input, total image cancellation was observed. The next three images (see Figs.4.4b - 4d) show the comparisons between a temporarily fixed reference and a moving object. While the overlapping parts cancel, the nonoverlapping parts are clearly visible. Finally, in the last image, (see Fig.4.4e), a total image cancellation caused by another reference update is shown. This completes a full cycle of a NOTNF operation. Here, although a discrete image sequence is displayed, when the sample and hold time is shorter

(e.g. every second video frame is used as a temporal reference), this visual discontinuity will be removed. It is noted that with the digital imaging board, depending on a different tracking application, the actual delay time is tunable from 30 ms (a single frame) to any longer delay time.

Using the same input image, three levels of its temporal pyramid are generated. The delay times for the three levels were 165, 330, and 495 ms, respectively. In Fig.4.5, the corresponding results are shown.

## 4.2 An Optical Programmable Real-Time Morphological Image Processor

### 4.2.1 Preliminary

The importance of morphological filtering (MF) to image processing has recently been recognized. Among the distinctive features of MF are its noise clean-up, median filtering, skeletonization, edge detection, size and shape extraction capabilities [3-4, 20-21]. The traditional digital electronic MF implementation uses a time-consuming 2D correlation matching operation [20]. Optical implementation of a MF (OMF) has been discussed by several authors [22-24]. O'Neill and Rhodes [23] proposed an incoherent OMF system. This system performs efficient parallel DILATION and erosion operation. However, due to defocusing, the structure element is limited to a small circular shape. A second OMF method, proposed by Goodman and Rhodes [24], uses an optical symbolic substitution-based scheme. Based on this method, recently, Casasent and Botha suggested a new optical architecture [25]. Here, the processor reads a coded input and then generates an OMF output symbol. Another closely related work using a shadow-casting scheme [25-26] has also been applied to image processing. However, before one can use an optical shadow-casting, a time consuming binary intensity to space receding step has to be incorporated. Recently, the use of an OMF has been extended to optical image algebra and to optical pyramidal image processing operations [27-28]. In this thesis, a new programmable real-time parallel OMF device is studied. With this new logic-oriented scheme, optical AND followed by INVERSION logic operations are performed by a lenslet array together with a projection lens, in stead of using either optical encoding or decoding operations.

The two primary morphological operations are image EROSION and DILATION. It can be shown that the DILATION of a binary image X by a given binary structuring element B denoted $\oplus$ is

$$X \oplus B = T_i(X * B), \qquad (4.1)$$

where * denotes an analog correlation and $T_1$ is an unity level threshold operation. On the other hand, the EROSION of X by B denoted $\ominus$ is

$$X \ominus B = T_M(X * B), \qquad (4.2)$$

where M is the number of bright elements in the structuring element B and $T_M$ represents binary threshold operation at level M. For a large M, due to intensity saturation, $T_M$ is difficult to implement. For this reason, the EROSION is performed via a DILATION operation. Thus, Eq.(4.2) can be rewritten as

$$X \ominus B = \overline{T_i(\overline{X} * B)}, \qquad (4.3)$$

where the overbar denotes binary logic INVERSION. Because the advantage of using optics for morphological processing will be overwhelming only for a large B corresponding to a large M which makes threshold operation at level M more difficult, this threshold level down conversion, that avoids the error caused by detector saturation at higher intensity, is important. The DILATION (EROSION) operation expands (shrinks) the image boundary in consonance with the specified structuring element.

Based on these two operations, morphological OPENING and CLOSING operations are defined as

$$X_B = (X \ominus B) \oplus B, \qquad (4.4a)$$

and

$$X_B = (X \oplus B) \ominus B, \qquad (4.4b)$$

respectively. In Fig.4.6 (Fig.4.7), a computer simulation of CLOSING (OPENING) operation via two optical DILATION (EROSION) operation together with optical INVERSION is shown. Both CLOSING and OPENING operations are capable of removing isolated noise elements, such as holes and inlets embedded both inside and outside of an image.

### 4.2.2 Optical Implementation

For the optical implementation of DILATION/EROSION operation, a new real-time optical primary morphological operation processor scheme is proposed. In Fig.4.8, the device schematic is shown. The optical elements, moving from the left to the right, are a spatial light modulator ($SLM_1$), a N X N element lenslet array ($L_1$) with focal length $f_1$, a large projection lens $L_2$ with focal length $f_2$, a second SLM ($SLM_2$), an analyzer (A), a ground glass screen (G), and a video camera. Starting from the left-hand side, a collimated light beam illuminates the device. The distance between lenses $L_1$ and $L_2$ is $f_1 + f_2$. The lenslet array converts the collimated input light beam into an array of delta functions. When the thus converted beam passes through $L_2$ and $SLM_2$, in the plane G, an intensity summation of different angularly projected uniform beams generates the correlation of the corresponding delta function array with the binary image X that is displayed on the $SLM_2$. It should be pointed out that a similar correlator has been used to perform optical shadow-casting logic operations [25-30]. To obtain this correlation, the combination of $SLM_1$and the lenslet array can also be replaced by a LED array. However, in terms of approximating a delta function, illumination

uniformity and divergence angle, all of which affect the quality of the correlation, the lenslet array scheme promises the best results. This analog correlation is needed for both morphological operations. Take the DILATION operation represented by Eq.4.1 as an example. For a centered N X N sample space for a binary structuring element, $SLM_2$ is programmed to switch on/off the apertures of the corresponding $L_1$ lenslet elements so that at the focal plane of $L_1$, the proper 2-D array of delta functions is formed. After the light beam passes through $L_2$, it contains different directional plane-waves ready to be incident on the image plane. At the output (G) plane, the projections of these beams represent an analog correlation of X with B, where

$$B(x,y) = \sum_{ij=-\frac{N}{2}}^{\frac{N}{2}} b_{ij}\delta(x - i\Delta, y - j\Delta) \qquad (4.5)$$

and

$$\Delta = \frac{dD_i}{f_2}, \qquad (4.6)$$

with $b_{ij}$ = 0, 1 and $D_1$ and d the diameter of the $L_1$ elemental aperture and the distance between $SLM_2$ and G, respectively. While the delta function spacing is $\Delta$, its correlation effect at the output screen depends also on d. For a fixed angular spacing, the larger the d the longer the spatial shift $\Delta$. This analog correlation forms an analog version of the dilated image. For a digital DILATION output, this analog output is thresholded at unity intensity level.

There are two input binary image encoding schemes: intensity levels or orthogonal polarization states. For an intensity-coded image, $SLM_2$ can be a

LCTV, while for a polarization encoded image, a LCTV without its back polarizer is needed. The polarization-encoding scheme offers the flexibility of adjusting the output contrast. Because a polarization-encoded image carries orthogonally polarized information, to extract the dilated image, an analyzer (A) is needed.

To perform an EROSION operation (see Eq.4.3), the input image needs to be inverted. After this step, the previous DILATION process is used resulting in an inverted eroded image. When a bright-true intensity-coded output is required, an additional image inversion, that can be performed either by an electronic logic gate array or by a second optical SLM, is needed.

For a device implementation, a number of technical problems need to be addressed. First, for a uniform and accurate threshold process, a uniform input illumination is needed. Since the off-axis lenslets introduce vignetting, the size of $L_1$ must be limited. For the given $f_1$, $f_2$, $D_1$ and $D'_2$, where $D'_2$ is the effective $SLM_2$ aperture, to reduce vignetting, in each dimension, the acceptable number of lenslet elements is

$$N \leq 1 + \frac{f_2}{f_1} - \frac{D'_2}{D_1}. \qquad (4.7)$$

For a large N, not only a large $f_2/f_1$ ratio is needed, but also the acceptable image size should be adjusted so that $D'_2/D_1 < f_2/f_1$ where $D_2$ is the diameter of $L_2$, to prevent a possible vignetting effect. In addition, for a required signal-to-noise ratio and an intensity threshold $T_1$, a minimum detectable output intensity $I_o$ must be guaranteed. This $I_o$ requires that the minimum input intensity illumination be

$$I_i = I_o\left(\frac{D_2}{D_1}\right)^2 \frac{1}{\alpha_L \alpha_A \alpha_{SLM_2}}, \qquad (4.8)$$

where $\alpha_L$, $\alpha_{SLM}$ and $\alpha_A$ are the transmissive loss coefficients of lens system, SLM and analyzer, respectively.

In Fig.4.9, an efficient real-time optical morphological image processor is shown. Combining of two identical optical primary morphological processors together with an optically addressable reflective SLM, both DILATION and INVERSION operations can be optically performed.

### 4.2.3 Experimental Results

To confirm the proposed concept, a proof-of-principle experiment was performed. As the input source, a noncoherent white light beam obtained from a slide projector was used. A custom-tailored 3 X 3 lenslet array with $D_1$ = 0.7 cm and $f_1$ = 2.5 cm was used. A projection lens $L_2$ with $f_2$ = 32 cm and $D_2$ = 12 cm was employed. The linear effective aperture $D'_2$ of $SLM_2$ (Radio Shack Pocketvision) was 4.5 cm. The spacing between the LCTV image encoder and the ground glass G was 4.5 cm. The analyzer located between LCTV and G was oriented so as to filter out the encoded background polarization. The input image (see Fig.4.10a) was recorded by a TV camera and displayed on the LCTV. This image contains two rectangular objects, and some noise elements, such as square holes and inlets. In the polarization encoding scheme, the objects and background were polarized vertically and horizontally. Similarly, the holes and inlets were also polarized horizontally and vertically, respectively. The size of the noise elements ranged approximately from 1.0 mm X 1.0 mm to 2.0 mm X 2.0 mm. To record Fig.4.10a, only the center lenslet was allowed to open. Next, a morphological CLOSING

operation was implemented. First, using two different structuring elements, two different DILATION operations were performed. In Figs.4.10(b) and 10(c), the DILATION results corresponding to the structuring elements $B_1$ (with the four upper right-hand corner lenslet elements open) and $B_2$ (with the four lenslet elements at the four corners of the array open) are shown. As expected, while the holes were removed, the objects and inlet noise were magnified. To remove the expanded inlet noise, an EROSION operation on image (see Fig.4.10c) with an area twice the size of the structuring element is needed. In our experiment, instead of increasing the size of the lenslet array, for an identical operation the image-to-ground-glass spacing (d = 9 cm) was doubled. Here, an inverted image from Fig.4.10c (see Fig.4.10d) was inserted into the image plane. In Figs.4.10e and 10f, using the two previous structuring elements $B_1$ and $B_2$, the corresponding results are shown. In Fig.4.10f, all the inlet elements were completely removed. Finally, in Fig.4.10g, the inverted and thresholded result of Fig.4.10f is shown. As expected, because of the use of a square structuring element for a rectangularly shaped object, no boundary distortion was observed.

## 4.3 Summary and Conclusion

In this chapter, two logic-oriented optical signal processors are presented. Based on optical EXCLUSIVE-OR logic operation, a white light optical pyramidal tracking novelty filter is implemented and experimental results are also presented. An optical programmable real-time morphological image processor based on optical AND followed by INVERSION logic operations is also presented together with experimental results.

To summarize, an optical temporal PIP technique has been proposed. A hybrid NOTNF which is a key element of the optical temporal PIP has been described. Using a white-light optical source, two inexpensive LCTVs, and a digital electronic delay system, the proposed NOTNF device was experimentally demonstrated. The unique features of the device have been studied. Because the proposed device uses noncoherent illumination and is tunable in real-time, it is suitable for an optical temporal PIP. A combination of the temporal and the various spatial image pyramids can help in the design of a future white light optical tracking and target recognition system for the various military and industrial applications.

Because of the use of commercially available inexpensive LCTVs, the image resolution was low. Also, because of nonuniform bias caused by both the LCTV's manufacturing process and our imperfect disassembly, it was difficult to obtain an uniform full-screen intensity cancellation. For a better LCTV-based NOTNF result, a high-quality directly-assembled two-layer LC composite structure is necessary. Although in our approach, for the time-delay a personal computer was used, it is possible to use a simplified device that contains a self-standing image digitizer, an A/D converter and a memory array. It is also possible to avoid the use of any digital system. As its possible replacement, a modified video recorder, where a recording head placed in front of a playing head is installed, can be utilized. In this case, the spacing between the two heads

determines the delay time.

In our experiment, for the preparation of the white-light source both a temporal and a spatial frequency filters were used. To lower the source requirement, an extended white-light source masked by a ground glass can also be used. In this case, to keep a one-to-one pixel relation between the two LCTVs, the two LCTVs must be separated into two planes, with one imaged onto another.

It is noted that this LCTV-based NOTNF can also be modified to perform other real-time image time domain processing. For example, when the output analyzer is rotated by $90^0$, instead of real-time differencing, the complement of differencing operation will be performed. Correspondingly, instead of the moving, the stationary part of the input is displayed. By cascading two LCTV-based NOTNFs, it is also possible to obtain a second order time-domain differencing operations. In this case, edges of a time-domain moving object will be extracted.

In comparison to the existing COTNF, the distinctive features of the new NOTNF can be summarized as follows: (1) because of using the LCTV polarization modulation, this NOTNF does not require a coherent source, (2) the NOTNF does not require vibration isolation that is necessary for many coherent processing systems, (3) unlike the phase-conjugation-based OTNF where the use of optical third-order nonlinearity requires a large optical power density, the NOTNF uses a LC material that demands a much lower optical power density is needed, and (4) unlike the phase-conjugation-based OTNF where with a particular nonlinear material, the reference signal time delay is fixed, the new NOTNF uses an electronically tunable time delay which is necessary for an optical temporal PIP. For the various military and industrial real-time tracking and target recognition applications, the proposed NOTNF-based optical temporal pyramid can be used in conjunction with the various optical noncoherent spatial image pyramids.

In case of new optical morphological processor, new efficient optical

morphological algorithm is introduced. In stead of performing CLOSING operation via a DILATION followed by a EROSION operation, optical DILATION-INVERSION-DILATION operations can performed CLOSING operation more efficiently on any size and shape of the structuring elements. Using optically addressed reflective SLM, the optical INVERSION logic operation is implemented.

Now, a comparison of this new OMF technique with other existing (both electronic and optical) MF approaches is given. First, to implement a parallel electronic MF, a mesh-type cellular array is required. In this case, wires are needed for the local interconnection among all the processing elements. For example, for a pixel to interconnect with its immediate neighbors for a N X N image, wires required for the local interconnect are

$$M_4 = 2(N-1), \qquad (4.9a)$$

$$M_8 = 2(2N-1)(N-1), \qquad (4.9b)$$

where the subscripts 4 (8) represents 4 (8) immediate neighbors. For a high resolution (N = 1024) image, more than four million wires are needed. When higher-order neighbors are connected, even more wires are necessary. On the other hand, for the proposed new OMF approach, these electronic interconnect wires are replaced by the 3D free-space propagation channels. To compare the new scheme to other OMF approaches, it is noted that in terms of the illumination coherence requirement, the new scheme is identical to the approach proposed in Ref.28, i.e. both coherent and noncoherent light beams can be used. As the number of optical elements comparison, the new scheme is a little more complex than the device of Ref.28 because of its trade for programmability. However, this device is more compact. While both devices possess the same lateral dimension

(i.e. the lens aperture D2) in the longitudinal dimension, to form an image, the device in Ref.28 uses a $4f_2$ the new scheme uses only $f_1 + f_2 + d$ as its longitudinal length. An added advantage of this scheme is its programming flexibility. While the previous approaches use a fixed isotropic structuring element, this new scheme allows any desirable structuring elements with size limited to the one specified by Eq.(4.7).

## 4.4 References


[1] P. J. Burt, "The pyramid as a structure for efficient computation," in *Multiresolution Image Processing and Analysis*, A. Rosenfeld, ed. (Springer-Verlag, Berlin, 1984) Ch. 2.

[2] Kou-Hu Tzou, "Progressive image transmission: a review and comparison of techniques," Opt. Eng. 26, 581 (1987).

[3] G. Eichmann, A. Kostrzewski, B. Ha, and Y. Li, "Parallel optical pyramidal image processing," Opt. Lett. 13, 431 (1988).

[4] C. Lu, G. Eichmann, J. Zhu, and Y. Li, "Pyramidal image processing using mathematical morphology," Proc. SPIE, 974, 30 (1988).

[5] T. Kohonen, *Self-Organization and Associative Memory* (Springer-Verlag, New York, 1984) Ch.4.

[6] D. Z. Anderson, D. M. Lininger, and J. Feinberg, "Optical tracking novelty filter," Opt. Lett. 12, 123 (1987).

[7] J. E. Ford, Y. Fainman and S. H. Lee, "Time integrating interferometry using photorefractive fanout," Opt. Lett. 13, 856 (1988).

[8] N. A. Vainos, "Real-time optical Winer-Kolmogorov and novelty filtering with phase conjugation," Opt. Lett. 14, 128 (1989).

[9] J. Feinberg, "Interferometer with a self-pumped phase conjugation mirror," Opt. Lett. 8, 569 (1983).

[10] S. R. Dashiell, A. W. Lohmann, and J. D. Michaelson, "Real-time coherent optical-electronic image subtraction," Opt. Comm. 8, 105 (1973).

[11] D. Zhao, and H.-K. Liu, "Real-time optical interferometric image subtraction by wave polarization," Appl. Opt. 21, 3864 (1982).

[12] S. Kwong, G. A. Rakuljic, and A. Yariv, "Real-time image subtraction and "exclusive or" operation using a self-pumped phase conjugation mirror," Appl. Phys. Lett. 48, 201 (1986).

[13] A. E. Chiou and P. Yeh, "Parallel image subtraction using a phase-conjugation Michelson interferometer," Opt. Lett. 11, 306 (1986).

[14] H. K. Liu, J. A. Davis, and R. A. Lilly, "Optical data processing properties of a liquid-crystal TV spatial light modulator," Opt. Lett. 10, 635 (1985).

[15] K. D. Hughes, S. K. Rogers, J. P. Mills, and M. Kabrisky, "Optical pre-processing using liquid crystal televisions," Appl. Opt. 26, 1042 (1987).

[16] F. Mok, J. Diep, H.-K. Liu, and D. Psaltis, "Real-time computer-generated hologram by means of liquid-crystal television spatial light modulator," Opt. Lett. 11, 748 (1986).

[17] F. T. S. Yu, S. Jutamulia, and D. A. Gregory, "Optical parallel logic gates using inexpensive liquid-crystal televisions," Opt. Lett. 12, 1050 (1987).

[18] M. Young, "Low-cost LCD video display for optical processing," Appl. Opt. 25, 1024 (1986).

[19] D. Casasent and S. F. Xia, "Phase correction of light modulators," Opt. Lett. 11, 398 (1986).

[20] J. Serra, *Image Analysis and Mathematical Morphology*, (Academic, New York, 1982).

[21] R. M. Haralik, S. R. Sternberg, and X. Zhuang, "Morphological Skeleton Representation and Coding of Binary Images," IEEE Trans. Acoust. Speech Signal Process. ASSP-34, 1228 (1986).

[22] P. Maragos, Opt. Eng. 26, 623 (1987).

[23] K. S. O'Neill and W. T. Rhodes, Proc. Soc. Photo-Opt. Instrum. Eng. 638, 41 (1986).

[24] S. D. Goodman and W. T. Rhodes, "Symbolic Substitution Applications to Image Processing," Appl. Opt. 27, 1708 (1988).

[25] D. Casasent and E. Botha, "Optical Symbolic Substitution for Morphological Transformations," Appl. Opt. 27, 3806 (1988).

[26] Y. Ichioka and J. Tanida, "Optical Parallel Logic Gates using A Shadow-Casting System for Optical Digital Computing," IEEE Proc. 72, 787 (1984).

[27] J. Tanida and Y. Ichioka, "Programming of Optical Array Logic 1: Image Data Processing," Appl. Opt. 27, 2926-2930 (1988).

[28] K. S. Huang, B. K. Jenkins, and A. A. Sawchuk, Proc. IEEE Computer Society Workshop on Computer Architecture for Pattern Analysis and Machine Intelligence, Seattle, Washington, Oct. (1987).

[29] G. Eichmann, C. Lu, J. Zhu, and Y. Li, "Pyramidal Image Processing Using Mathematical Morphology," Proc. Soc. Photo-Opt. Instrum. 974, (1988).

[30] J. S. Jang, S. Y. Shin, and S. Y. Lee, "Adaptive Two-Dimentional Quadratic Associative Memory Using Holographic Lenslet Arrays," in Technical Digest, Topical Meeting on Optical Computing (Optical Society of America, Washington, DC, 1989), pp. 40-43.

[31] M. M. Mirsalehi, T. K. Gaylord, D. C. Fielder and C. C. Guest, "number Representation Effects in Truth-Table Look-Up Processing: 8-Bit Addition Example," Appl. Opt. 28, 1931-1939 (1989).

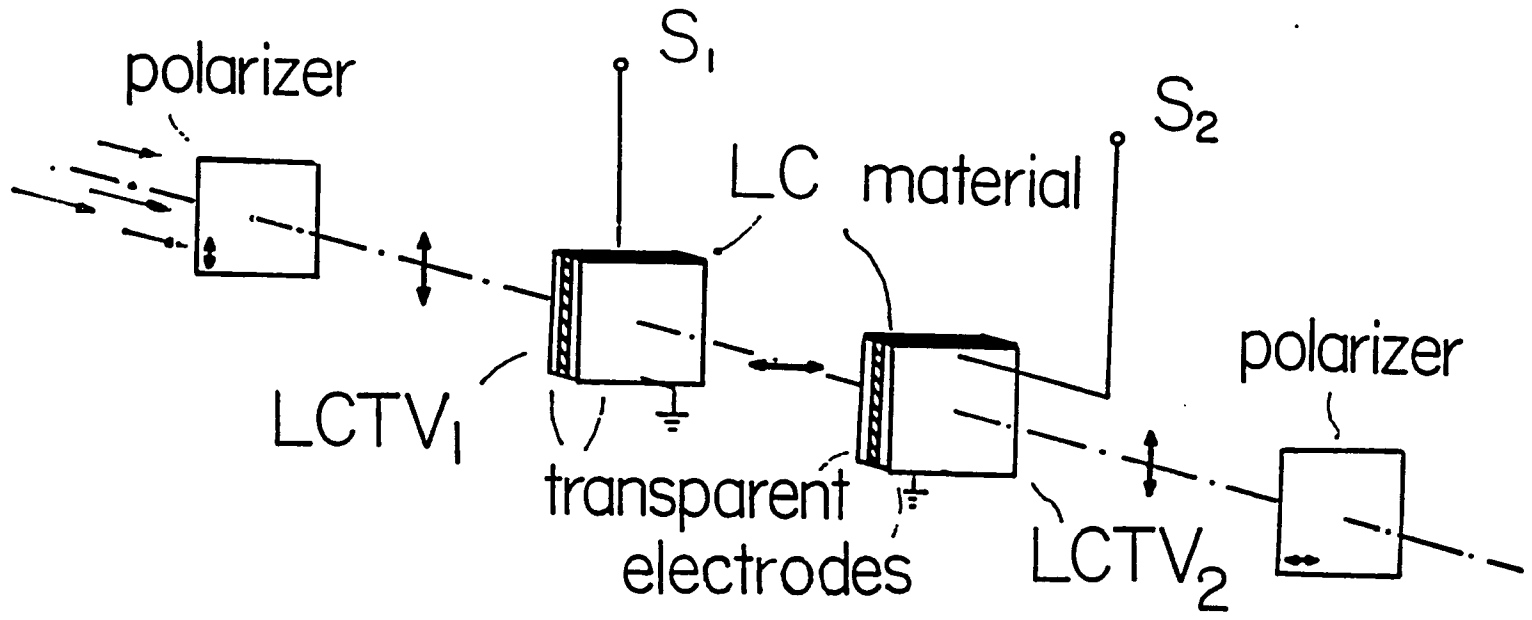


Fig.4.1 Schematic of a LCTV-based real-time image temporal differencing device. Two LCTVs, with their front and back polarizers removed, sandwiched between two cross polarizers, are used. For a real-time differencing operation, at the two LCTV's RF input ports, video signal $S_1$ and its delayed version $S_2$ are applied.

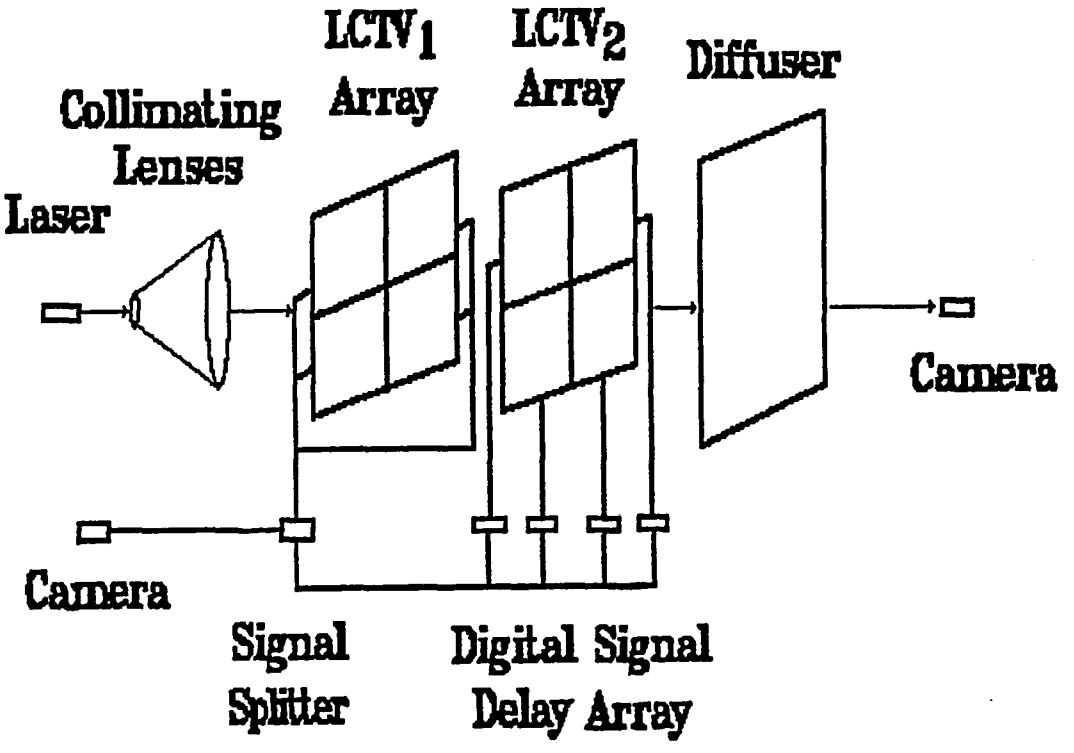


Fig.4.2 Schematic of a LCTV-based temporal pyramidal TNF.

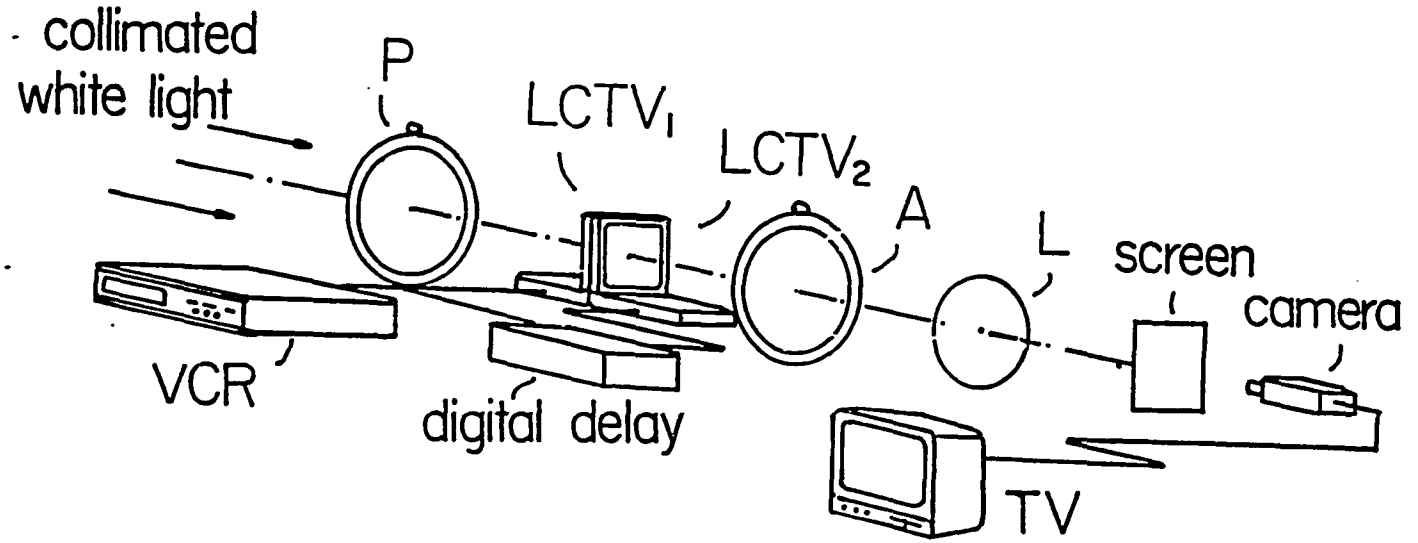


Fig.4.3 Schematic of an experimental white-light tracking novelty filter (NOTNF) system. In addition to a collimated white-light optical source, two LCTVs, a polarizer (P), and an analyzer (A), an imaging lens (L) that transmits the result to an output screen to be monitored by a video camera is used. The real-time signal from a video recorder (VCR) is split into two parts: with one signal directly connected to $LCTV_1$ and the other signal passed through a digital delay device (implemented by a digital imaging board) to $LCTV_2$.

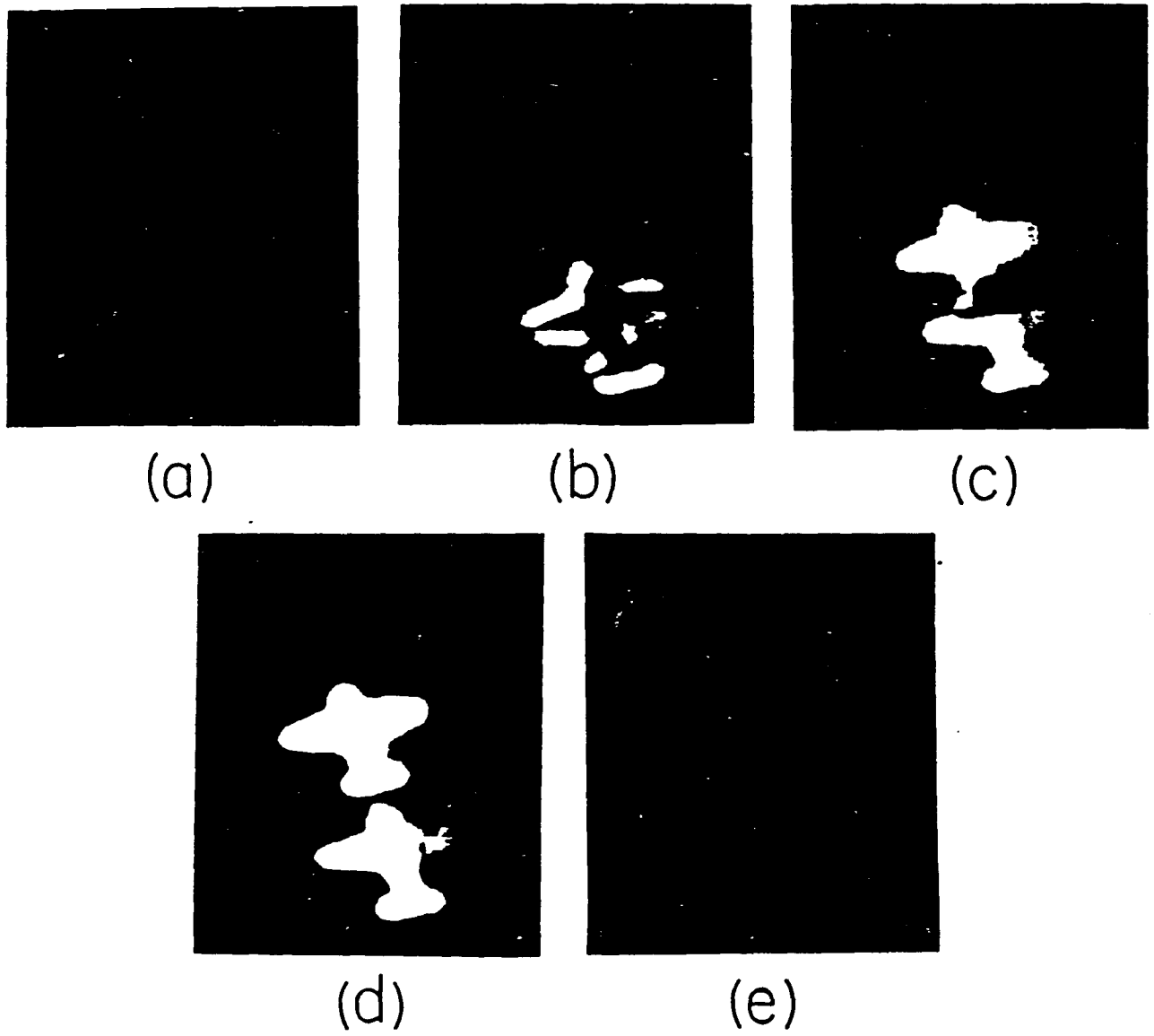


Fig.4.4 The real-time NOTNF experimental results. A moving air plane, recorded by a video camera, serves as a real-time video input. The reference image was updated at every 330 ms (equivalent to ten video frames). Five images generated within the reference update period are shown: (a) the scene obtained right after the reference image was updated; (b)-(d) three different scenes showing the subtraction between a temporarily fixed reference and a real-time image, and (e) the scene obtained right after a new reference image update.

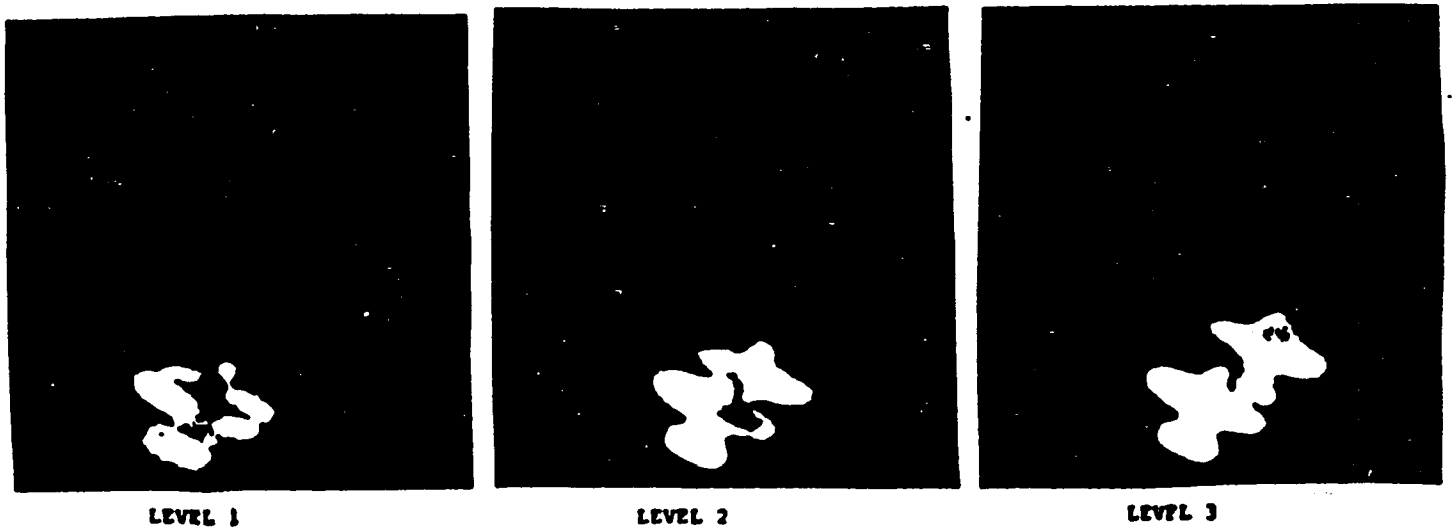


Fig.4.5 Experimental results of a three level temporal pyramid.

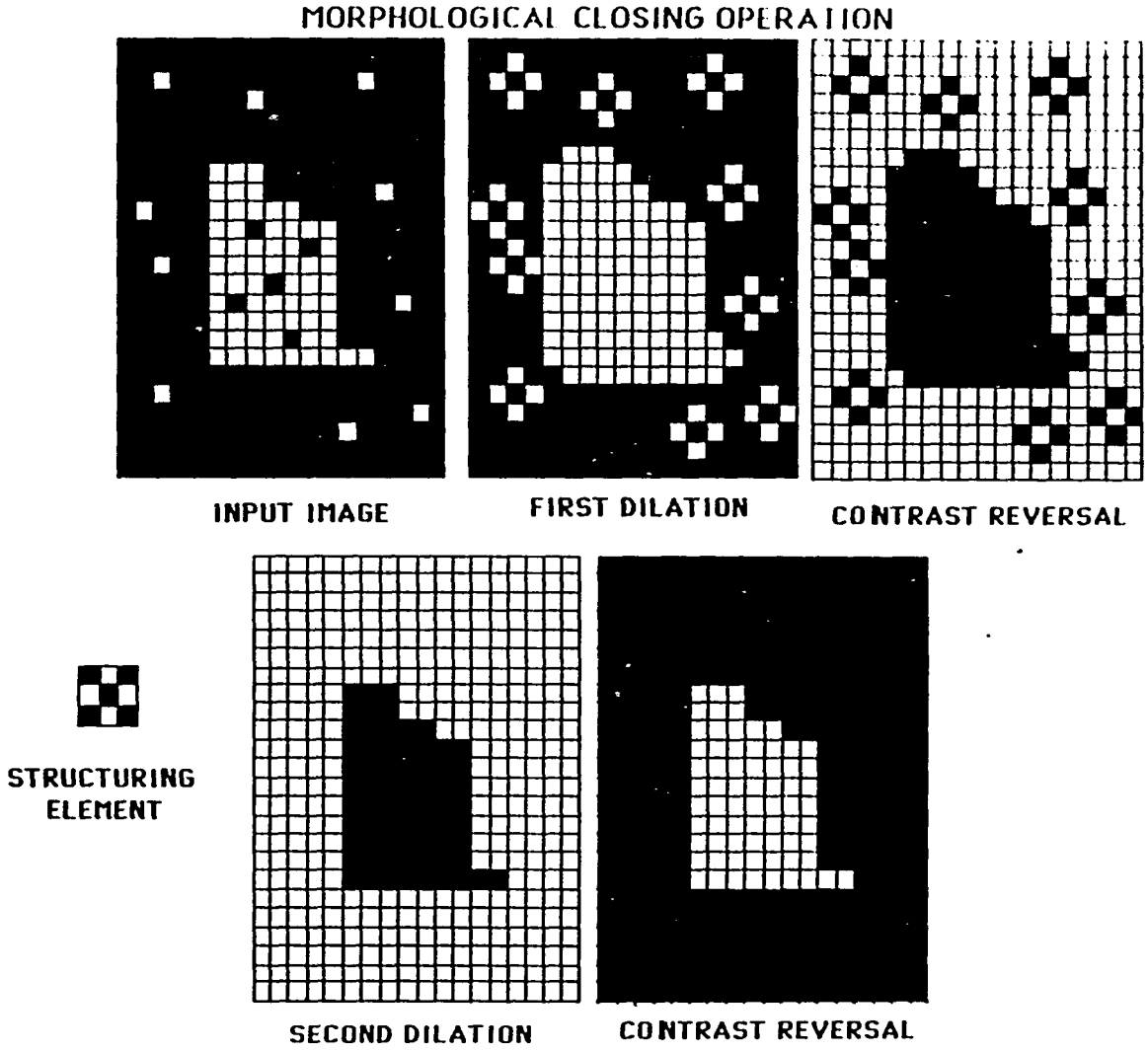


Fig.4.6 Computer simulation of a morphological CLOSING operation via an optical DILATION followed by inversion operation.

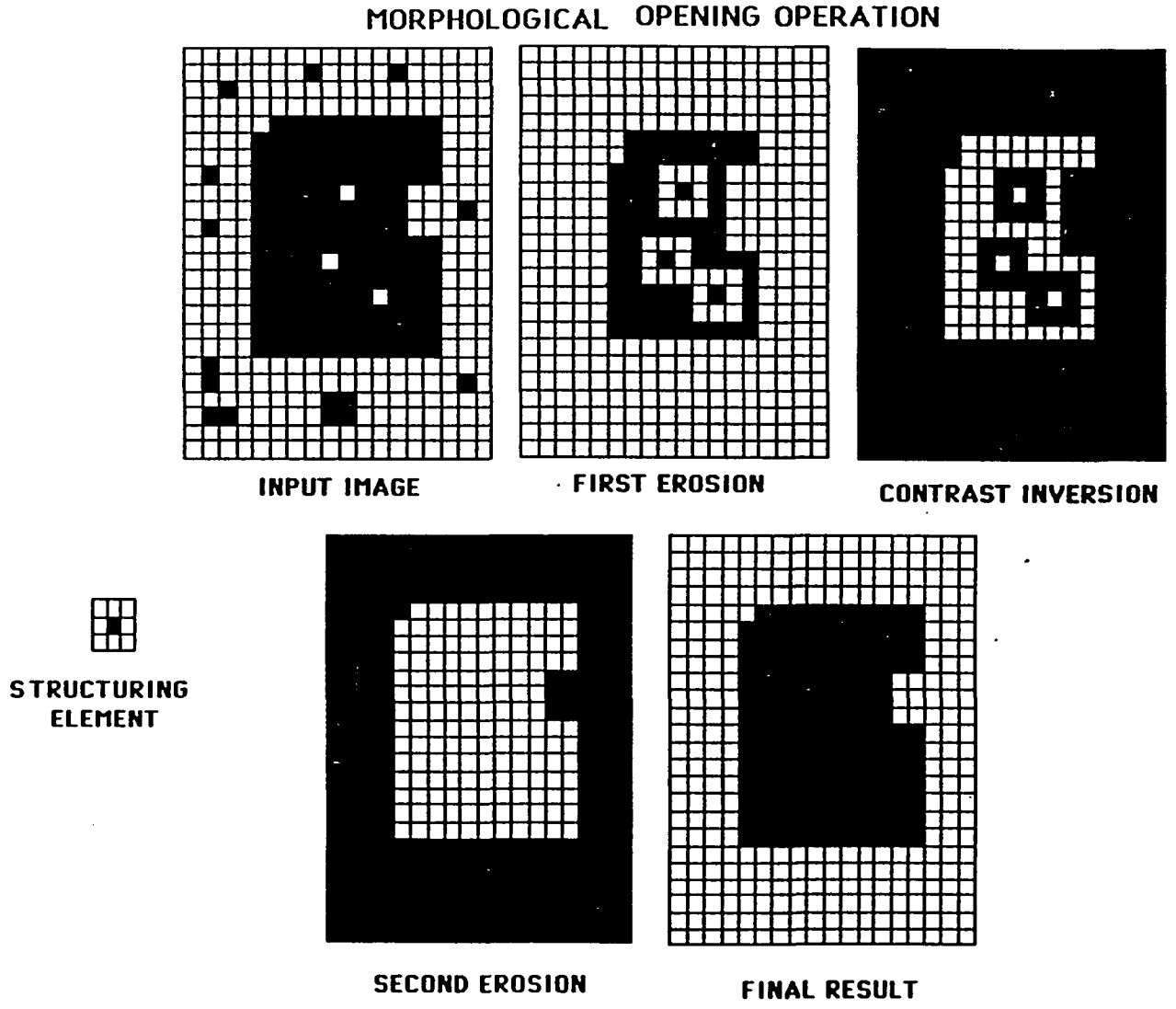


Fig.4.7 Computer simulation of a morphological OPENING operation via an optical EROSION followed by inversion operation.

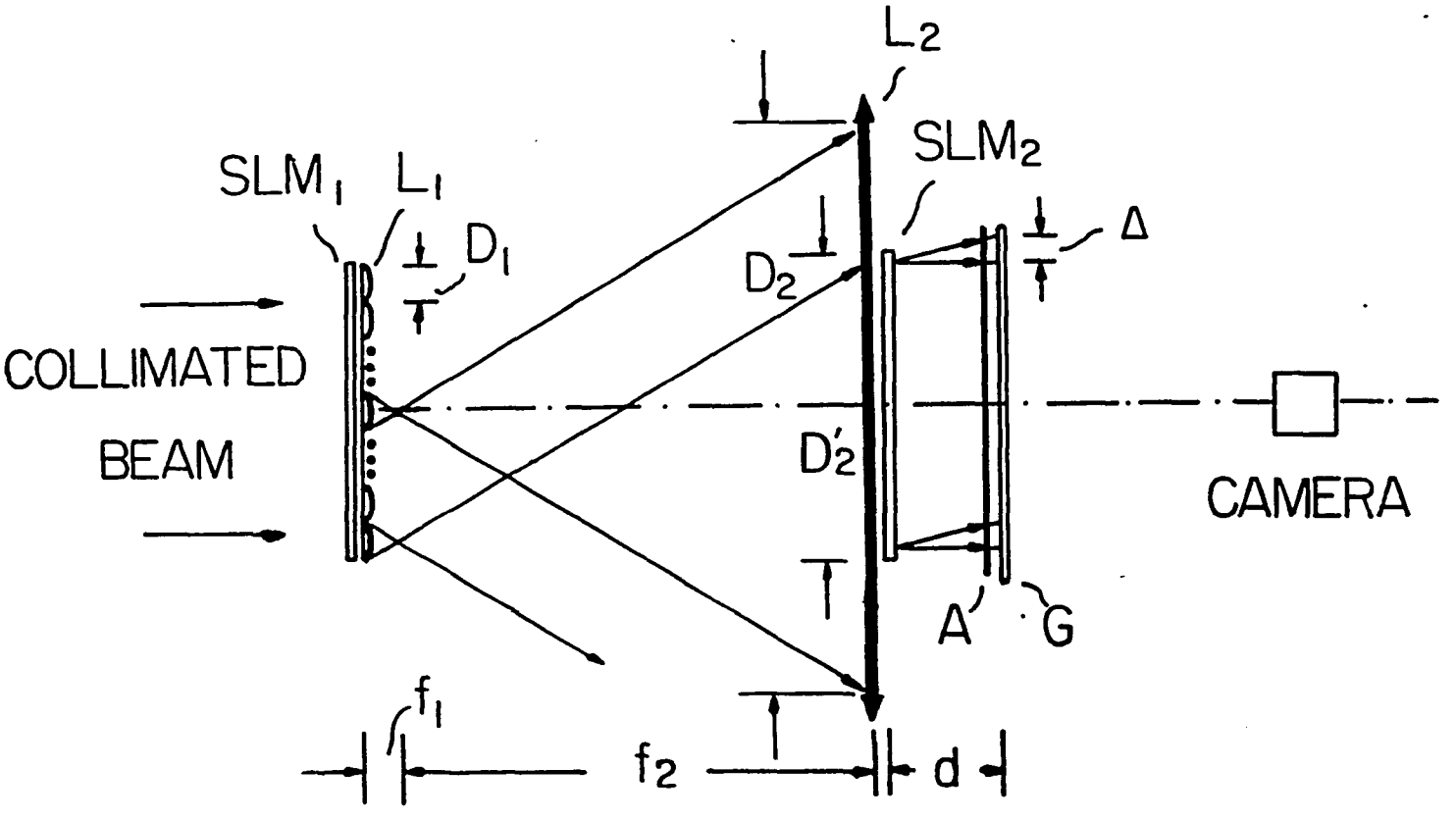


Fig.4.8 Schematic of a programmable optical parallel primary morphological operation processor. SLM, spatial light modulator; $L_1$, 2D lenslet array; $L_2$, projection lens; A, polarization analyzer; and G, ground glass screen. The $SLM_1$ is programmed to select $L_1$ lenslet elements which serve the role of a structuring element for a morphological operation. The selected $L_1$ elements together with $L_2$ convert the collimated input beam to the various angular projections to be incident on the image (displayed on $SLM_2$) to be morphologically processed. The overall projections on G represent an analog version of morphological DILATION result. For a digital morphological DILATION, this analog output is threshold by the video camera (placed after G). When a polarization encoded image is used, an analyzer A is employed. For an erosion operation, an inverted image is created on $SLM_2$. After an identical DILATION operation, an additional image inversion is also required.

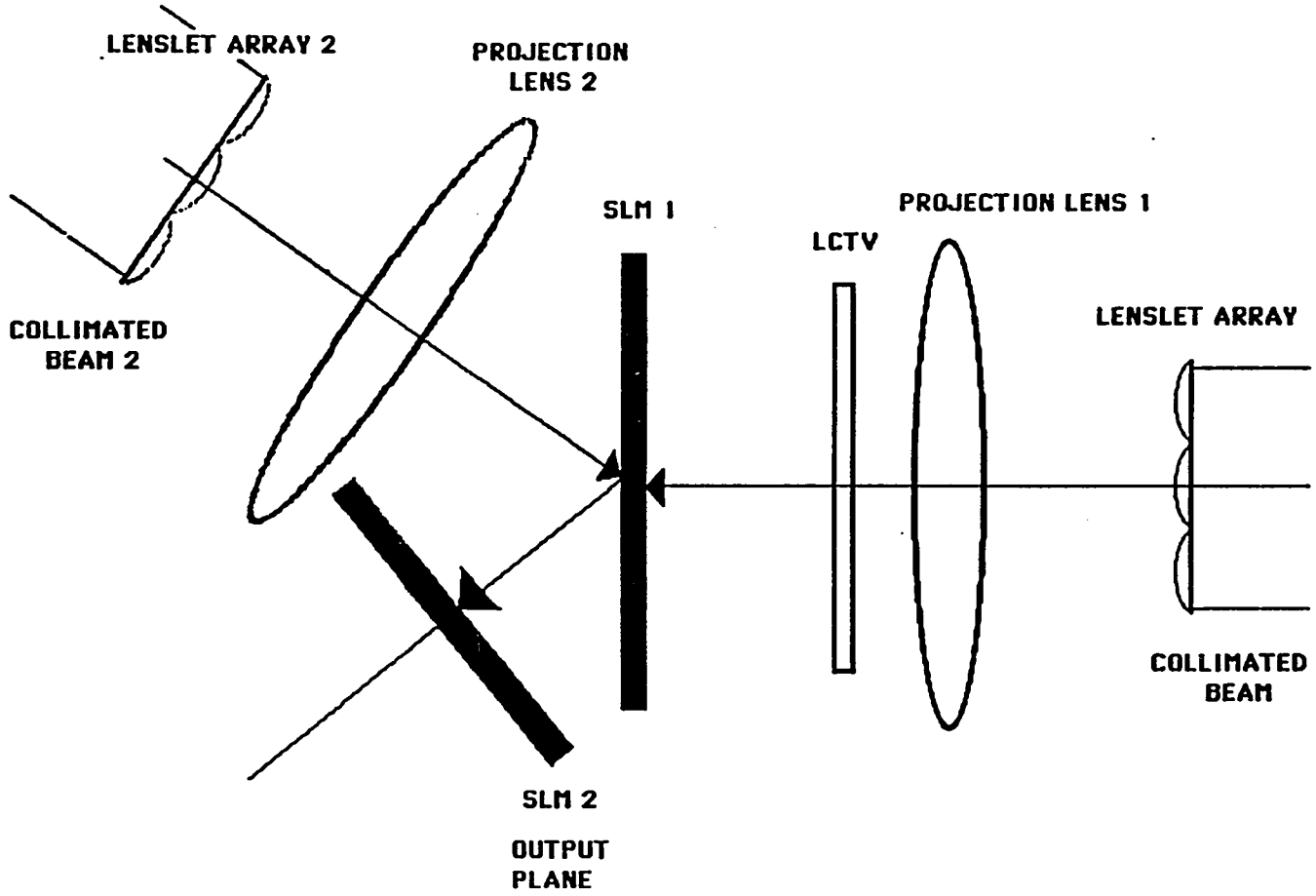


Fig.4.9 Schematic of the real-time optical morphological processor.

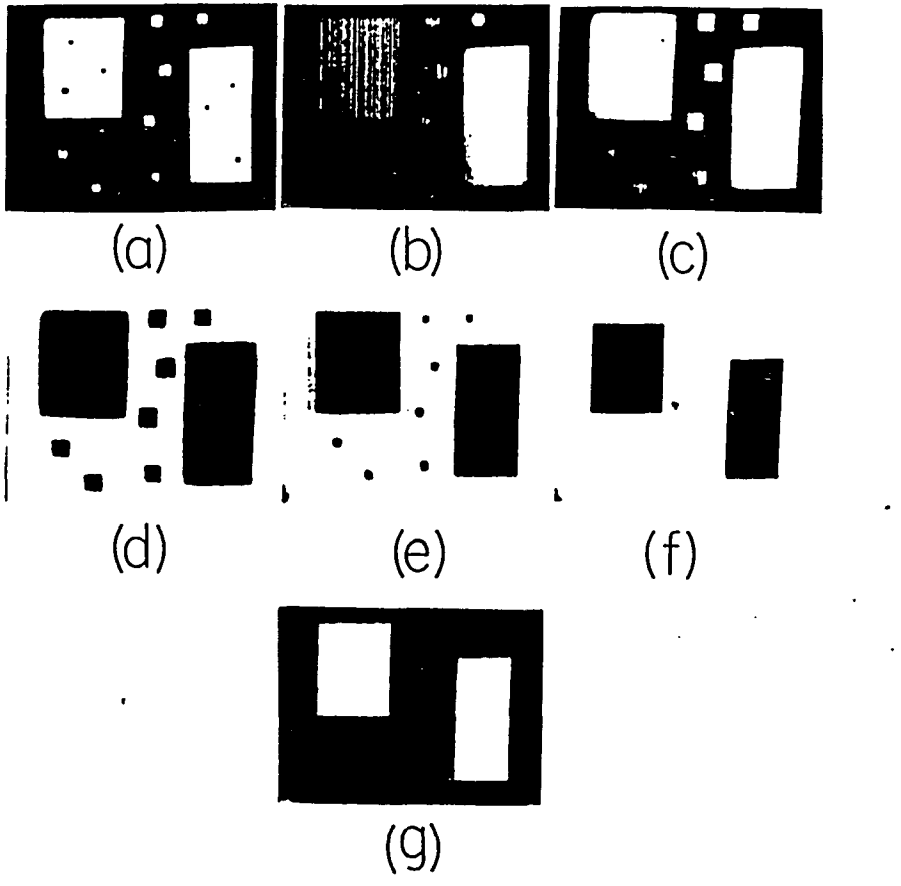


Fig.4.10 Real-time experimental result of the optical pyramidal CLOSING operation. (a) the input image with two bright objects together with hole and inlet noise elements. (b) and (c), the results of dilation using two different structuring elements. In (c) the holes are completely removed. (d) the contrast reversal of (c) as performed by a LCTV. (e) and (f) the two DILATION results of (e). (g) the final morphological CLOSING result of (a) using a contrast reversal of (f).

# V MEMORY-ORIENTED OPTICAL SIGNAL PROCESSOR

In case of optical signal processing, an alternative to a logic-oriented approach is the use of memory based schemes. In this case, all possible inputs and their outputs are precalculated, tabulated, and codified as a truth-table. In this chapter, using two types of optical memory such as content-addressable memory (CAM) and associative memory (AM), two memory-oriented optical signal processors are studied.

To perform an optical parallel arithmetic operation, the use of a modified-signed digit (MSD) number system, because of its weak inter-digit dependence [1], has been suggested. Unlike the three-stage MSD logic based implementations [2-4], CAM based approaches [5-7] that precalculate and store the processing results are yielding speed efficiency. However, the present holographic optical CAM approach suffers from its difficulty of alignment and inconvenient recording problems. The purpose of this chapter is to propose a new, simple and compact optical CAM architecture for an efficient optical MSD arithmetic processing. Compared to the existing optical MSD approaches, this architecture offers a number of practical advantages, such as faster processing speed, ease of implementation and alignment, and a better functional distribution of its optical and electronic processing elements.

Because of the signal retrieving and error correcting capabilities with incomplete or imperfect input information [8], AM has been applied for optical signal processing. In this chapter, an optical parallel register transfer processor based on a holographic AM is presented. To utilize the signal retrieving and error correcting capabilities of AM, input and output pairs are recorded on holographic materials during the recording stage. In the reading stage, the prerecored holographic AM is illuminated by only the input as a reference beam, then the output is retrieved.

## 5.1 A CAM-Based Single-Stage Optical MSD Processor

### 5.1.1 Preliminary

In this section, a non-holographic CAM-based MSD processor is studied. Using a CAM, a number of practical advantages, such as fast processing speed and ease of implementation, relatively simple architecture of multi-channel scheme, and less stored information using logic reduction scheme. For a single-stage parallel MSD addition operation, it has been shown [5] that each output digit $s_i$ is a function of six trinary input digits ($x_{i+1}$, $y_{i+1}$, $x_i$, $y_i$, $x_{i-1}$, and $y_{i-1}$). Using standard logic reduction schemes and don't care bit assignments, the overall $3^6 = 729$ logic minterms can be reduced to 56 reference product terms. To generate the 1 and $\bar{1}$ outputs, each 28 reference terms are needed, and when neither a 1 nor $\bar{1}$ is obtained, it presents a result 0. To memorize optically the 56 six-variable reference patterns, an optical either associative memory (AM) [9] or CAM [10] can be used. The main difference between an AM and a CAM is that while the former is designed to be able to cope with incomplete or imperfect input information the latter is designed to deal with complete knowledge of its input.

### 5.1.2 Optical Implementation

To illustrate the new optical non-holographic CAM write and readout procedures, a single six-variable reference pattern example is given (see Fig.5.1). Here, a reduced six-variable reference pattern ($d_{\bar{1}}$ 1 d 0 1 $d_{10}$), where d and $d_{xx}$ denote a total and partial don't care digits, is used. To write into this CAM, after a three-channel bit-wise position encoding, a 6 X 3 = 18 pixel CAM mask is designed so as to block the transmission of all possible light appearance position combinations. For a CAM readout, any input digit

combination corresponding to a stored reference pattern will generate, at the cylindrical lens back focal plane, a dark output. The thus detected "zero" intensity is thresholded and electronically inverted. On the other hand, input combinations that do not match the coded reference pattern will produce some residue light which after a logic inversion yields a zero signal indicating a pattern mismatch. Using this scheme, all the 56 reference patterns can be encoded as a 56 X 18 pixel mask array serving as the MSD CAM for the generation of a 1-bit MSD addition result (see Fig.5.1(b)).

For an N-bit parallel MSD addition, a straightforward extension of the Fig.5.1(b) device may lead to an unacceptably large space-bandwidth product. To minimize the size of the CAM MSD system, an angular multiplexing scheme that uses a 56 X 18 pixel CAM MSD addition mask and N+1 angularly multiplexed input patterns is employed (see Fig.5.2). Each of the N+1 six-digit 1-D input devices (SLMs) is connected to six electronic input ports where the dotted line indicates a constant zero input. Past the array of input SLM, a 1-D prism wedge array is placed. Each wedge element deflects its output to a common but shared CAM MSD mask. The matching results are spatially integrated by a single cylindrical lens positioned immediately past the mask. At the lens back focal plane, the integrated results are displayed as N+1 vertically displaced horizontal channels. At this plane 56(N+1) electronic threshold logic inverters are located. These results are connected to a device that outputs N+1 bit MSD summation results where each output bit is represented by three position coded MSD channels. While, in principle, the number of bits N can be large, but due to diffraction and lens off-axis aberration-induced angular resolution limits, this number is limited. For example, assuming that the spatial width of each input channel to be l =100 $\mu m$, to perform a two 32-bit MSD (equivalent to 32-bit signed binary) number

addition, a lens with an effective aperture $D_{eff} > 18 \times 33 \times 1 = 6$ cm must be used. Also, for a large N, to reduce the diffraction loss, an imaging lens linking the input and the mask should be used.

### 5.1.3 Experimental Results

Some proof-of-principle experiments were performed. First, a 6.4 cm X 1.8 cm CAM mask (see Fig.5.3a) that contains two 28 X 18 pixel sub-masks (one for an output 1 and the other for $\bar{1}$) was made photographically through a Hughes LCLV illuminated by an $Ar^+$ Ion laser. The same SLM was then used to project a 6-digit MSD input bar array onto the mask. The output signal was spatially integrated by an f = 7.5 cm cylindrical lens. For the final electronic thresholding and logic inversion, the integrated intensity was recorded by a digital computer linked video camera. This CAM system was tested by three groups of six digit inputs, e.g. 111111, 01001$\bar{1}$, and 1010$\bar{1}$1 (see Figs.5.3b, 3e and 3h for their encoded inputs). For the input of Fig.5.3b, in the top and bottom parts of Fig.5.3c and 3d, for the output channels 1 and $\bar{1}$ the masked and integrated intensity and its electronically thresholded and inverted results are shown. These results indicate that for this particular six-digit input, an output bit 1 was generated. In Figs.5.3f, 3g, 3i and 3j, corresponding to the remaining input groups, the obtained $\bar{1}$ and 0 CAM summation results are also shown. Because of the use of a 20:1 contrast LCLV, in our experiment, the intensity threshold level $I_{th}$ was set at $0.5I_p$ where $I_p$ is the pixel intensity. In general, $I_{th}$ should be set between the highest possible intensity "zero", e.g. $10/C_I$, and lowest possible intensity "one", e.g. $1 + 5/C_I$, where $C_I$ is the input device's intensity contrast. For the correct result, $C_I$ should be greater than 1:5. For the processing of the angularly-multiplexed inputs, a second experiment was performed. Three spatially encoded input masks corresponding to the first, second and last six-digits of the two

five-digit MSD addends, X = $0\bar{1}101$ and Y = $\bar{1}0\bar{1}11$, e.g., $0\bar{1}\bar{1}01\bar{1}$, $\bar{1}01\bar{1}01$, and $1\bar{1}0111$ after a distribution to three channels (see also the top part of Fig.5.4), were lined from the top to the bottom rows on an input plane device that was located at a distance of 15 cm from the shared CAM mask. The three input groups were illuminated by three angularly multiplexed ($0^0$ and $\pm 75^0$) optical beams each of which was aligned to project its input on a common CAM mask. The masked results that represent the angularly multiplexed CAM matching results were spatially integrated and displayed at the lens back focal plane (see the bottom part of Fig.5.4). The three expected CAM results were 0, 1 and $\bar{1}$. The alignment of a large number of multiplexing channels is more difficult. However, since only a position-matching rather than a phase-matching, as is the case with a holographic approach, is required, the alignment of N channels is more straightforward than in other, for example a N channel holographic, schemes.

## 5.2 An Optical Holographic Associative Memory-based Parallel Register Transfer Processor

### 5.2.1 Preliminary

A combinatorial logic circuit is an interconnected array of logic gates or switches. However, for various arithmetic operations, iterative sequential computation is needed. To furnish feedback for combinatorial circuits, memory elements, such as flip-flops or registers, must be utilized. With this feedback, the overall logic circuit is a finite-state sequential logic machine. To perform fast combinatorial logic the use of optics was suggested [11-12]. However, for the proposed sequential logic schemes the efficient feedback generation is an active research area. To generate a sequential logic circuit, a viable hybrid approach is to use optics for both fast parallel combinatorial logic and interconnect functions and high-speed bit-addressable electronics for storage and feedback [11]. An example is the emitter-hologram-SLM-hologram-detector combination used for opto-electronic residue arithmetic processing [13]. In this section, a hybrid sequential computing module, where an optical array processor performs the combinatorial logic and interconnect operations between high-speed electronic parallel addressed storage registers, is described. This hybrid system is able to perform fast optical register transfer microoperations (ORTMOs), operations that represent the primitive operations required for an general-purpose optical digital computer. Using these operations, other, such as residue arithmetic operations can be constructed. This new system will be referred to as an optical register transfer processor (ORTP).

For the design of a digital computer, the so-called register transfer language (RTL) [14] plays an important role. Based on an interconnected set of logic gates, registers, etc., RTL serves as the most primitive language that

links a physical digital machine and its programming environment. Any sophisticated iterative computation can be decomposed into a sequence of primitive logic and transfer operations. In Table 5.1, some typical register transfer (a) and logic (b) microoperations [14] are listed. Here, the source and destination registers are denoted as A and C, respectively. It can be shown [14] that for both a single bit and a full-length word, register parallel load, clear, rotate and shift as well as transfer operations are executable. These operations together with a complete set of binary logic microoperations (see Table 5.2) can be combined for other more sophisticated arithmetic operations, such as addition, subtraction, and multiplication [14].

### 5.2.2 Optical Implementation

For an optical register transfer microoperation (ORTMO) implementation, the recently developed symbolic substitution technique [15-18] can be used. Here, an optical holographic associative symbolic substitution (OHASS) technique, proposed by Yu et. al. [17-18] is employed. The two logic states 0 and 1 are encoded as two spatial orthogonal symbols (see Fig.5.5). In the OHASS filter preparation stage, the interference pattern between the Fourier spectra of the input and the precalculated output symbols are recorded. To process either a single or two-variable ORTMO, at the correspondingly partitioned recording plane either two or four exposures are affected. To generate an output, these input symbols are used as reference beams. The OHASS filter construction details can be found in Refs. [16-17].

For the various ORTMOs, in the input plane, a set of N-bit input optical symbols

$$c(x,y)=\sum_{i=0}^{N-1}[a(x-ix_0,y-y_0)+b(x-ix_0,y-2y_0)$$

$$+c^*(x-ix_0,y+y_0) \qquad (5.1)$$

where ($x_0$, $y_0$) are spatial shifts, a, b and $c^*$ are the two inputs and a reference pattern, respectively, is allowed to overlap with a pattern duplicating filter g(x, y). In the system's Fourier plane, the corresponding output pattern O is

$$O(x,\eta)=C(x,\eta)\oplus G(x,\eta)=\sum_{k=0}^{M-1}C(x,\eta-k\eta_1)$$

$$=\sum_{i=0}^{N-1}\sum_{k=0}^{M-1}\{A(x-ix_0,\eta-k\eta_1)\exp[-jy_0(\eta-k\eta_1)]$$

$$+B(x-ix_0,\eta-k\eta_1)\exp[-j2y_0(\eta-\eta_1)]$$

$$+C^*(x-ix_0,\eta-k\eta_1)\exp[+jy_0(\eta-k\eta_1)]\} \quad (5.2)$$

where $\oplus$ denotes a convolution operation, A, B, C and $C^*$ are the 1-D Fourier transform of the input patterns. Eq.5.2 represents a 1-D (vertical) replica of a horizontal Fourier hologram array. The synthesis of a proper duplication filter g has been reported [19-21].

Based on the above-described OHASS and pattern duplication scheme, an optical register transfer processor (ORTP) can be implemented. In Fig.5.6, a schematic of an ORTP is shown. The four N-bit A, B, C, and $C^*$ electronic registers are employed. To generate the optical inputs, input electronic registers are used to drive a parallel 1-D array of fast laser diode emitters. A fast detector array feeds into an ORTP output register. For iterative

computing, an one-to-one electronic feedback loop connecting the registers A to C can be utilized. The register B also acquires input data from an electronic output port. In a learning phase, to load a reference pattern the register $C^*$ is used. For the M possible N-bit microoperations, using the M vertical Fourier spectrum replica, M consecutive associative holograms are prepared. To ensure that all the two-variable input combinations are available, for each hologram four OHASS bit-wise partitioned exposures are required. When all the M ORTMOs are encoded, the register $C^*$ is deactivated. To control the ORTP's sequencing, located at the back of the hologram array, a 2-D spatial light modulator (SLM) is programmed to select, one at a time, one of the M horizontal slices. The thus selected result, after passing through the second cylindrical lens $L_2$, is detected and stored in the register C.

Because an ORTP is a bit-serial word-parallel processor that processes in a sequential operation fashion two input variables at a time, optical fanout is determined by the number of logic and transfer operations independent of the word length. It has been shown [22] that for a holographic interconnect to be superior to its electronic counterpart, the interconnect line-length, efficiency, rise-time, fanout, and source threshold power must be optimized. It has been indicated [22] that for a given rise-time (e.g. 1 ns in a capacitance limited region), the use of long interconnect line-length (> 1 mm), large fanout (> 1), low source threshold (< 2 mw) and high hologram efficiency (> 9 %) can provide an over-all superior interconnect performance for optics than for electronics. For an existing optical semiconductor laser source with a maximum power of 50 mW operated with a 1 ns rise-time, a maximum fanout of 67 is possible [22]. This fanout places an upper limit on the number of ORTP microoperations (more than what is required for primitive operations). Since all the registers store for a short period of time the parallel data and the intermediate results, and because no serial intra-register operations are required, fast GaAs-based GHz electronic registers together with a fast system

clock can be used. For an all-optical ORTP, optical memory elements, such as the recently developed SEED [23] device, that can offer dynamic storage for as long as 30 sec., may be used. In addition, because all microoperations require an identical processing circuitry, clock synchronization is relatively easy. Finally, because of the ORTP speed is independent of the word length, by using a large space-bandwidth product optical system, the implementation of a multi-variable ORTP may also be possible.

### 5.2.3 Experimental Results

In our proof-of-principle ORTP experiment, various parallel OHASS bit transfer, logic complement and AND operations were performed. For the duplication of the Fourier spectrum into three laterally displaced spatial locations, two beam splitters and a mirror were used. These three Fourier spectra were used, for bit transfer, logic complement and AND microoperations, respectively. For each operation there are k possible input bit configurations where for transfer k = 2 and for logic k = 4. Corresponding to a particular operation, a hologram was partitioned into k sections. Depending on which operation, transfer or logic, is to be performed, a k step hologram generation process is used where in each step, the contents of registers A and $C^*$ or A, B, and $C^*$ are used. During the associative recall process, for either the transfer or logic, the entire hologram was illuminated by either A or A and B. Using the associative recall process, at the output register C plane, the result was retrieved. In Fig.5.7a and 7b, the result of these transfers are shown. To select the desired microoperation, at the Fourier plane, a binary mask was employed. On the left-most Fourier spectrum, an optical bit transfer microoperation was performed. Since there are two bit transfer cases, i.e the transfer of either a 0 or a 1, the hologram associated with these two transfers was divided into two vertical parts. At each exposure, two identical input

symbols taken from the input registers A and $C^*$ were used. For a bit complement logic operation, the central Fourier spectrum was used. In this case, for each exposure, a different pair of binary symbols were used. In Fig.5.8a and 8b, the two OHASS logic complement results are shown. To perform a two-variable logic AND operation, the right-most Fourier spectrum was utilized. In this case, a four quadrant composite hologram was constructed. At each exposure, the three other spectral quadrants were covered. Also, for the four exposures, the four input symbol pairs were inserted. In Fig.5.9, an experimental OHASS logic AND results are shown.

## 5.3 Summary and Conclusion

In this chapter, memory-oriented optical information processing was investigated. Two types of optical memories, CAM and AM, were drafted. As an conclusion, utilizing the advantages of CAM and AM, an efficient MSD single-stage adder and transfer register processor were implemented. The merits of the non-holographic CAM are reduced minterms by logic reduction, less hardware complexity, less number of used optical elements, and fast processing speed. For the holographic AM, the advantages are fast processing speed limited by only source modulation speed and the detector response time, one step processing by precalulating input and output combination, and an ease of parallel processing scheme with either an array of holographic AM or photorefractive crystal (volume holograms).

In Table 5.3, a comparison summary of the new MSD adder with the various existing optical MSD addition schemes is presented. It is assumed that after each optical processing stage, an electronic detection and an electronic gain element is required. For this comparison, the active optical operations include switch and logic functions, while the passive optical operations imply beam splitting and combining, pixel masking and lens integration. In principle the holographic CAM-based approach is efficient, but to generate the N CAM addition bits, N+1 holographic crystals (each processing 56 holograms) must be used. On the other hand, our non-holographic opto-electronic CAM uses the fewest number of optical elements for the largest number of single optical stage parallel operations. Despite the large number of optical operations, it requires fewer active (switching) operations than the other schemes. Its main advantage, however, is its processing speed. As compared to an electronic CAM [24] where about ten times more electronic logic gates are required, this opto-electronic approach shifts a large part of the computational burden from electronics to optics. This shift is important since when higher-level computations, e.g. multiplication and

matrix operations, need to be performed, only a free-space optical scheme allows for multiplexing thereby greatly reducing the number of operations. Another advantage of this approach is that when a picosecond semiconductor laser is used as a driving source, an overall 50 MHz rate MSD processing is possible. On the other hand, a typical kilo-bit CMOS CAM that has a fastest 140 ns cycle time can only operate at an overall rate of 5 MHz [24].

In this chapter, a hybrid sequential computing module, where an optical array processor performs the combinatorial logic and interconnect operations between high-speed electronic parallel addressed storage registers, was presented. This hybrid system experimentally demonstrated the capability of performing fast ORTMOs. Combining the multi primitive operations, any types of logic and arithmetic processing can be performed for an general-purpose optical digital computer. As examples, an interregister transfer, a logic complement, and logic AND operations were experimentally performed. In case of the logic AND operation, both input and output patterns were illuminated during the learning stage to generate a hetro-associative memory at the Fourier plane. Only input pattern, during recall stage, was illuminated the holographic hetro-associative memory. As a result of the signal recovery of associative recall, the output pattern was retrieved at the output plane. For multiple variable AND operation, some crosstalks were observed. This drawback can be improved by more elaborated spatial symbols which provide more distinction between two spatially orthogonal symbols. Also, the signal to noise ratio can be improved by using higher diffraction materials such as photorefractive crystal and dichromated gelatin.

## 5.4 References


[1] A. Avizienis, IRE Trans. Electronic Computers, EC-10, 189 (1961).

[2] B. L. Drake, R. P. Bocker, M. E. Lasher, R. H. Patterson, and W. J. Miceli, Opt. Eng. 25, 38 (1986).

[3] P. A. Ramamoorthy and S. Anthony, Opt. Eng. 26, 1169 (1987).

[4] K. Hwang and A. Louri, "Optical Multiplication and Division using Modified-Signed-Digit Symbolic Substitution," Opt. Eng. 28, 364-372 (1989).

[5] M. M. Mirsalehi and T. K. Gaylord, Appl. Opt. 25, 3078 (1986). 25, 2277 (1986).

[6] Y. Li and G. Eichmann, "Conditional Symbolic Modified Signed-Digit Arithmetic using Optical Content-Addressable Memory Logic Elements," Appl. Opt. 26, 2328-2333 (1987).

[7] M. J. Murdocca, "Theory and Applications of Free-space Digital Optical Computing," Ph.D. Dissertation, (The State University of New Jersey at Rutgers, 1988). Ch.6.

[8] T. Kohonen, *Self-Organization and Associative Memory* (Springer-Verlag, New York, 1984) Ch.4.

[9] M. Sakaguchi, N. Nishida, and T. Nemoto, "A New Associative Memory Systems Utilizing Holography," IEEE Trans. Comput. C-19, 1174 (1970).

[10] M. M. Mirsalehi and T. K. Gaylord, "Truth-Table Look-up Parallel Data Processing using on Optical Content-Addressable Memory," Appl. Opt. 17, 2277-2283 (1986).

[11] R. Arrathoon, "Logic based spatial light modulators," Proc. SPIE, 881 230-239 (1988).

[12] P. S. Guilfoyle and W. J. Wiley, "Combinatorial logic based digital optical computing," Appl. Opt. 27, 1661-1673 (1988).

[13] S. F. Habiby and S. A. Collins, Jr., "Implementation of a fast digital optical matrix-vector multiplier using a holographic lookup table and residue arithmetic," Appl. Opt. 26, 4639-4651 (1987).

[14] M. M. Mano, *Computer System Architecture*, (Prentice-Hall, NJ, 1982) ch.4.

[15] K. H. Brenner, A. Huang, and N. Streibl, "Digital optical computing with symbolic substitutions," Appl. Opt. 25, 3054-3060 (1986).

[16] Y. Li, G. Eichmann, R. Dorsinville, and R. R. Alfano, "An AND operation-based symbolic pattern recognizer," Opt. Comm. 63, 375-379 (1987).

[17] F. T. S. Yu and S. Jutamulia, "Implementation of symbolic substitution logic using optical associative memories," Appl. Opt. 26, 2293-2294 (1987).

[18] F. T. S. Yu, C. Zhang and S. Jutamulia, "Applications of one-step holographic associative memory to symbolic substitution," Opt. Eng. 27, 399-402 (1988).

[19] L. P. Boivin, "Multiple imaging using various types of simple phase gratings," Appl. Opt. 11, 1782-1792 (1972).

[20] P. Matthijsse, "Multiple imaging with thin phase filters: a signal processing approach," J. Opt. Soc. Am. 68, 733-738 (1978).

[21] W. H. Lee, "High efficiency multiple beam gratings," Appl. Opt. 18, 2152-2158 (1979).

[22] M. R. Feldman, S. C. Esener, C. C. Guest, and S. H. Lee, "Comparison between optical and electronical interconnects based on power and speed considerations," Appl. Opt. 27, 1742-1751 (1988).

[23] G. Livescu, D. A. B. Miller, J. E. Henry, A. C. Gossard, and J. H. English, "Spatial light modulator and optical dynamic memory using a 6 times 6 array of self electro-optic-effect devices," Opt. Lett. 13, 297-299 (1988).

[24] T. Ogura, S.-I. Yamada, and T. Nikaido, IEEE J. Solid State Circuits SC-20, 1277 (1985).

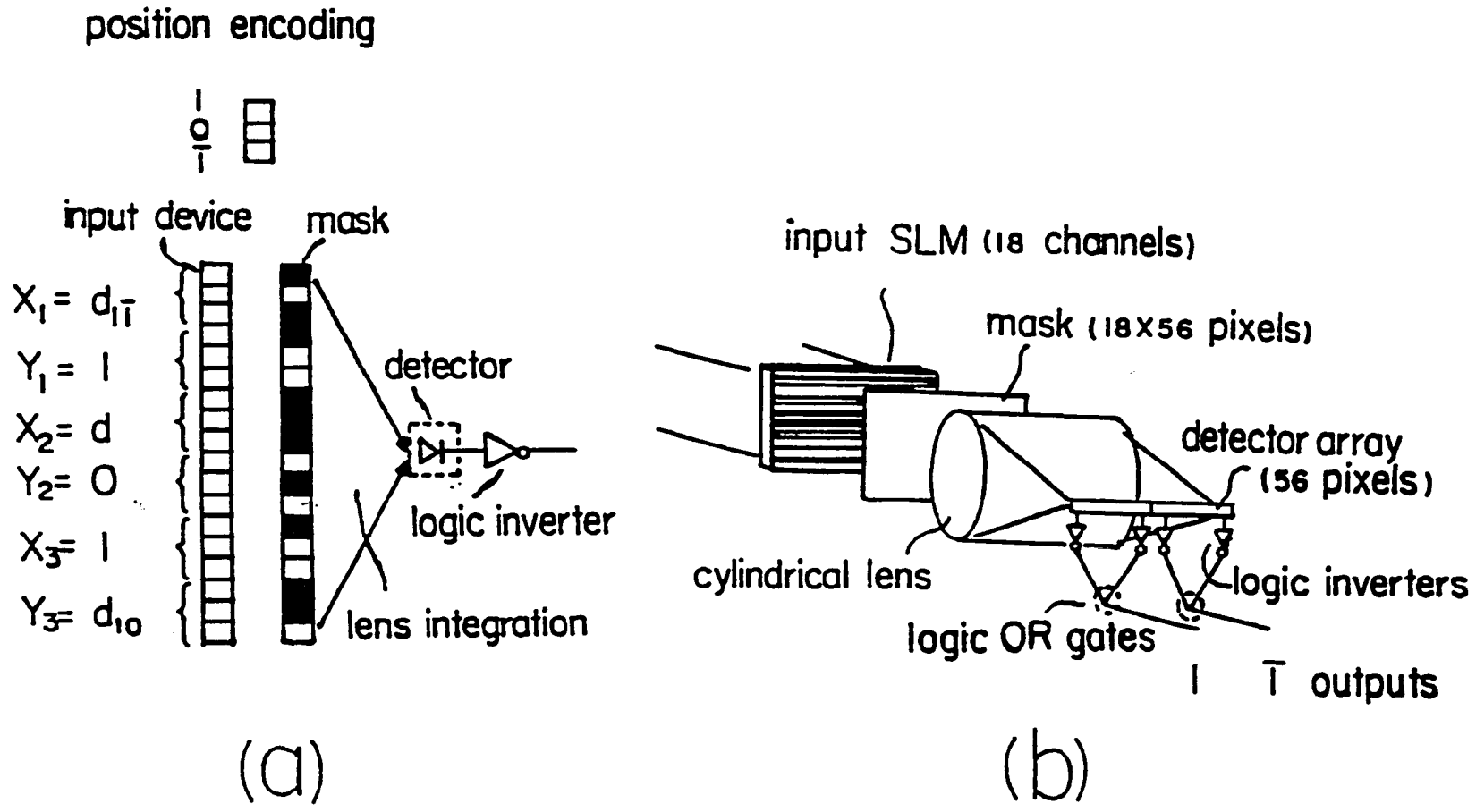


Fig.5.1 Schematic of a position encoded optical non-holographic CAM. (a) A six-variable reference pattern CAM. (b) A 56 reference pattern CAM for an MSD addition processor. For the 1 and $\bar{1}$ output channels, the CAM readouts are separately processed.

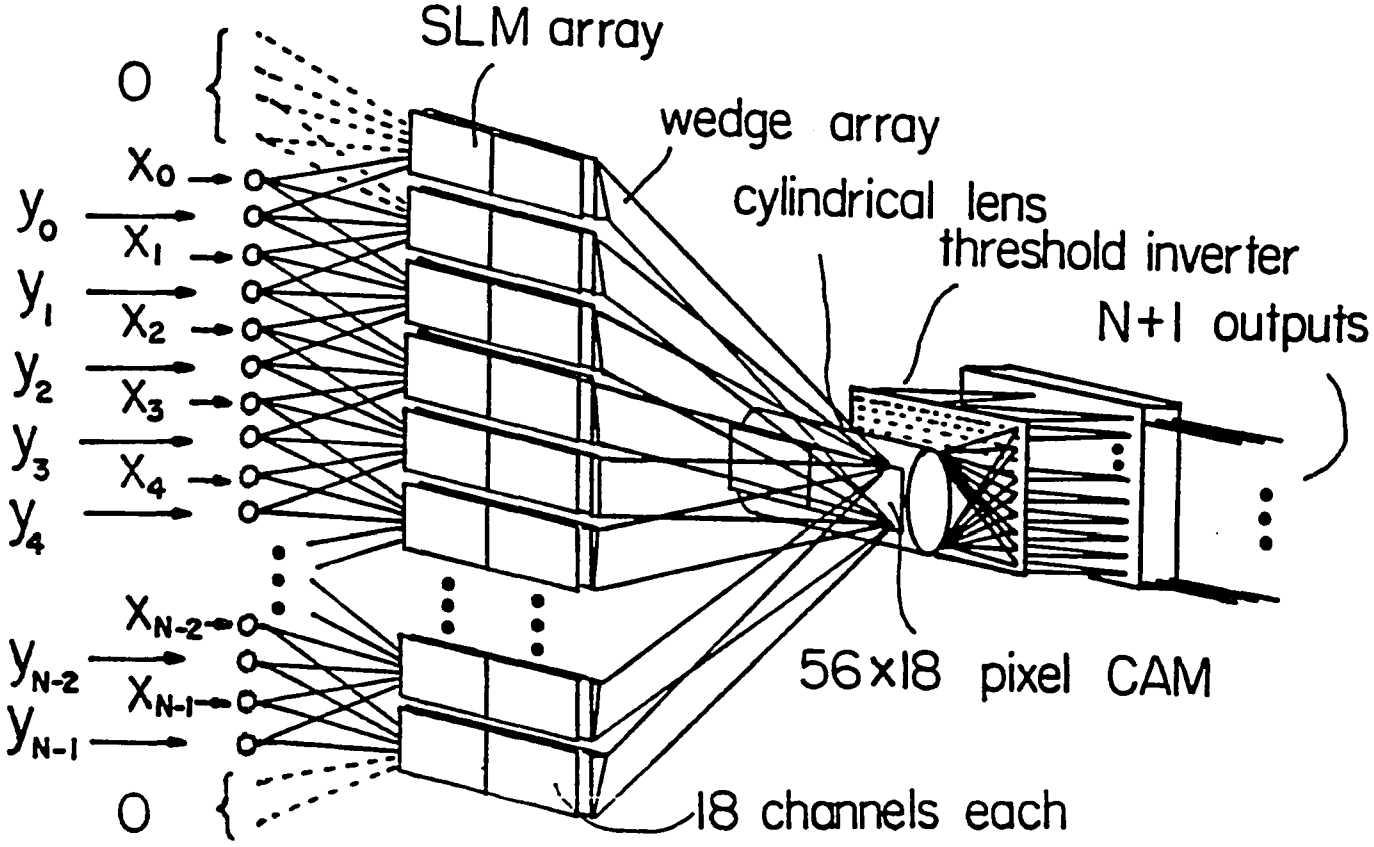


Fig.5.2 Schematic of an N-digit angularly-multiplexed CAM processor. N+1 input devices (SLMs) each of which is covered by a prism wedge are used. The dotted lines are connected to a constant zero inputs. 56(N+1) electronic detection cells with threshold inverters are used.

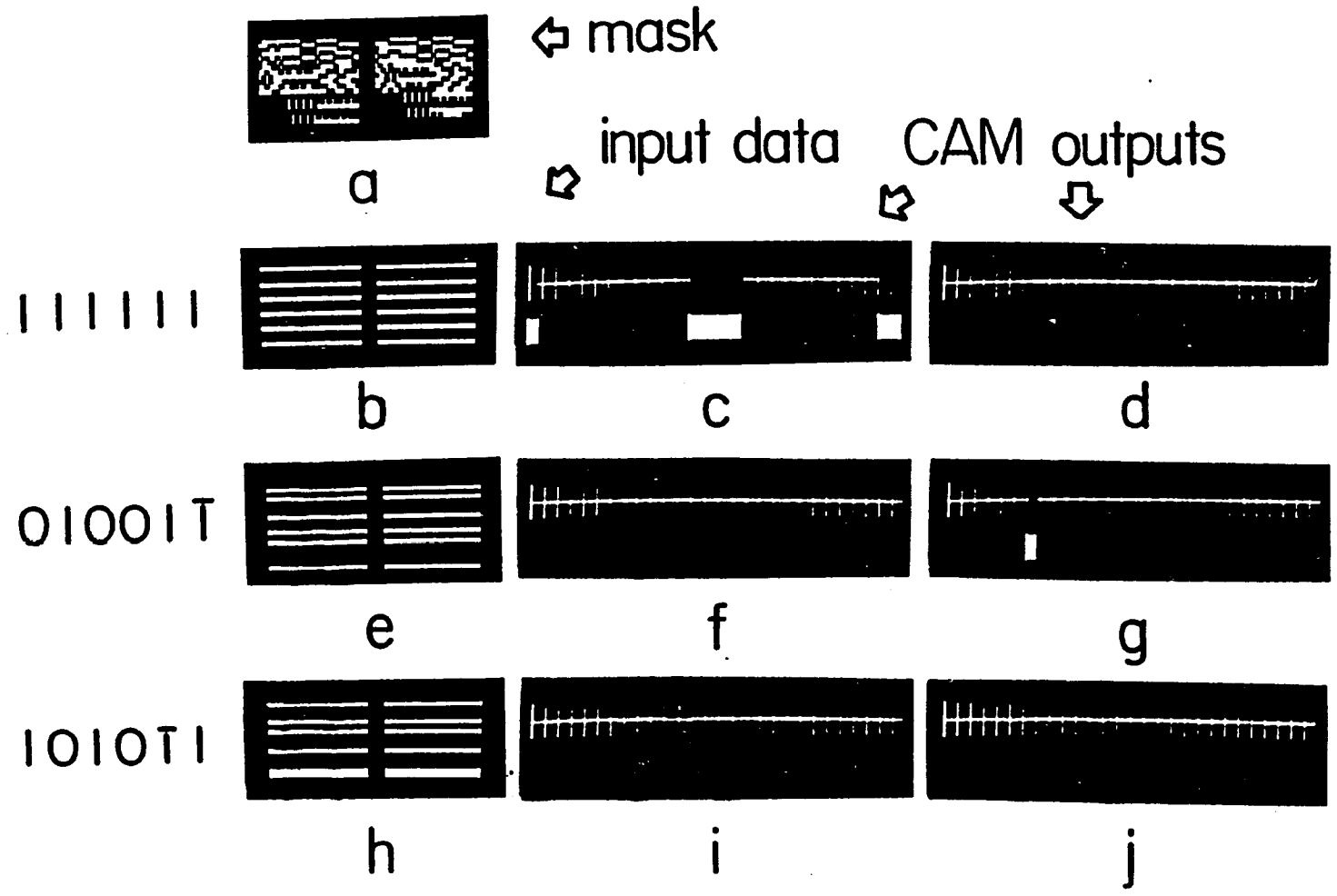


Fig.5.3 (a) A composite CAM mask for a MSD addition (the left- (right-) hand side submask is for the 1 ($\overline{1}$) output). (b) a six-digit input data group. (c) - (d), the corresponding masked intensity results for the output channel 1 and $\overline{1}$ in the lens back focal plane (top) and their thresholded and inverted outputs (bottom) respectively. (e) - (j) two other input data groups and their corresponding results.

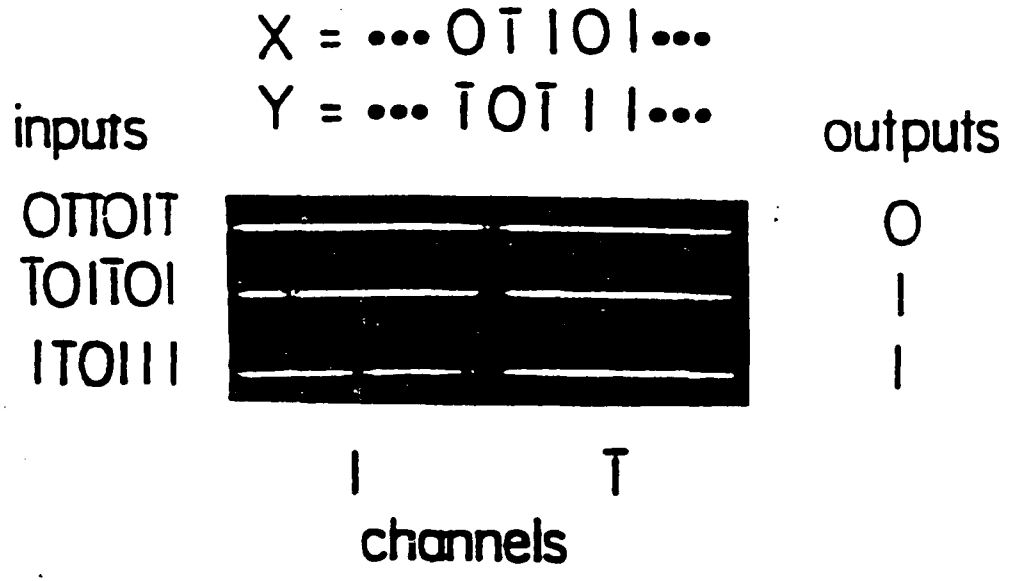


Fig.5.4 Results of a three angularly multiplexed CAM processing. For this example, the two 5-digit MSD numbers X and Y (top) are used. The inputs to the top, middle and bottom CAM channels, are the first, second and last 6-digit groups of X and Y. In the bottom part, the corresponding lens integrated results for the output channels 1 and $\bar{1}$ are shown. The three output digits are 0, 1, and 1, respectively.

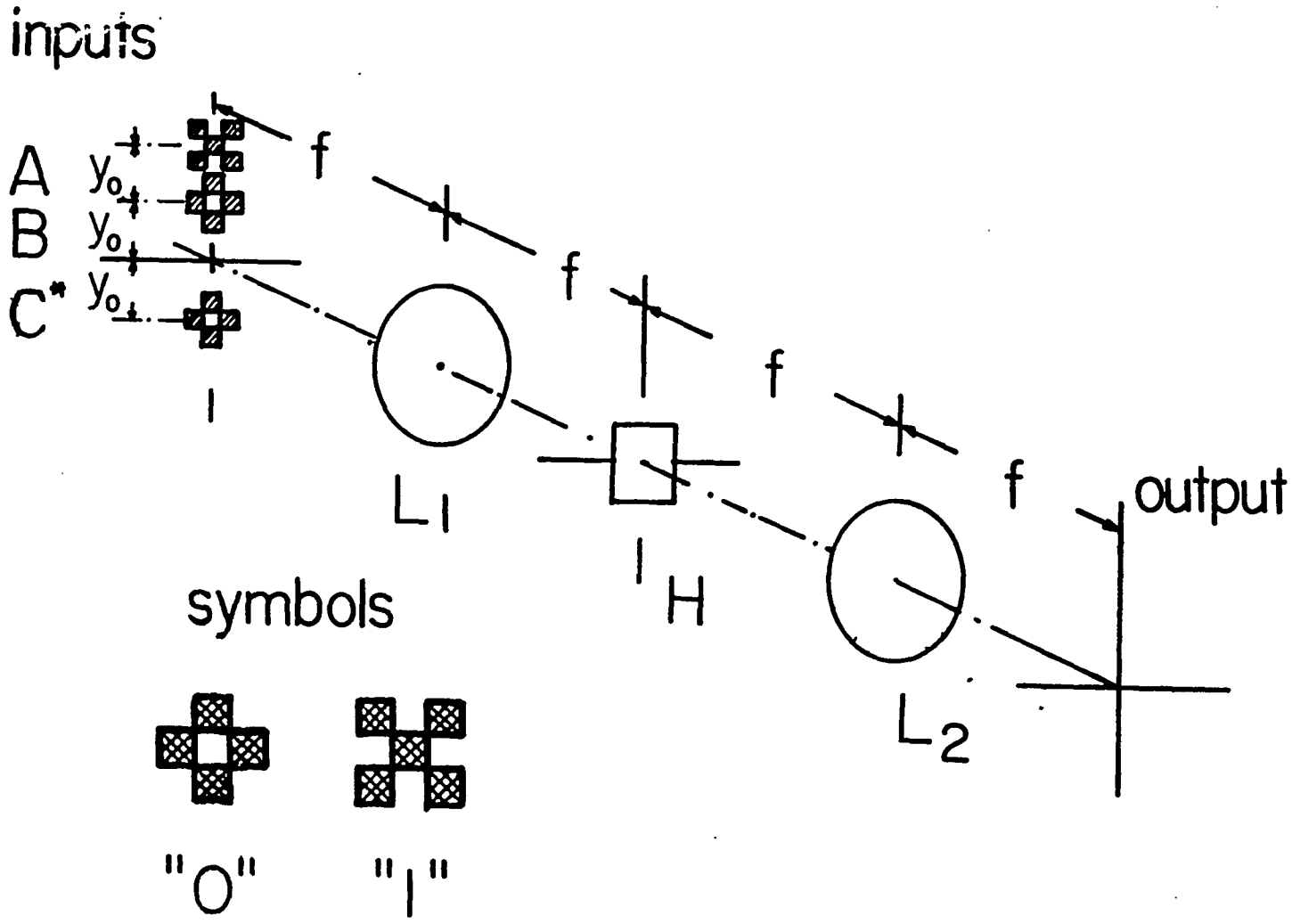


Fig.5.5 Schematic of a 1-bit OHASS processor. Input binary symbols are encoded into orthogonal patterns. $L_1$, $L_2$ and H, are two identical Fourier lenses and a hologram. The two logic and a reference symbols are inserted at the input plane. For the recording of the four associative subholograms, the Fourier spectrum is divided into four quadrants. For logic processing, depending on the inputs, at the system's output plane an associated output will be detected.

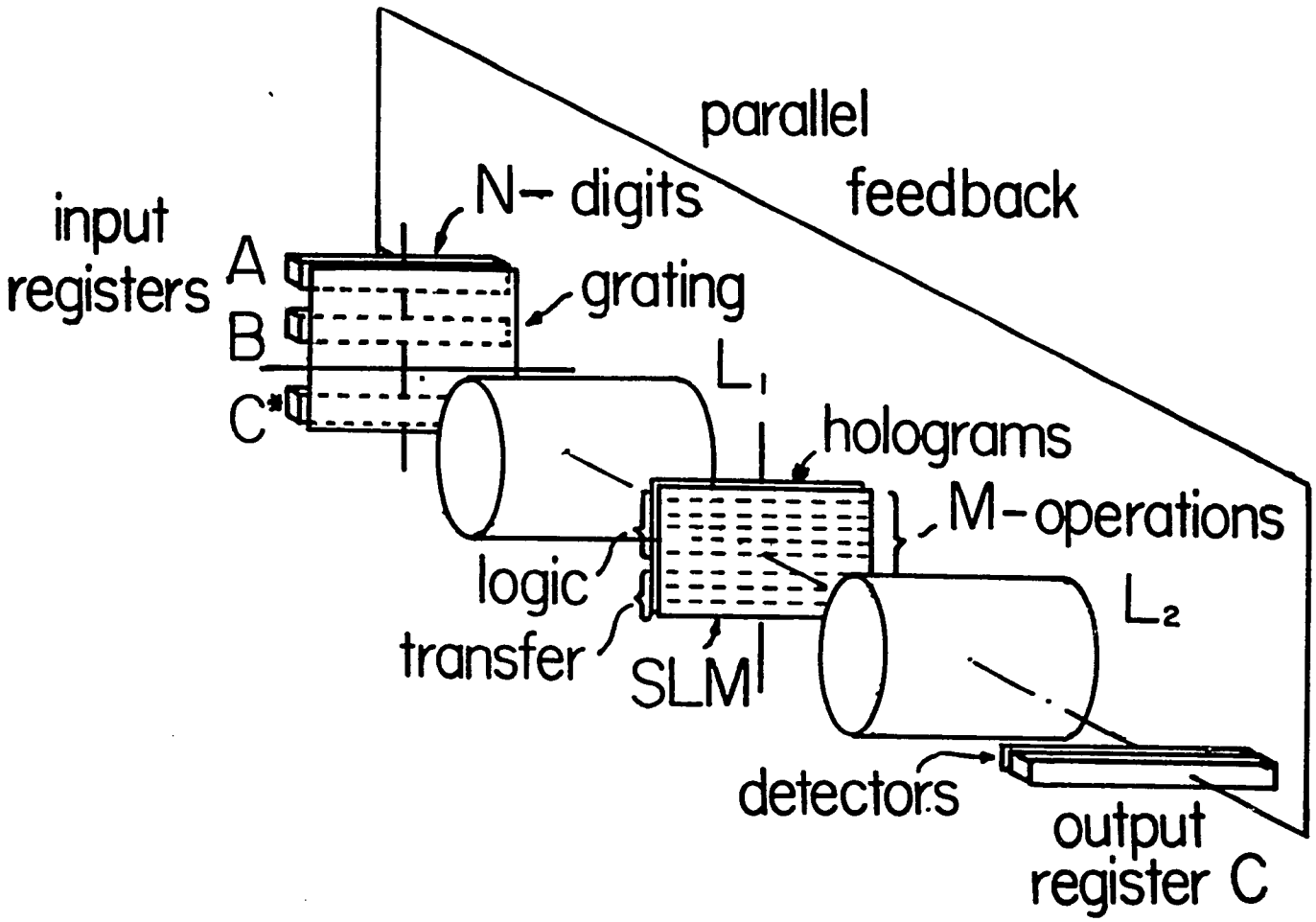


Fig.5.6 Schematic of a N-bit OHASS iterative processor. A, B and C*, are three N-bit input registers driving channelized laser diodes; C, an N-bit output register storing the result of optical threshold detector array. In addition to the lenses, holograms, and an input duplication grating, a Fourier plane 2D SLM and a parallel electronic feedback are used.

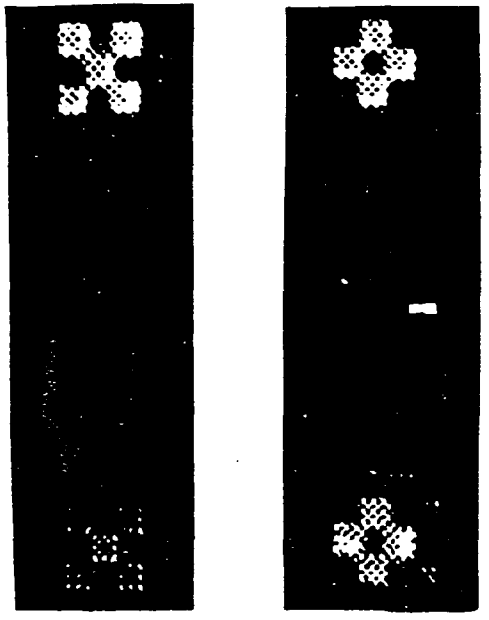


Fig.5.7 Results of a 1-bit OHASS interregister transfer micro-operation. (a) and (b), an associative transfer of a symbolic 1 and 0, respectively. The top and bottom patterns are the input and output symbols.

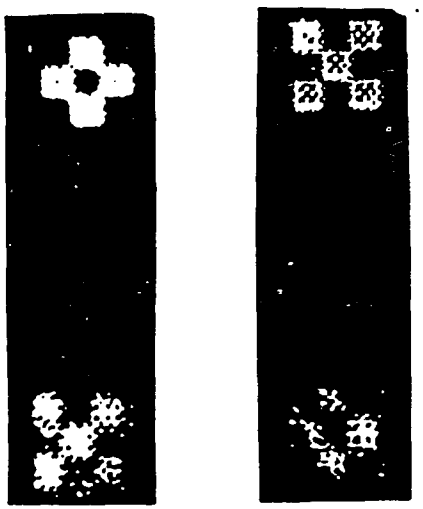

Fig.5.8 Results of a 1-bit OHASS logic complement micro-operation. (a) and (b), the associative complement of a symbolic logic 0 and 1, respectively.

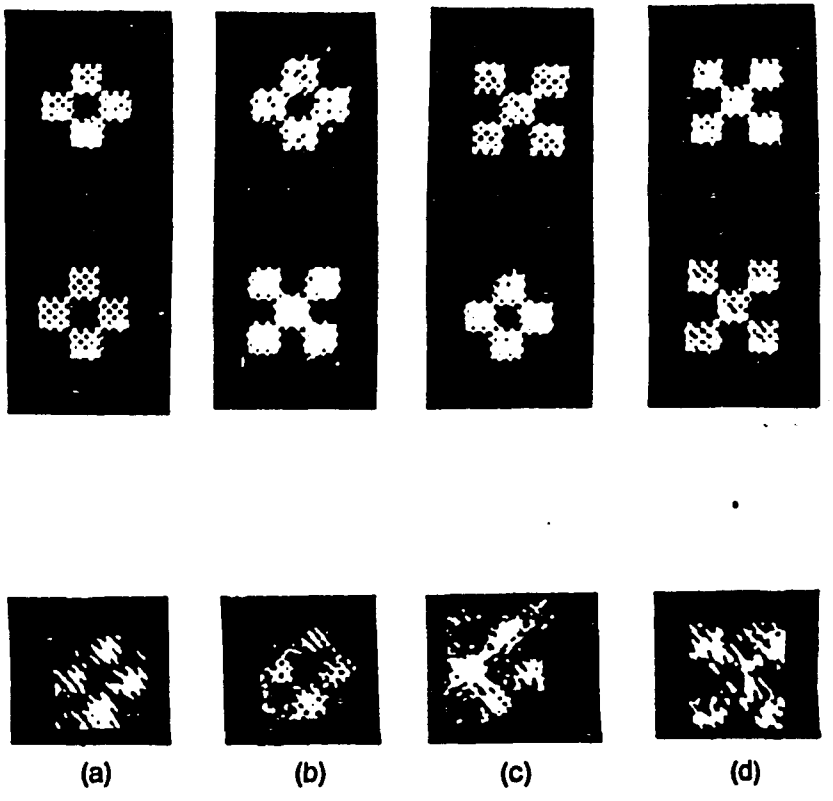


Fig.5.9 Results of a 1-bit OHASS logic AND micro-operation. (a)-(d), the associative AND operation results of the four input binary symbol pairs.

| Processors | Bistable[2] | Holographic[5] Mapping | Symbolic[3-4] Substitution | Holographic[6] CAM | Nonholographic CAM |
|---|---|---|---|---|---|
| **Parameters** | | | | | |
| Active Input Channels | 6(3N-4) | 6(3N-4) | 12(N+1) | 18(N+1) | 18(N+1) |
| Additional Optical Elements | 18(3N-4)Hs<br>18(3N-4)Ws<br>18(3N-4)Es | 18(3N-4)Hs<br><br>2(3N-4)Ls | 54(N+1)Bs<br>27(N+1)Ms<br>108(N+1)Is | (N+1)Cs<br><br>(N+1)Ls | Hs<br>(N-1)Ws<br>1L |
| Optical Operations | | | | | |
| 1. active | 6(3N-4) | 4(3N-4) | 114(3N-4) | 6(N+1) | 6(N+1) |
| 2. passive | 2(14N-17) | 2(3N-4) | 219(3N-4) | 392(N+1) | 392(N+1) |
| Electronic Operations | | | | | |
| 1.detection | 2(3N-4)† | 2(3N-4)† | 2(5N+4)† | 56(N+1)† | 56(N+1)† |
| 2. logic | 0 | 0 | 0 | 59(N+1) | 59(N+1) |
| System Dimensions | | | | | |
| 1. lateral | (18N)Ps | (6N)Ps | 36(N+2)Ps | 18(N+1)Ps | 18(N+1)Ps |
| 2.longitudinal | 6d | 3d+3f | 6d | d+f | d+f |
| Processing Steps | 9 | 6 | 9 | 4 | 4 |
| Processing speeds | $3T_o+3T_h+3T_d$ +6d/c | $3T_h+3T_d$ +3(d+f)/c | $3T_o+3T_h+3T_d$ +6d/c | $T_h+T_d+2T_l$ +(d+f)/c | $T_h+T_d+2T_l$ +(d+f)/c |

LEGENDS:
CAM, content-addressable memory; N, N-bit addition; B, beamsplitter; H, hologram; C, holographic crystal; M, mask; W, wedge; L, lens; E, etalon; I, optical inverter; P, pixel; d, lens-less beam travel distance; f, focal length; c, speed of light; $T_o$, optical switching time; $T_h$, electro-optic switching time; $T_d$, detector response time; $T_l$, electronic logic operation time; †, a detection gain is required, and ‡, a threshold detection is required.

Table 5.1 A performance comparison summary of the various optical MSD N-digit number addition schemes.

| Microoperation | Explanation |
|---|---|
| $C \leftarrow A$ | Transfer A into C |
| $C \leftarrow srA$ | Shift A right by 1-bit and transfer into C |
| $C \leftarrow slA$ | Shift A left by 1-bit and transfer into C |
| $C \leftarrow rrA$ | Rotate A right by 1-bit and transfer into C |
| $C \leftarrow rlA$ | Rotate A left by 1-bit and transfer into C |
| $C_i \leftarrow A_j$ | Transfer $j^{th}$ bit of A into $i^{th}$ bit of C |

Table 5.2 List of inter-register transfer micro-operations.

| Binary logic | Microoperation | Explanation |
|---|---|---|
| $O_0 = 0$ | $C \leftarrow 0$ | Reset |
| $O_1 = 1$ | $C \leftarrow 1$ | Set |
| $O_2 = A$ | $C \leftarrow A$ | A |
| $O_3 = B$ | $C \leftarrow B$ | B |
| $O_4 = \overline{A}$ | $C \leftarrow \overline{A}$ | Complement |
| $O_5 = \overline{B}$ | $C \leftarrow \overline{B}$ | Complement |
| $O_6 = A \bullet B$ | $C \leftarrow A \bullet B$ | AND |
| $O_7 = A \bullet \overline{B}$ | $C \leftarrow A \bullet \overline{B}$ | Inhibition |
| $O_8 = \overline{A} \bullet B$ | $C \leftarrow \overline{A} \bullet B$ | Inhibition |
| $O_9 = A + B$ | $C \leftarrow A + B$ | OR |
| $O_{10} = A + \overline{B}$ | $C \leftarrow A + \overline{B}$ | Implication |
| $O_{11} = \overline{A} + B$ | $C \leftarrow \overline{A} + B$ | Implication |
| $O_{12} = A \oplus B$ | $C \leftarrow A \oplus B$ | XOR |
| $O_{13} = \overline{A \oplus B}$ | $C \leftarrow \overline{A \oplus B}$ | XNOR |
| $O_{14} = \overline{A \bullet B}$ | $C \leftarrow \overline{A \bullet B}$ | NAND |
| $O_{15} = \overline{A + B}$ | $C \leftarrow \overline{A + B}$ | NOR |

Table 5.3 List of register logic micro-operations.

# VI SYMBOLIC SUBSTITUTION-ORIENTED OPTICAL SIGNAL PROCESSORS

## 6.1 Preliminary

Because of the advantages of optical signal processing such as, massive parallelism, high temporal and spatial bandwidth, high processing speed and noninterference communications, it has recently elicited a lot of attention. Technical improvements of spatial light modulators (SLMs) and the applications of nonlinear optics lead to new advances in the field of optical computing. In this chapter, several new higher-order spatial symbol recognition methods for optical symbolic substitution-based calculations are presented. In case of logic processing, higher-order symbolic substitution (SS) rules can implement multi-variable logic functions. For binary arithmetic calculations requiring carry propagation by simultaneously processing a number of bits, the computational speed increases. Finally, in image processing, the higher-order SS rules allow the use of larger local windows. For a higher-order spatial symbol recognition, both multiplicative and additive logic techniques are discussed. Three different higher-order SS recognition optical architectures are suggested: a multi-reflecting technique using an optical cavity, a lenslet array, and a content-addressable memory, are suggested.

For the optical cavity approach, by placing an encoded mask (SLM) inside an optical cavity optical implementation of logical AND functions is achieved. For noncoherent correlation approach, to generate shifted replicas of an input image, a new simple lenslet array-based architecture is proposed. To optically implement higher-order symbol recognition, using a CAM techniques, an input image is superimposed with a fixed binary mask (CAM). This CAM approach utilizes a binary periodic mask which is a bit-wise complemented image of the search symbol. Either dual-rail (DR) or triple-rail (TR) spatial encoding is

employed for these symbolic signal processing. Also, several new spatial encoding techniques are suggested. And, some preliminary experimental results are also presented.

One of the most frequently mentioned optical parallel computing techniques is the so-called symbolic substitution (SS). Symbolic substitution, proposed by Huang [1] as a powerful means for optical parallel digital computing, is a pattern replacement operation. The basic SS is a two step operation; (1) recognition of a particular pattern in the input data array and (2) its replacement with another pattern according to a given substitution rule. The original SS binary addition rule was described by Huang [1] but other several-bit SS, also called higher-order SS, rules were suggested by Kozaitis [2]. For example, using a dual-rail (DR) encoding scheme (see Fig.6.1a), sixteen higher-order 2-bit addition substitution rules are shown. An optical system for implementing SS must consist of two subsystems; a pattern recognizer including both optical linear and nonlinear devices that perform thresholding and complementing operations, respectively, and a pattern substituting device. Recently, various optical SS implementation techniques, such as associative memory, spatial filtering, phase-only hologram, optical correlation, grating, etc., have been suggested [3-14].

There are two basic SS pattern recognizing techniques; the additive and the multiplicative pattern techniques. With an additive pattern technique, the location of a search pattern is ascertained by either a correlation or a superposition of the shifted data copies [5-11]. The additive pattern technique, using either an optical intensity or polarization coding, requires an optical NOR operation. With a multiplicative pattern technique, light is either transmitted through several transparencies using spatial filters or reflected using an optical cavity [12-14]. The multiplicative pattern technique is an optical AND operation. Unlike the multiplicative pattern technique, the additive pattern technique, because it is a NOR operation, need a logic inversion. The required inversion is time-consuming and needs the support of additional optical or electronic

devices. To achieve a shift with phase-only hologram based SS, a technique suggested by Mait and Brenner [6], not only holograms but also prisms are required. In addition, since this system is not programmable, for each search symbol a different phase-only hologram is required. Symbolic recognition using spatial filters, a method suggested by Brenner et al [13], requires multiple passes through a data mask. Such filters are suitable for relatively simple search symbols.

The SS digital computing is applicable to optical arithmetic, logic, and image processing operations. For arithmetic operations, there are several operations such as binary, residue and modified-signed-digit (MSD) number SS representations [15-17]. With conventional binary number SS rules, since only two bits are processed at the same time, implies that for an n-bit number an n-stage computation is required. Using higher-order SS rules, since longer words are now processed, higher computational speed can be expected. For longer than 2-bit numbers, applying some of the rules of Fig.6.1b, the number of computational steps is reduced (see Fig.6.1c, for the addition of two binary numbers 0011 and 1010). For SS logical operations, Casasent and Botha have suggested SS rules for the realization of all 16 binary two-variable logical functions [18]. By applying higher-order SS rules in a single step, multivariable logical functions can be evaluated. Using SS rules various image processing techniques, such as skeletonization, morphological processing, median filtering, syntactic pattern recognition, and local image processing, have also been suggested [19-22]. Here, the higher-order SS rules allow the use of larger window elements.

## 6.2 Spatial Encoding for Optical Higher-Order Symbolic Processing

In this section, to help understand the SS schemes to be studied later, dual-rail (DR) and triple-rail (TR) higher-order SS spatial symbol encoding techniques are discussed. The binary digits "0" and "1" can be encoded using various primitive spatial symbols (see Fig.6.1a for DR and Fig.6.2a for TR encoding schemes). Compare to DR, the TR encoding can deliver a better signal-to-noise ratio (SNR). When one type of primitive symbols (e.g. "1") occurs more often in an input string, TR encoding can be more energy efficient. Such cases may occur, for example, in the case of image skeletonization. Also, TR encoding may be of choice with MSD arithmetic. The more elaborate TR symbols (see Fig.6.2b), however, require a larger space for their representation leading to less efficient use of the space-bandwidth product (SBP). In some applications, however, such as the associative memory based SS, the more elaborate symbols have shown satisfactory results [3-4]. By designing larger primitive symbols, at the expense of the system complexity, better detection SNR can be achieved.

For an n-bit operation, each input sequence is composed of a group of n primitive spatial symbols. To represent an n-bit input, symbols to be substituted can be arranged either as a 2-D matrix or as a 1-D vector. In Figs.6.2c and 2d, the TR spatial encoding of a binary string 001 in a 2-D matrix and 1-D vector form, respectively, are shown. To recognize a particular sequence of primitive symbols (the search symbol), the two basic processing techniques can be used. The additive technique performs on the search symbols a logical NOR operation on all the low intensity pixels, while the multiplicative technique performs a logical AND operation on all the high intensity pixels.

The primitive symbol representing the binary digit "0" ("1") is characterized by the logical functions $F_{0i}$ ($F_{1i}$). For a DR encoding rule, the corresponding functions $F_{0i}$ and $F_{1i}$ are

$$F_{0i} = x_{1i} \qquad (6.1a)$$

$$F_{1i} = x_{2i} \qquad (6.1b)$$

where x is the logic value of the high intensity pixel, the first and the second subscripts represent the rail position and the bit position in an input binary string, respectively. In the case of DR encoding, the symbol "1" is encoded using the spatial primitive symbol

$$x_{1i} = 0 \qquad (6.2a)$$

$$x_{2i} = 1 \qquad (6.2b)$$

while the primitive symbol "0" is encoded as

$$x_{1i} = 1 \qquad (6.2c)$$

$$x_{2i} = 0 \qquad (6.2d)$$

where i ranges from 0 to n-1. Because of the orthogonal encoding scheme, the following condition is always satisfied:

$$x_{1i} = \overline{x_{2i}} \qquad (6.3)$$

where the bar represents complement operation.

To recognize a particular binary input combination, a combined AND operation on the logical functions $F_{0i}$ and $F_{1i}$ is performed. For example, for a binary input string 110 and using a DR encoding scheme, the combined logical function F(110) is

$$F^k = F(110) = F_{11}F_{12}F_{03} = x_{21}x_{22}x_{13} \qquad (6.4)$$

where superscript k (for the input 110, k is equal to 6) stands for the input index number (the decimal equivalent of the input binary number). For any other 3-bit input symbol, $F^6$ results in a logic "0". The search for a particular symbol (characterized by the input index number k) among an aggregate of M higher-order symbols requires an array of M AND gates, where each gate is an implementation of a particular logical function $F^k$. The spatial location of the output logic value of "1" indicates the search symbol's spatial location. For an N-bit input number, there are $2^n$ different substitution rules (k is from 0 to $2^n$ -1). In Table 6.1, for a DR encoding rule of a 3-bit input, is of all the possible input combinations and their corresponding logical functions $F^k$ is shown. If the $i^{th}$ digit of the binary input number is equal to 0 (1), $x_{1i}$ ($x_{2i}$) is applied as the operand of the composite AND function $F^k$. The logical function $F^k$ uniquely represents a particular input data combination. The location of all the input data search symbols can be obtained by checking simultaneously, and in parallel, the logic values of all the $F^k$ functions.

For a TR encoding rule, the corresponding logical functions $F_{0i}$ and $F_{1i}$ are

$$F_{0i} = x_{2i} \qquad (6.5a)$$

$$F_{1i} = x_{1i} x_{3i}, \qquad (6.5b)$$

where the AND operation is to be performed on all the high intensity pixels. In Table 6.2 for the TR encoding rule with a 3-bit input, the listing of all the possible input combinations and their corresponding logical functions $F^k$ are shown. Using the same DR encoding, the function $F^6(110)$ for the TR encoding rule is expressed as

$$F^6 = F(110) = F_{11} F_{12} F_{03} = x_{11} x_{31} x_{12} x_{32} x_{23}. \qquad (6.6)$$

It is also possible to use the other alternative, the additive logic for SS operations. There is a group of optical architectures that utilizes for symbol recognition a NOR gate-based SS rules. First, the logical OR operation is performed on all the low intensity pixels in the search symbol and, next, an intensity inversion is accomplished. In this case, the logic function $F^k$ can be expressed as a function of all the low intensity pixels in the search symbol. As an example, for the DR encoding rule, consider again the function $F^6$ (see Eq.6.4):

$$F^6 = \overline{\overline{F^6}} = \overline{\overline{x_{21} x_{22} x_{13}}}. \qquad (6.7)$$

Using DeMorgan's theorem and Eq.6.3, the function $F^6$ can be written as

$$F^6 = \overline{x_{11} + x_{12} + x_{23}}. \qquad (6.8)$$

Equation (6.8) represents a logical NOR function performed on all the low intensity pixels of the spatial symbol representing binary input 110.

In case of the TR encoding rule, symbol's complement representing the "0"

element is

$$\overline{x_{2i}} = x_{1i} + x_{3i} \tag{6.9}$$

and the symbol's complement representing the "1" element is

$$\overline{x_{1i}x_{3i}} = x_{2i}. \tag{6.10}$$

Due to DeMorgan's theorem and using Eqs.(6.9), (6.10), and Eq.(6.6) is expressed as

$$F^6 = \overline{x_{21} + x_{22} + x_{13} + x_{33}}. \tag{6.11}$$

Equation (6.11) represents a logical NOR operation to be performed on all the low intensity pixels of a search symbol. To implement a NOR operation optically, a number of input image copies need to be generated. By superimposing the various shifted copies, an optical OR gate is implemented. The number of required shifts is equal to the number of low intensity pixels in the search symbol. To establish the positions of the search symbol, the result of the OR operation is ANDed with a fixed binary mask. In this case, the low intensity pixels indicate the position of the search symbol. To represent the search symbol's position by a high intensity pixel, before an AND operation with a fixed mask, a logic inversion should be performed.

## 6.3 A Lenslet Array-Based Higher-Order Symbolic Processor

### 6.3.1 Preliminary

Lenslet array (often called dragon-fly eyes lens) is a very useful optical passive element. Using a lenslet array, various optical information and image processing techniques have been implemented [23-25]. Using an N X N element lenslet array of a focal length $L_1$ together with collimated beams, an array of delta functions ($N^2$) can be generated. The delta function array can be used to generate multiple input sources, multiple images and multiple switches. This unique property of the lenslet array broadens the practical applications of optical information processing such as optical discrete Fourier transform (DFT), optical morphological filter and optical interconnect. In this section, to generate shifted replicas of an input image, a new simple lenslet array architecture, to be used for a higher-order optical symbol recognition, is investigated.

### 6.3.2 Optical Implementation

The input image is illuminated by a number of collimated beams. Each beam is incident on the input data mask at a different angle, where each angle corresponds to a different spatial shift. To generate a specific shift configuration, an array of diverging point sources (an array of 2-D delta functions), where each point source is associated with a different shift is provided. To sustain a specific number of shifts (here, all low intensity pixels in the search symbol should be superimposed), the lenslet array opening configuration must correspond to the low intensity pixel distribution in the search symbol.

In Fig.6.3, the proposed lenslet array SS recognition processor is shown.

By illuminating the lenslet array with a collimated beam, an array of point sources is obtained. Behind a spherical projection lens $L_2$, the $SLM_2$ inputs to the system a 2-D data A(x,y). The lenslet and the projection lens focal lengths are $f_1$ and $f_2$, respectively. The distance between the lenslet $L_1$ and the projection lens $L_2$ is $f_1 + f_2$. If the diameter of $L_1$ is $D_1$ and the distance between lens $L_2$ and the output plane is d, then the neighboring replicas of the input data array A(x,y) are shifted by a distance $\delta$ where

$$\delta = \frac{dD_1}{f_2}. \qquad (6.12)$$

The result of the optical OR operation on the shifted copies of the input image is obtained on the output plane. By masking the resulting OR operation, the location of the low intensity pixels indicates the location of the search symbols. In this case, the output plane image O(x,y) is the analog correlation of the input image A(x,y) with the array of delta functions and it is

$$O(x,y) = A(x - i\delta, y - j\delta), \qquad (6.13)$$

where, for an N X M lenslet array, i = 1, 2, ....,N and j = 1, 2, ....,M. For a fixed $D_1$ and $f_2$, the longer distance d leads to the larger shift $\delta$. To generate a pixel distance shift, the $\delta$ must be equal to the pixel size a. For a pixel shift, the distance d is

$$d = \frac{af_2}{D_1}. \qquad (6.14)$$

To minimize the crosstalk in the recognition stage, the precise alignment

of the optical system is important. Due to material nonuniformity, signals transmitted through different SLM pixels have different intensities, leading to an increase in crosstalk and a reduction of the system SNR.

To recognize a number of different symbols, a programmable lenslet array is employed. To recognize an N X M pixel symbol, an N X M lenslet array is needed. By blocking some lens opening, using a transmission-type SLM for corresponding high active intensity pixels in the search symbol, the required number of shifts is accomplished. For this scheme, the lenslet array can replaced by an LED/LD array [26]. However, because a lenslet array promises a more uniform angular illumination and hence is nearer to a delta function approximation, it gives a better result. In Fig.6.4a and 4b for a 3-bit operation with a 1-D TR spatial symbol encoding for search symbol 111 and 110, the corresponding lenslet array opening configurations are shown.

### 6.3.3 Experimental Results

In the optical lenslet array setup of Fig.6.3, an $Ar^+$-Ion laser was employed as a coherent light source. A custom-tailored 3 X 3 lenslet array with $D_1$ = 1 cm and $f_1$ = 1.6 cm and a projection lens $L_2$ with $f_2$ = 37 cm and $D_2$ = 7 cm were employed. For the data, the pixel area was 0.45 X 0.45 cm. The distance between SLM and the ground glass was 16.65 cm. The resulting output was recorded by a computer-linked TV camera. The input data, consisting of 3 X 12 array of binary pixels, was displayed as a 2-D matrix. In Figs.6.5a and 5b, respectively, the binary and the spatially encoded TR input sequences are shown. For symbols 111 and 110, a two-channel symbol recognition was performed. First, the $SLM_1$ was programmed to recognize the occurrence of a higher-order symbol 111. In this case, the aperture of lenses $L_{21}$, $L_{22}$ and $L_{23}$ were opened while all other lens apertures were blocked (see Fig.6.4a). This lenslet configuration corresponds to two unit shifts. In

Fig.6.5c, the superposition of the shifted copies of image in Fig.6.5b is shown. Using the mask of Fig.6.5e, the complemented copy in Fig.6.5c is masked. In Fig.6.5d, the final result is shown. Here, in the input data the high intensity pixels represent the positions of the search symbol 111. Next, at a second channel, a search for the location of symbol 110 was performed. In this case to provide for three unit shifts the aperture of lenslet lenses $L_{21}$, $L_{22}$, $L_{13}$ and $L_{33}$ were allowed to remain open (see Fig.6.4b). In Fig.6.5f shows the result of the OR operation (the superposition result), while Fig.6.5g shows the locations of the search symbol.

## 6.4 A CAM-based Optical Higher-Order Symbolic Processor

### 6.4.1 Preliminary

Optical CAM architecture has been described for a variety of optical information processing applications [22, 26-27]. A CAM based processor compares the input data with all previously stored reference patterns. When the input matches a stored CAM pattern, an output is generated. For an optical CAM, an angularly multiplexed volume hologram can be utilized. However, due to its alignment problems, this method is difficult to implement. In this section, a new optoelectronic CAM based symbol recognition scheme is introduced.

Consider, a 1-D binary 12-bit string of primitive elements B:

$$B = 0011 \quad 0110 \quad 0111. \qquad (6.15)$$

Here, the objective is to find the locations of a 4-bit sequence, i.e. 0110 (the search symbol S), in the bit string B. First, using a DR scheme, the primitive elements "0" ("1") in the string B and in the search symbol S are encoded as "01" ("10") producing substituted strings $B_e$ and $S_e$ ($S_e$=10010110). Complementing the string $S_e$ and repeating it three times, a periodic copy $P_e$ is generated. Performing a logical AND on the strings $B_e$ and $P_e$, the string $A_e$ (see Eq.6.16) is obtained. An 8-bit string of all zeros indicates the position of the search symbol:

$$\begin{array}{l} B_e = 01011010 \quad 01101001 \quad 01101010 \\ P_e = 10010110 \quad 10010110 \quad 10010110 \\ \hline A_e = 00010010 \quad 00000000 \quad 00000010 \end{array} \qquad (6.16)$$

### 6.4.2 Optical Implementation

To optically implement a CAM higher-order symbol recognition, an input image (the spatially encoded sequence of symbols shown in Fig.6.6a) is superimposed with a fixed binary mask (CAM) (see Fig.6.6b). The resulting image is shown on Fig.6.6c. This CAM approach utilizes as the binary periodic mask the bit-wise complemented image of the search symbol. To established the locations of the search symbols, at each symbol's aperture the light intensity is integrated. To perform this light intensity, a lenslet array is employed. The size of the elemental lenslet aperture is identical to the size of the search symbol. The lack of integration result indicates the locations of search symbol. As a final step, to point the search symbol,s locations by means of high intensity pixels, a light intensity inversion is performed.

To recognize all possible $2^n$ symbols, in general, $2^n$ channels are used. Using an angularly multiplexed scheme, a number of different output channels, a number of different output channels, where each channel corresponds to a different search symbol and is equipped with a different CAM mask, are incorporated. In Fig.6.7 the optical architecture for a three channel optical symbol recognizer is shown. The three lenses (input lenslet array) together with a projection spherical lens produce the three collimated beams. The input data symbols are displayed on an SLM that is positioned in the front focal plane of lens $L_4$. The CAM masks are aligned so that there is no overlap between any two CAM masks. This condition is satisfied when the spacing between two neighboring input lenslet array elements is equal to the SLM linear dimension d. The longitudinal dimension of the system is equal to $f_1 + 3f_2 + f_3$, while the transverse dimension depends on the number of multiplexed channels. For k channels, the transverse dimension equals to kd. Because of the rotational symmetry, and to more efficiently utilize the 3-D space, the light point sources are arranged as a 2-D array. To point to the

locations of the search symbols, at the output plane, either an array of optoelectronic inverters or an SLM is used.

The overall performance of the proposed system depends on the type of SLM used. The system's SNR is proportional to the contrast ratio of the SLM. For a DR encoding, half of each search symbol's area is masked. Since each element of the output lenslet array preforms integration over an area equal to the area of a single search symbol (over n X n pixels), the proper symbol detection is achieved for an SLM whose contrast ratio C is greater than $n^2/2$. Thus, using a DR encoding and for an SLM whose C equal to 500:1, the largest detectable search symbols is about 30 X 30 pixels. An additional limitation on the maximum size of the search symbol is due to the crosstalk between symbols that occurs during the lenslet array integration. By precise alignment of the output lenslet array, the crosstalk can be minimized.

### 6.4.3 Experimental Results

For the CAM based symbol recognizer, the input data were TR encoded. In Fig.6.8a the binary input data consisting of a 3 X 12 binary pixel matrix is shown, while in Fig.6.8b the corresponding spatially encoded input data are shown. In this experiment, a search for the two 3-bit symbols 011 and 110 was performed. First, the two masks corresponding to the search symbols 011 and 110 were generated. In Fig.6.8c (Fig.6.8d) the masks for the symbol 011 (110) containing the periodically repeated sequence of the complement of the search symbols are shown. Using a two-channel system, the recognition of the two search symbols can simultaneously be performed. By illuminating the input data mask with two angularly multiplexed collimated beams, an AND operation between the input data and search masks was performed. In Fig.6.8e (8f) for channels 011 (110), the result of the AND operation are

shown. Finally, using a 3 X 4 lenslet array, an intensity average of each 3 X 3 AND plane pixels was obtain. In Figs.6.8g and 8h, the averaged and the thresholded versions of the images in Figs.6.8e and 8f are shown. Here, the low intensity pixels indicate the locations of search symbol. The lenslet array, used in the experiment, consisted of 12 square aperture lenses. By introducing a photographic film in the beam path, Figs.6.8g and 6.8h images were generated. These images were also recorded by a computer-linked TV camera.

## 6.5 An Optical Cavity-based Higher-Order Symbolic Processor

### 6.5.1 Preliminary

Higher-order SS can be implemented using integrated optics approach [28-32]. Alignment and packaging is one of the difficult tasks for complex optical signal processing systems. This problem occurs, for example, when free-space optics is used for an optical digital computer or switching system. To reduce the alignment problems of many optical components, it is necessary to reduce the number of degrees of freedom by integrating these components on either optical cavities or common substrates. In this section, an optical symbolic processor based on an optical-cavity which consists of only mirrors with different distance is presented.

### 6.5.2 Optical Implementation

By placing an encoded mask (SLM) inside an optical cavity (see Fig.6.9), the optical implementation of logical AND functions is achieved. To simplify the system architecture, a DR spatial encoding technique is employed. Using a TR encoding to recognize the same binary input sequence, a larger number of passes (in comparison to the DR encoding) inside the cavity would be required. Here, the search symbol consists of three primitive symbols aligned along one direction (1-D vector). With a 1-D vector encoding, the output beam reflected from both mirrors $M_1$ and $M_2$ is also located in the input beam plane. The input beam, after passing through the mask at angle $\Theta$, is first reflected by $M_1$ and then it passes through the mask again. Next it is reflected by $M_2$, finally passes through the mask, and is detected at the output plane. By varying the distances $d_1$ ($d_2$), where $d_1$ and $d_2$ are the distances between the mask and mirrors $M_1$ and $M_2$, respectively, all possible logic functions

$F^k$ (see Table 6.1) can be implemented. In Table 6.3, for logic functions, distances $d_1$ ($d_2$) are given. The smallest distance d between the mask and one of the mirrors is

$$d = \frac{a}{2\tan\theta} \qquad (6.17)$$

where a is the SLM's pixel size.

Another way of implementing an array of optical cavities is to use half-mirrors together with some binary masks (see Fig.6.10). The masks $MA_1$ ($MA_2$) consist of one pixel wide vertical openings with separation between the openings that is equal to six pixels. In Fig.6.10, a particular input beam trajectory is shown.

For an n-bit input, a parallel recognition of $2^n$ input patterns is performed. Here, the encoded image is split into $2^n$ channels, where each channel employing an optical cavity with different distances $d_1$ ($d_2$) (see Table 6.3). In this case, the occurrence of all possible search patterns is simultaneously identified. As a result, with each image pointing to the position of a different search pattern, n simultaneous output images are generated.

### 6.5.3 Experimental Results

For an experimental implementation of the optical cavity-based symbol recognizer, a vector type DR encoding technique was utilized. In Figs.6.11a and 11b, the binary input and its spatially encoded version are shown. While the 3-bit search symbol was arranged as a 1-D vector, the input data were arranged as a 9 X 9 matrix with twenty-seven recognizable symbols. In this experiment, two-half mirrors $M_1$ and $M_2$ were utilized. For each group of three primitive symbols, a separate light beam was generated. To illuminate

a binary mask that was superimposed on halfmirror $M_1$ and/or $M^2$, a collimated $Ar^+$-Ion laser beam was employed. The mask consisted of vertical bars (openings) with bar separation equal to six times of the input data pixel size. The pixel size was 4 mm, the incident angle $\Theta$ was equal to 10°, with the distance d of 11.34 mm. For the recognition of two search symbols 000 (010), from Table 6.3 the distance $d_1$ was equal to 2d (3d) and $d_2$ was equal to 2d (2d). In Figs.6.11c and 11d, respectively, the locations of the search symbols 000 (010) are shown. Because now the high intensity pixel indicates the location of a search symbol, as opposed to the additive approach, neither an intensity inversion nor masking was required.

## 6.6 Summary and Conclusion

One of the major advantages of a higher-order SS processor is its speed. In addition, a second advantage over a 2-bit SS processor stems from a consideration of the practical cascadability of any optical SS scheme. Because of the long existing problems of cascading, such as the noise associated with repetitive amplification that seriously limit the SNR, the critical reduction of speed due to the existing 2D SLMs speed limit, an one-step SS processor may be a preferred approach. One advantage of use free-space optics is its capability to trade space for time. In solving a specific problem, it may also be possible to save both space and energy with a higher-order SS scheme. For example, for a single-step N-bit binary addition problem, instead of memorizing all the possible $2^N$ specified input configurations, a logic prereduction using Quine-McCluskey method can be applied. It has been shown [26] that, with this reduction, a factor of two or more reduction can be achieved. Also, for a specific problem, for example, when ternary and trinary symbols are needed, a TR encoding may be more advantageous to use than DR encoding. In general, the design of a higher-order SS processor is problem dependent. Ultimately, it is the combination of speed, energy, and space-bandwidth product (SBP) requirements associated with a specific application that determines the choice of a processor. In general, an optical SS scheme that uses local interconnets with refractive optical elements, the SBP has an upper limit of $10^8$ which is less than an obtainable $10^{11}$, using global interconnects with diffractive optical elements [33]. In fact, the main reason for the use of an optical SS scheme is that it can be implemented with space-invariant geometric optical elements such as lenses, beam splitters, etc., elements.

In this chapter, a higher-order SS technique symbol recognition stage was discussed. The higher-order SS method was applicable to arithmetic, logic as well as to image processing operations. Four different higher-order SS optical

architectural approaches were presented. To point to the location of the search symbol via a high intensity pixels, the recognition methods can be classified into two groups. Optical architectures in the first group require an intensity inversion, while for those in the second group this step is unnecessary. The first group includes the CAM-based and the lenslet-based approaches, while the second group consists of an optical cavity-based scheme. While the CAM recognition system utilizes angularly multiplexed channels to perform simultaneous search symbol recognition, the lenslet array-based system can be used to perform search symbol recognition either in parallel or in a sequential programmable mode. The input lenslet array together with SLM is used to program for the recognition of a particular search symbol. In an optical cavity-based recognition process, the high intensity output pixels indicate the search symbol's location. In the optical cavity-based symbol recognition architecture, an optically addressable SLM can be used.

## 6.7 References


[1] A. Huang, "Parallel Algorithms for Optical Digital Computers," Proceeding of the Tenth International Optical Computing Conference, 13-17 (IEEE Computer Society, Los Angeles, 1983).

[2] S. P. Kozaitis, "Higher-Ordered Rules for Symbolic Substitution," Opt. Comm. 65, 339-342 (1988).

[3] F. T. S. Yu, C. Zhang and S. Jutamula, "Applications of One-step Holographic Associative Memory to Symbolic Substitution," Opt. Eng. 27, 399-402 (1988).

[4] G. Eichmann, A. Kostrzewski, D. H. Kim and Y. Li, "Optical Parallel Register Transfer Microoperations using Holographic Symbolic Substitution," Appl. Opt. 28, 3860-3863 (1989).

[5] M. J. Murdocca, "Digital Optical Computing with One-Rule Cellular Automata," Appl. Opt. 26, 682-688 (1987).

[6] J. N. Mait and K-H. Brenner, "Optical Symbolic Substitution: System Design using Phase-only Holograms," Appl. Opt. 27, 1692-1700 (1988).

[7] D. P. Casasent and E. C. Botha, "Multifunctional Optical Processor based on Symbolic Substitution," Opt. Eng. 28, 425-433 (1989).

[9] K. H. Hwang and A. Louri, "Optical Multiplication and Division using Modified-Signed-Digit Symbolic Substitution," Opt. Eng. 28, 364-372 (1989).

[9] K-H. Brenner, "Programmable Optical Processor based on Symbolic Substitution," Appl. Opt, 27 1687-1691 (1988).

[10] R. Thalmann, G. Pedrini, B. Acklin and R. Dandliker, "Optical Symbolic Substitution Using Diffraction Gratings," Proceeding SPIE 963, 635-641 (1988).

[11] J. N. Mait, "Design of Dammann Gratings for Optical Symbolic Substitution," Proceeding SPIE 963, 646-652 (1988).

[12] M. T. Tsao, L. Wang, R. Jin, R. W. Sprague, G. Gigioli, H. M. Kulcke, Y. D. Li, H. M. Gibbs and N. Peyghambarian, "Symbolic Substitution using ZnS Interference Filters," Opt. Eng. 26, 41-44 (1987).

[13] K-H. Brenner, A. W. Lohmann and T. M. Merklein, "Symbolic Substitution Implemented by Spatial Filtering Logic," Opt. Eng. 28, 390-395 (1989).

[14] Y. Li, G. Eichmann, R. Dorsinville and R. R. Alfano, "An AND Operation-based Optical Symbolic Recognizer," Opt. Comm. 63, 375-379 (1987).

[15] Y. Li, G. Eichmann, R. Dorsinville and R. R. Alfano, "Parallel Digital and Symbolic Optical Computation via Optical Phase Conjugation," Appl. Opt. 27, 2025-2032 (1988).

[16] C. D. Capps, R. A. Falk and T. L. Hook, "Optical Arithmetic/Logic Unit based on Residue Arithmetic and Symbolic Substitution," Appl. Opt. 27, 1682-1686 (1988).

[17] R. P. Bocker, B. L. Drake, M. E. Lasher and T. B. Henderson, " Modified-Signed Digit Addition and Subtraction using Symbolic Substitution," Appl. Opt. 25, 2456-2457 (1986).

[18] D. Casasent and E. Botha, "Optical Symbolic Substitution for Morphological Transformations," Appl. Opt. 27, 3806-3810 (1988).

[19] G. Eichmann, J. Zhu and Y. Li, "Optical Parallel Image Skeletonization using Content-addressable Memory-based Symbolic Substitution," Appl. Opt. 27, 2905-2911 (1988).

[20] P. A. Ramamoorthy, S. Antony and T. A. Grogan, "Symbolic-Substitution-based Median Filters," Opt. Eng. 27, 409-412 (1988).

[21] S. D. Goodman and W. T. Rhodes, "Symbolic Substitution Applications to Image Processing," Appl. Opt. 27, 1708-1714 (1988).

[22] G. Eichmann and S. Basu, "Parallel Optical Syntactic Pattern Recognizer," Appl. Opt. 26, 1859-1865 (1987).

[23] Y. Li, A. Kostrzewski, D. H. Kim and G. Eichmann, "A Compact Real-Time Programmable Optical Morphological Image Processor," Opt. Lett. 14, 981-983 (1989).

[24] J. S. Jang, S. Y. Shin and S. Y. Lee, "Adaptive Two-Dimensional Quadratic Associative Memory using Holographic Lenslet Arrays," Optical Computing in 1989 the Technical Digest Series, 40-43 (OSA, Salt Lake City, 1989).

[25] J. Tanida and Y. Ichioka, "Programming of Optical Array Logic. 1: Image Data Processing," Appl. Opt. 27, 2926-2930 (1988).

[26] M. M. Mirsalehi, T.K. Gaylord, D.C. Fielder, and C.C. Guest, "Number representation effects in truth-table look-up processing: 8-bit addition example," Appl. Opt. 28, 1931-1939 (1989).

[27] M. M. Mirsalehi and T. K. Gaylord, "Truth-Table Look-up Parallel Data Processing using on Optical Content-Addressable Memory," Appl. Opt. 17, 2277-2283 (1986).

[28] J. Jahns and A. Huang, "Planar Integration of Free-space Optical Components," Appl. Opt. 28, 1602-1605 (1989).

[29] K.-H. Brenner and F. Sauer, "Diffractive-Refractive Optical Interconnects," Appl. Opt. 27, 4251-4254 (1988).

[30] J. B. McManus, R. S. Putnam and H. J. Caulfield, "Swithed Holograms for Reconfigurable Optical Interconnection: Demonstartion of a Prototype Device," Appl. Opt. 27, 4244-4250 (1988).

[31] A. Wuthrich and W. Lukosz, "Holographic with Guided Optical Waves," Appl. Phys. Lett. 21, 55-58 (1980).

[32] R. K. Kostuk, M. Kato and Y-T Huang, "Substrate Mode Holograms for Optical Interconnect," Technical Digest of OSA Topical Meeting on Optical computing, Salt Lake City, Utah, Feb. 27 - Mar. 1, Vol. 9, 168-171 (1989).

[33] F. Kiamilev, S. C. Esener, Y. Fainman, C. C. Guest, and S. H. Lee, "Programmable Optoelectronic Multiprocessor and their Comparison with Symbolic Substitution for Digital Optical Computing," Opt. Eng. 28, 396-409 (1989).

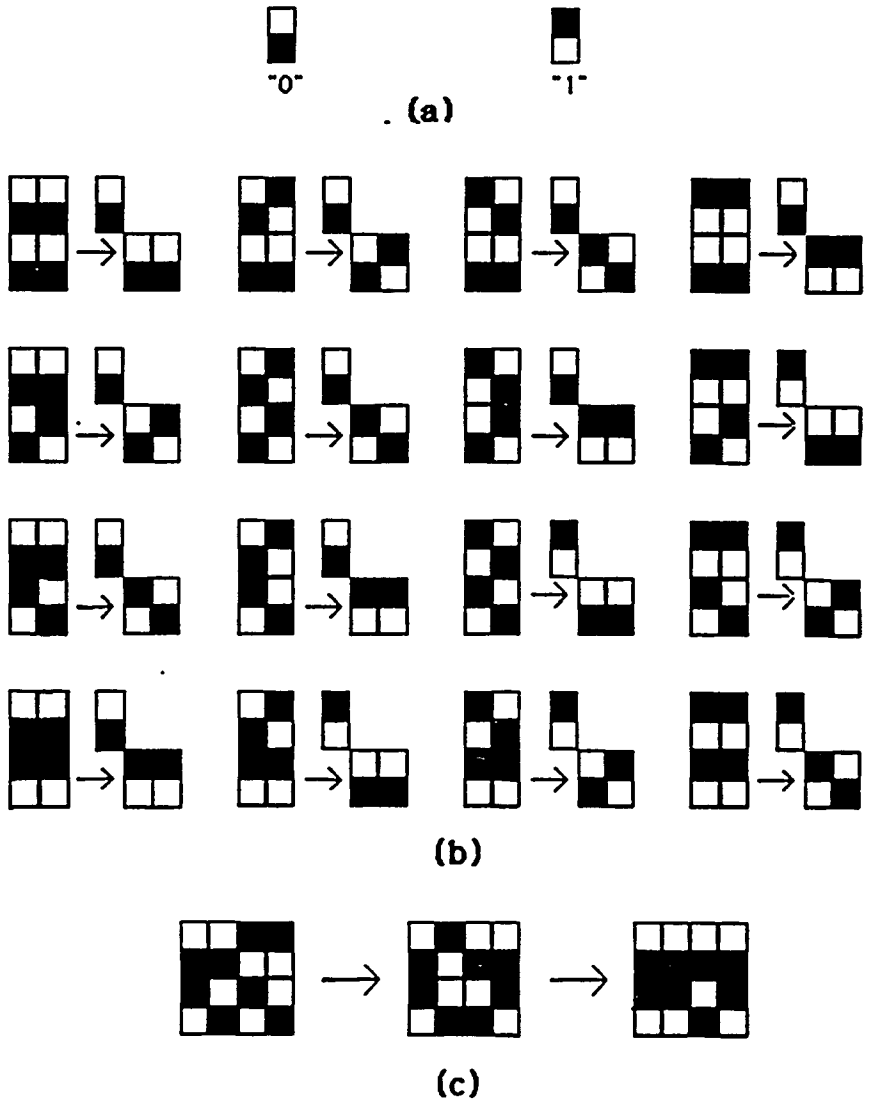


Fig.6.1 (a) Spatially DR encoded primitive elements "0" and "1". (b) Higher-order SS rules for the addition of two 2-bit binary numbers. (c) Using the addition rules in (b) we obtain a two-step addition example for binary numbers 0011 and 1010.

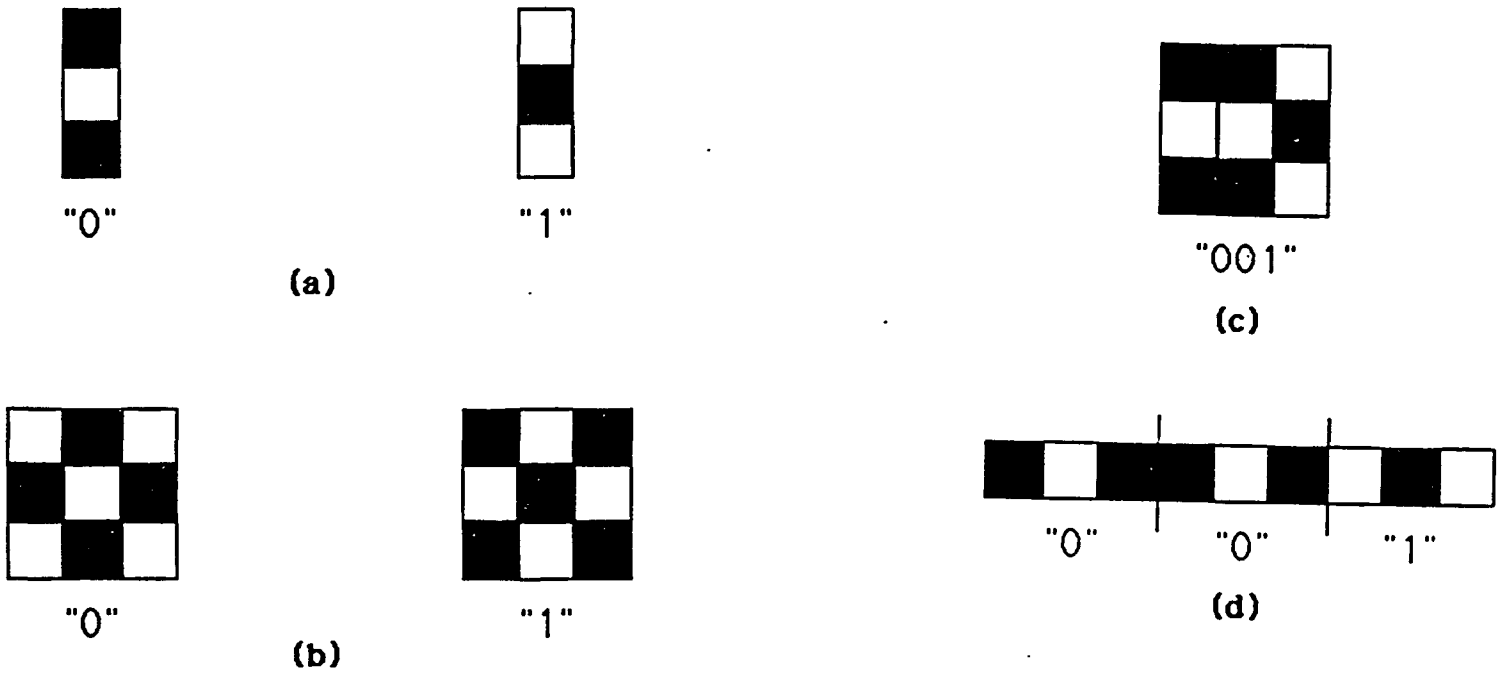


Fig.6.2 (a) Triple-rail (TR) encoding rule for the primitive elements "0" and "1". (b) Murdocca's encoding rule [5] for the primitive elements "0" and "1". (c) The spatially encoded binary number 001 using a matrix TR coding rule. (d) The spatially encoded binary number 001 using a vector TR coding rule.

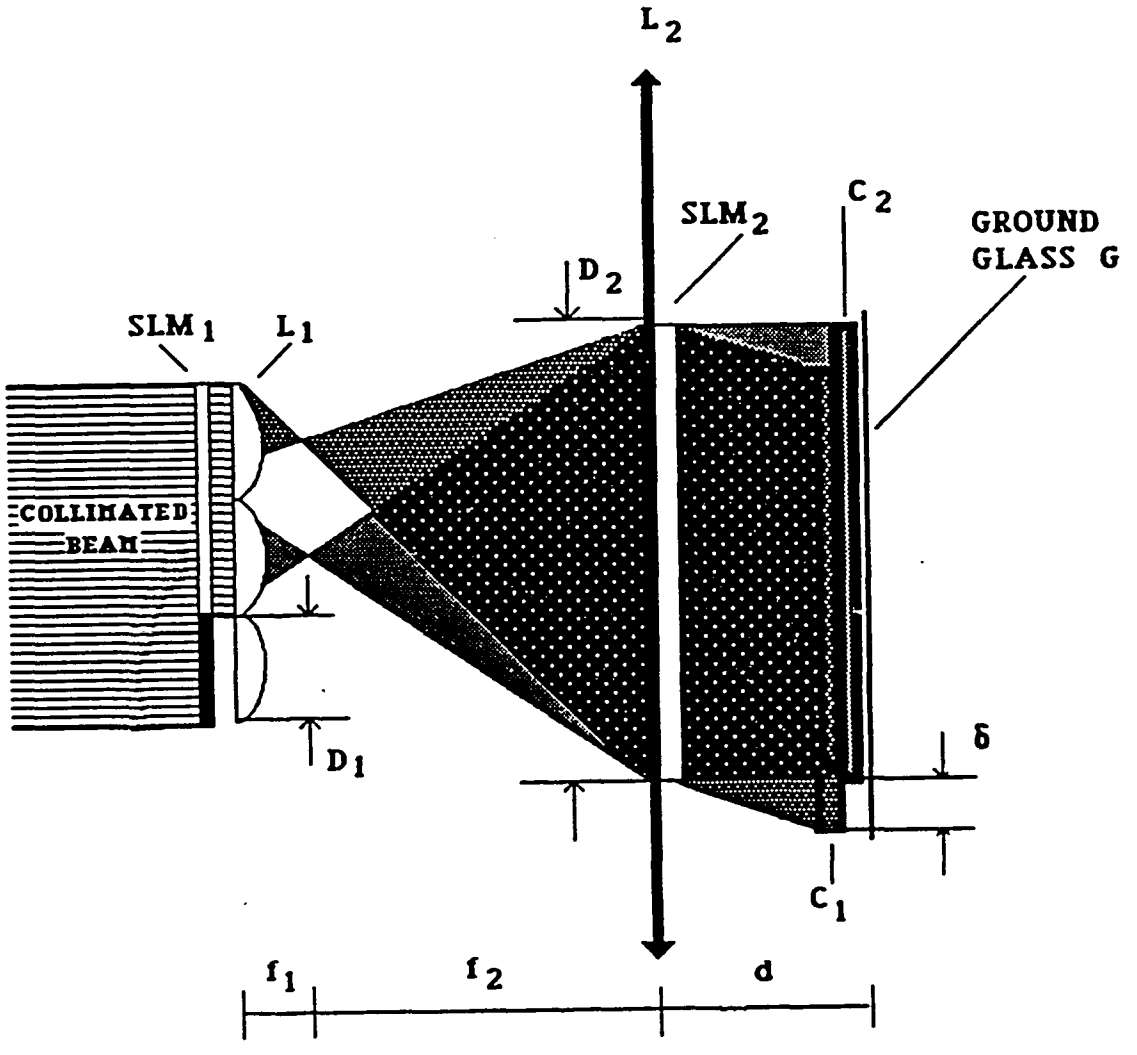


Fig.6.3 Diagram of a lenslet array based recognition system. The programmable lenslet array consists of $SLM_1$ and the lenslet array $L_1$ with an elemental aperture equal to $D_1$. The encoded data are displayed on $SLM_2$ with a dimension of $D_2$. The smallest shift at the output plane is $\delta$. At the output plane, at distance d from lens $L_2$, five shifted copies of the input image are shown.


Fig.6.4 Lenslet array switch configuration corresponding to input symbols: (a) 111 and (b) 110.

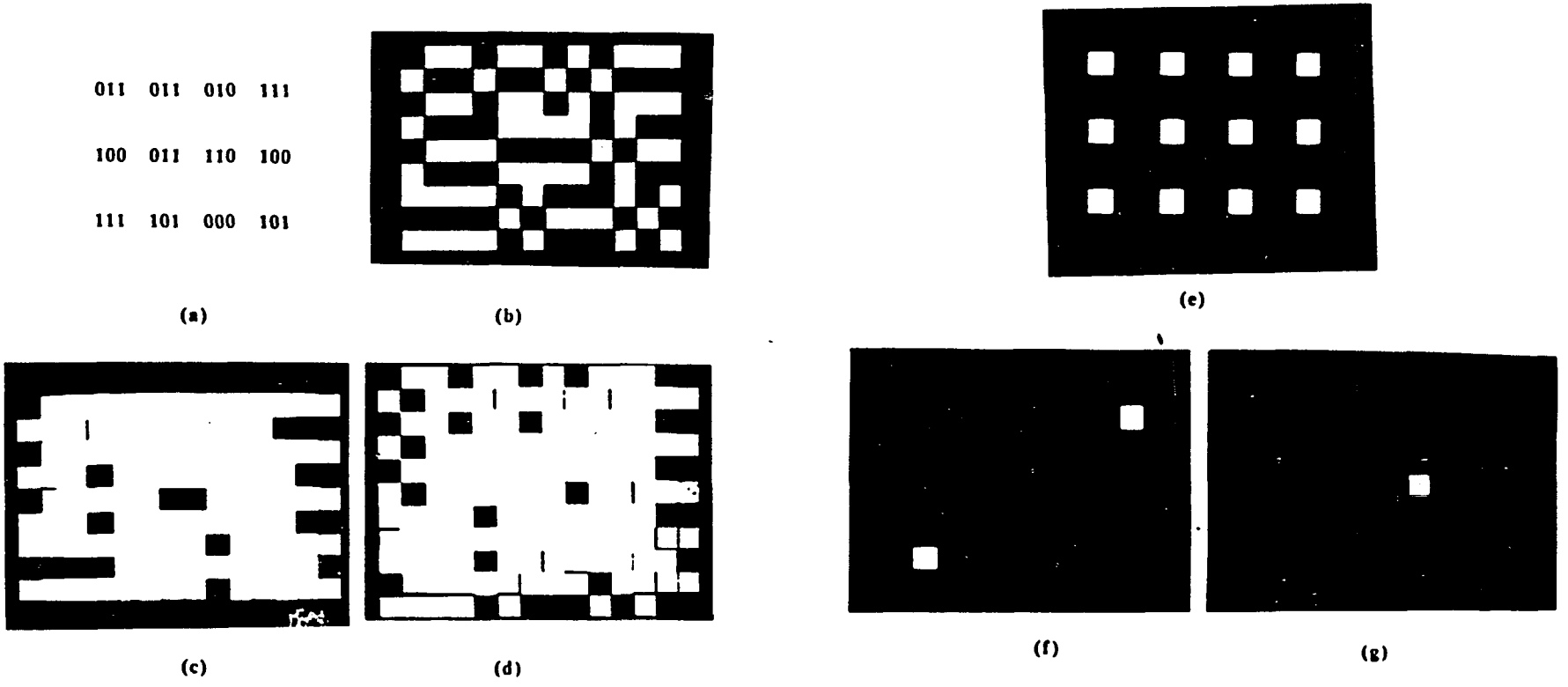


Fig.6.5 Experimental results for a lenslet array based higher-order symbol recognition: (a) binary input data; (b) TR spatially encoded input data; (c), (d) three superimposed shifted copies of the input image used in the recognition of the search symbol 111 (110); (e) binary mask to mask the images of (c) and (d); and (f), (g) results of the image operations. The locations of the high intensity pixels indicate the positions of the search symbol 111 (110) in the input data.

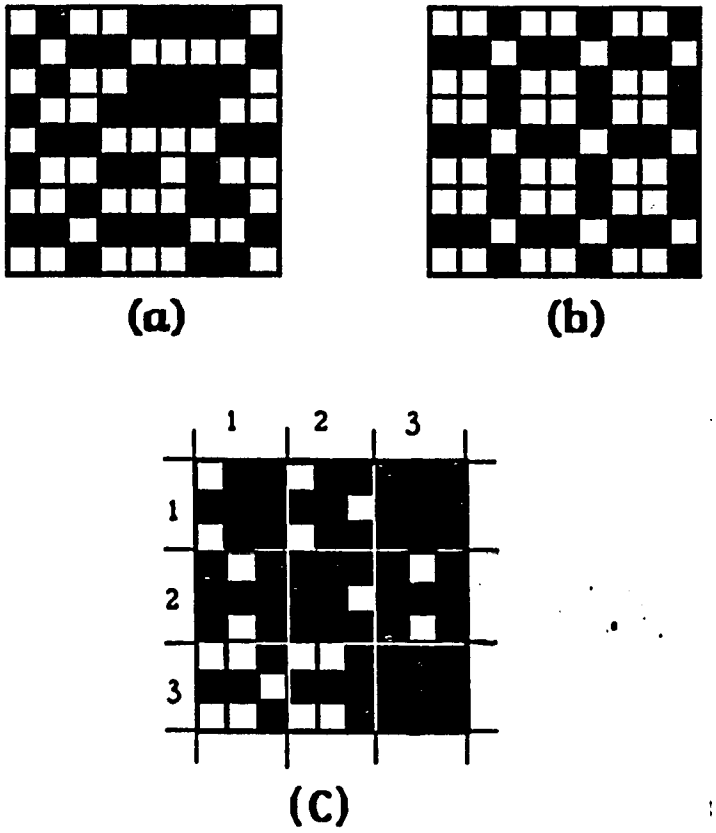


Fig.6.6 (a) Spatially TR encoded input data for a CAM based symbol recognition. (b) The corresponding CAM mask for search symbol 001. It consists of a periodically replicated spatially encoded complemented symbol 100. (c) The result of a CAM recognizer. The location of the search symbol is indicated by a completely blocked 3 X 3 pixel area. Search symbol 001 is located at positions (1,3) and (3,3).

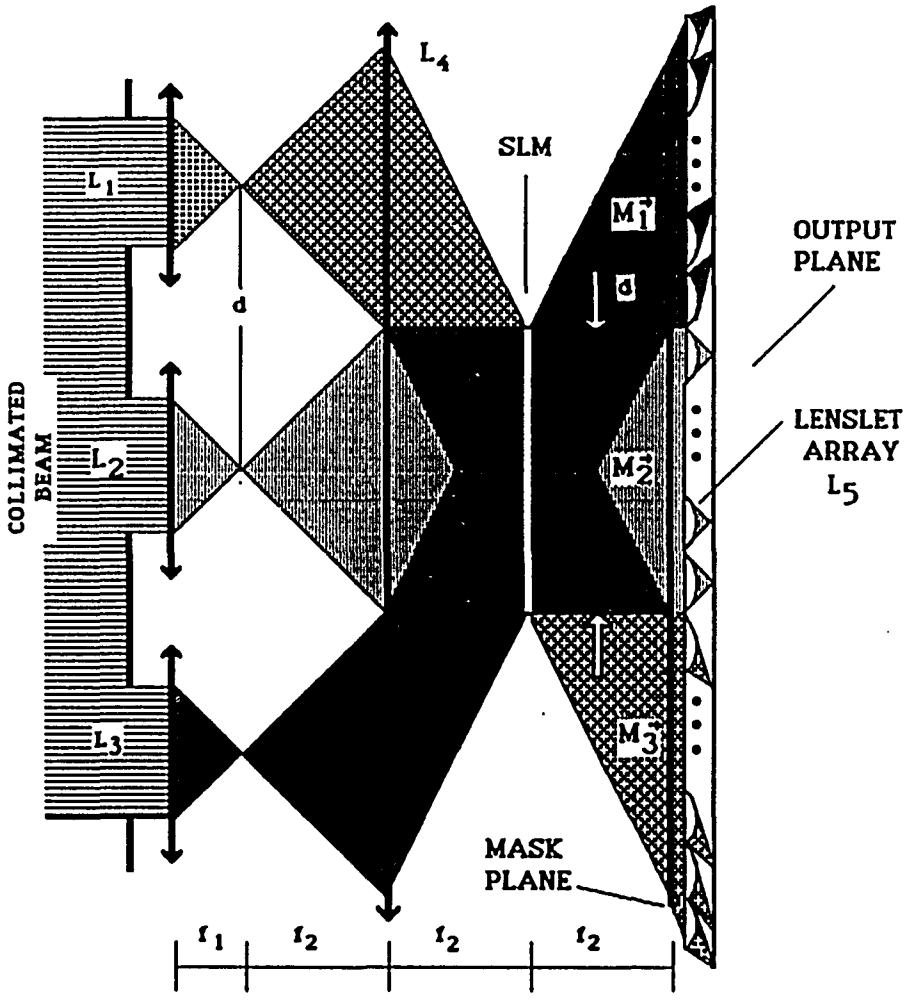


Fig.6.7 A CAM-based system for a three channel symbol recognition. $L_1$ - $L_3$ are lenses of a lenslet array. Lenses $L_1$ - $L_3$ together with a projection lens $L_4$ generate three angle-multiplexed beams, where each channel is used to recognize a different search symbol. The input data is displayed on the SLM. The spacing d between two adjacent light sources is equal to the linear SLM dimension. To recognize three search symbols at the mask plane, three masks ($M_1$, $M_2$ and $M_3$) are placed. Lenslet array $L_5$ performs the light intensity integration over each symbol's aperture.

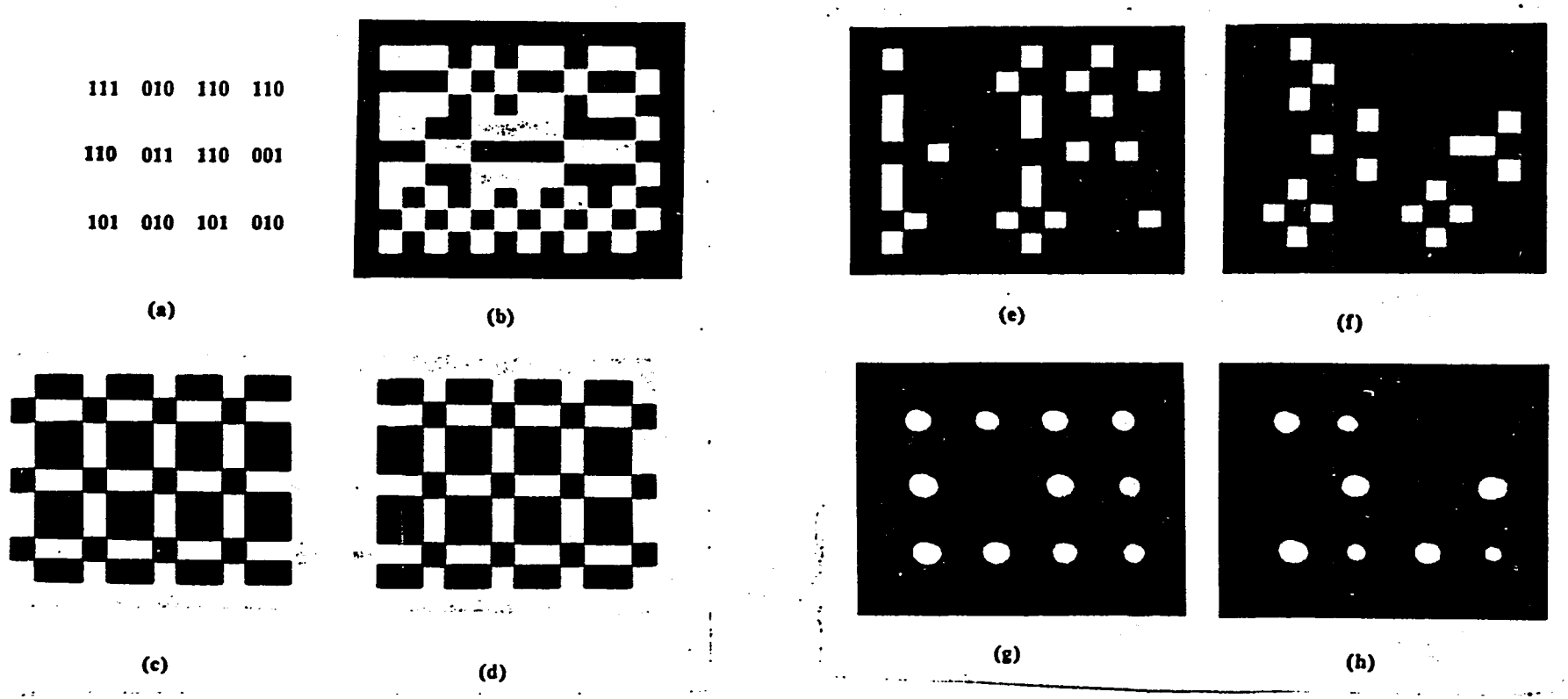


Fig.6.8 Experimental results for a CAM based higher-order symbol recognition: (a) binary input data; (b) TR spatially encoded input data; (c), (d) binary mask to recognize the search symbol 011 (110); (e), (f) masked version of the input image used to recognize the search symbols 011 (110); and (g), (h) for symbols 011 (110), the integration for each of 3 X 3 pixel area results. The positions of the low intensity pixels indicate the position of the search symbol.

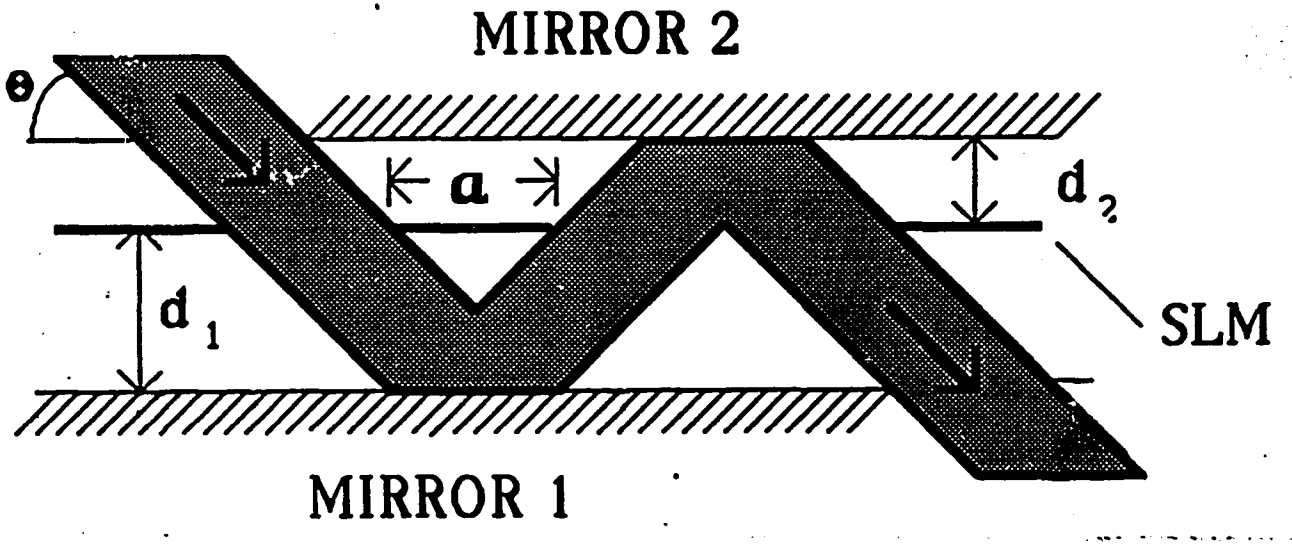


Fig.6.9 Schematic of an optical cavity based multiplicative symbol recognizer: $M_1$ and $M_2$ are mirrors. The spatial symbols (input data) are displayed on the SLM in a vector format. The incident beam angle is $\Theta$ and the SLM pixel dimension is a.

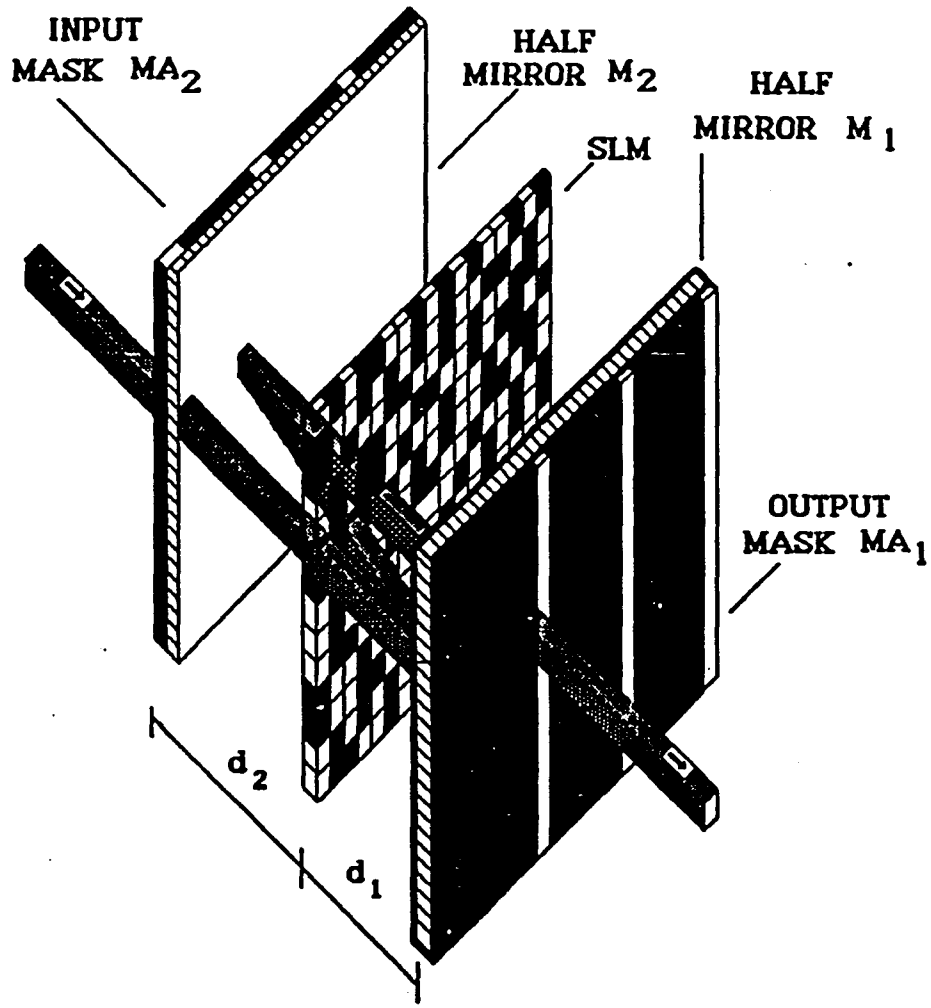


Fig.6.10 Optical architecture of an optical cavity-based symbol recognizer. $MA_1$ and $MA_2$ are binary masks with vertical openings; $M_1$ and $M_2$ are half mirrors. The encoded input data is displayed on the SLM.

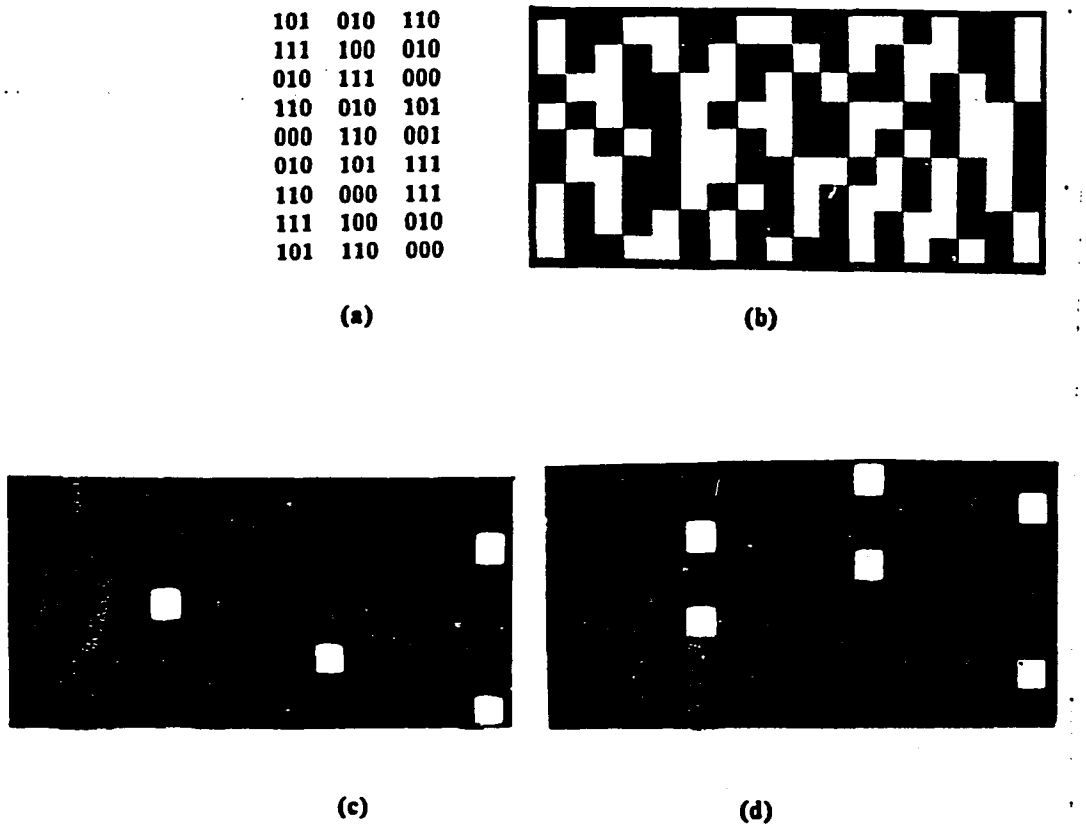


Fig.6.11 Experimental results for an optical cavity-based higher-order symbol recognition: (a) binary input data; (b) spatially DR encoded input data; and (c), (d) positions of the high intensity pixels indicating the locations of search symbols 000 (010) in the input data.

| Input number index | Bit configuration | AND function |
|---|---|---|
| 0 | 000 | $F^0 = x_{11}x_{12}x_{13}$ |
| 1 | 001 | $F^1 = x_{11}x_{12}x_{23}$ |
| 2 | 010 | $F^2 = x_{11}x_{22}x_{13}$ |
| 3 | 011 | $F^3 = x_{11}x_{22}x_{23}$ |
| 4 | 100 | $F^4 = x_{21}x_{12}x_{13}$ |
| 5 | 101 | $F^5 = x_{21}x_{12}x_{23}$ |
| 6 | 110 | $F^6 = x_{21}x_{22}x_{13}$ |
| 7 | 111 | $F^7 = x_{21}x_{22}x_{23}$ |

Table 6.1 Logical function $F^k$ as function of high intensity pixels for 3-bit binary numbers for a dual-rail (DR) encoding scheme.

Superscript k represents input index number. $x_{ij}$ represents high intensity pixels in a 3 bit search symbol. Subscript i is a rail position of the high intensity pixel and subscript j is a bit position in the string of n-bit binary number.

$$F^0 = \overline{x_{21}x_{22}}x_{13} = 0$$
$$F^1 = \overline{x_{21}x_{22}x_{13}} = 0$$
$$F^2 = \overline{x_{21}}x_{22}x_{13} = 0$$
$$F^3 = \overline{x_{21}}x_{22}\overline{x_{13}} = 0$$
$$F^4 = x_{21}\overline{x_{22}}x_{13} = 0$$
$$F^5 = x_{21}\overline{x_{22}x_{13}} = 0$$
$$F^6 = x_{21}x_{22}x_{13} = 1$$
$$F^7 = x_{21}x_{22}\overline{x_{13}} = 0$$

Table 6.2 Logical function representation for 3-bit binary numbers for a triple-rail (TR) encoding scheme.

Superscript k represents input index number. $x_{ij}$ represents high intensity pixels in a 3 bit search symbol. Subscript i is a rail position of the high intensity pixel and subscript j is a bit position in the 3-bit binary number.

| Input number index | Bit configuration | Distance $d_1$ | Distance $d_2$ |
|---|---|---|---|
| 0 | 000 | $2d$ | $2d$ |
| 1 | 001 | $2d$ | $3d$ |
| 2 | 010 | $3d$ | $d$ |
| 3 | 011 | $3d$ | $2d$ |
| 4 | 100 | $d$ | $2d$ |
| 5 | 101 | $d$ | $3d$ |
| 6 | 110 | $2d$ | $d$ |
| 7 | 111 | $2d$ | $2d$ |

Table 6.3 The distances $d_1$ and $d_2$ from the input mask to mirrors $M_1$ and $M_2$, respectively, for the different 3-bit inputs.

For different search symbols, the smallest distance d between the mask and one of the mirrors is equal to $a/2\tan\Theta$, where a is the elemental pixel size and $\Theta$ is the beam incident angle.

# VII SUMMARY AND FUTURE RESEARCH

## 7.1 SUMMARY

In this thesis, several optical information processing approaches, such as switching-, logic-, memory-, and symbolic substitution-oriented optical signal processing techniques, were presented. To maximize the major advantage of optical information processing that is massive parallelism, an appropriate number system for a particular application was investigated. Those number systems are binary number, residue number, and modified signed-digit number systems. Also, various types of optical memories such as content addressable-memory and associative memory were engaged, since the former allows to reduce minterms using logic minimization, while the later provides both the error correcting and information retrieving capability with imperfect or incomplete input data, respectively. As the result of the same purpose, position coded look-up table processing technique was applied to providing fast crossbar switching operation. Lenslet array, because of its unique property to provide easily programmability, multiple replicas images, and multiple sources of delta function. To apply to integrated optical processing, some optical cavity-based approaches were also introduced.

Because of the frequent usage of the BN system in conventional computers, ease of input/output interfacing is achieved using BN system. The major drawback of BN system is the time-consuming and hardware complexity due to carry propagation. This drawback was easily and efficiently overcome by drafting carry look-ahead addition algorithm and content addressable-memory [1-3].

Residue number system is one of the frequently applied for optical arithmetic processing. Since the number system provides relatively high dynamic range using larger moduli, ease decomposition offering more efficient parallel

processing architecture, and non-carry propagation yielding less hardware complexity and fast processing speed.

The modified signed-digit number representation is an attempt to have the best of both worlds: easy-to-use fixed radix numbers and carryless concurrent calculations. One advantage of the MSD number system is its parallel addition and subtraction capability. The addition and subtraction operation can be performed using an array of four 2-bit MSD logic gates. Using the above logic gates requires three cascading stages which yields hardware complexity. This drawback is overcome by applying content addressable memory and logic minimization. In this thesis, using all the previously mentioned number systems and optical elements, four types of optical information processing schemes were implemented such as switching-, logic-, memory-, and symbolic substituion-oriented optical signal processors.

In case of the switching-oriented optical signal processors, using an optical cavity and two identical inexpensive LCTVs together with hologram an optical programmable logic array processor and a LCTV-based optical position coded residue processor were implemented, respectively. For the optical logic array processor, there are two major advantages. First, using the normal incidence angles, unlike other existing SLM-based multiple beam path schemes, this architecture provided the best SLM performance. Second, using the folded 4f imaging system this processor offered less diffraction noise and capability of the integrated architecture. For the PCRN processor, the use of a single laser source together with two commercial LCTVs eliminated the complexity of the LED arrangement. Using a number of moduli, high dynamic range computation and decomposition processing scheme were obtained. As a switching operation, using angularly multiplexing reference beams and together with a projection lens, the results were mapped for each truth-table point to a proper PCRN results plane position which reduce, the number of detectors by only the number of different outputs.

In case of the logic-oriented optical signal processors, two optical signal processing schemes were implemented. First, using an EXCLUSIVE-OR logic operation, a noncoherent optical pyramidal tracking novelty filter was presented. In this approach, an optical image subtraction technique was drafted using two identical inexpensive LCTVs. This image subtraction scheme provided fast processing speed and less hardware complexity compared to conventional electronic processing. Second, based on AND (performed via SHIFT-OR-THRESHOLD operation) followed by an INVERSION logic operation, an optical morphological image processor was presented. There are three major advantages of this scheme. First, any shape and size of structuring element can be processed. This advantage is achieved by varying the distance between the lenslet array and the second SLM located on the output plane. Second, unlike the electronic mesh-type celluar array, to realize real-time parallel architecture it does not need massive wire interconnects causing hardware complexity. Finally, the CLOSING operation can be performed by only cascading two optical DILATION operations followed optical inversion, which leads to less hardware complexity and simple processing algorithm.

For the memory-oriented signal processors, two optical arithmetic processors were implemented. In case of the CAM-based single-stage optical MSD processor, both MSD number system and optical non-holographic CAM were engaged. Unlike the time-consuming and hardware complexing three-stage scheme, the suggested new single-stage scheme offered fast processing speed, less minterms yielding high space-bandwidth-product, and capability of processing multi-channel processing. The other memory-oriented optical signal processor is the optical holographic associative memory-based parallel register transfer processor. This processor utilized the unique property of the associative memory such as signal recovery and error correcting capability. As the result of the property of the associative memory, the output pattern was detected on the output plane.

Finally, in this thesis, symbolic substitution-oriented signal processors were

presented. For the optical cavity approach, by placing an encoded mask (SLM) inside an optical cavity optical implementation of logical AND functions was achieved. Varying the distance between SLM and the mirrors, each channel processor was implemented for all the possible input combinations. For non-coherent correlation approach, to generate shifted replicas of an input image, a new simple lenslet array architecture was proposed. In this scheme, using SLM and the lenslet array, any multi-bit search symbol recognition was achieved. To optically implement higher-order symbol recognition, using a CAM techniques, an input image was superimposed with a fixed binary cam mask. This CAM approach utilized a binary periodic mask which is a bit-wise complemented image of the search symbol.

## 7.2 FUTURE RESEARCH DIRECTION

During my doctoral studies, I have conducted research in three major fields in optical signal processing: optical image, arithmetic and symbolic processing. To implement efficient optical processors, various number system and memory issues have been investigated and utilized. My future research goal will be to improve and modify the proposed schemes, and to develop new schemes.

In this thesis, only symbolic recognition scheme has been studied and implemented. In future research, I will conduct the research for parallel processor array based on optical symbolic substitution, with implementing symbolic substitution schemes. The potential capability of parallel multi-processor computational system can be fully utilized with fast parallel interconnect network. Optical processing can relieve some problems associated with electronic multi-processor systems. Symbolic substitution can be used to design highly parallel computing systems with more than $10^5$ parallel processors working in a single instruction multiple data (SIMD) or multiple instruction multiple data (MIMD) modes.

Present day digital electronic computers based on BN system can perform arithmetic operations with certain accuracy. In order to represent rational numbers in a binary computer, inevitable truncation error is made when an infinite string of digits must be substituted by a finite representation. However, digital computers can perform error-free computations for integer addition and multiplication. By mapping rational numbers (fractions) onto an corresponding integer set, only addition and multiplication are needed to perform subtraction and division operations, respectively. To perform so called "error-free" arithmetic computations, Hensel code, multiple residue periodic number system, can be used. The Hensel code based error-free computations can be implemented using content addressable memory. Due to large memory capacity requirements for high dynamic range calculations, a novel optical CAM is needed. Major

advantages of the optical CAM are high storage capability, reducibility of minterms by applying logic minimization and don't care term, ease in optical implementation and high processing speed.

Another goal of my future research is to investigate multi-radix number system-based arithmetic computation, especially decimal number-based computation. Although this approach causes carry propagation and hardware complexity, it can provides extremely high dynamic range, fast computation speed, free of number conversion from decimal to binary and vice versa, and user friendly system by utilizing optical CAM together with the major advantage of optics; spatial frequency (spatial encoding technique).

Other future research directions include optical interconnects based on the $N^4$ weighted neuron-based interconnect technique, optical neural networks based on the multi-wavelength multiplexing technique and an associative memory, and syntactic discrimination/estimation filters based on an optical holographic associative memory and Hough transformation.

## VIII APPENDIX

List of Abbreviation used in the Thesis

| | |
|---|---|
| AM | - associative memory |
| BN | - binary number |
| CAM | - content addressable memory |
| CCD | - charge-coupled device |
| CLA | - carry look-ahead adder |
| COTNF | - coherent optical tracking novelty filter |
| DFT | - discrete Fourier transform |
| DR | - dual-rail |
| E-SLM | - electrically addressed spatial light modulator |
| LAM | - location addressable memory |
| LC | - liquid crystal |
| LCSLM | - liquid crystal spatial light modulator |
| LCTV | - liquid crystal television |
| LD | - laser diode |
| LED | - light emitting diode |
| MF | - morphological filtering |
| MSB | - most significant bit |
| MSD | - modified signed digit |
| MQW | - multiple quantum well |
| MVLPT | - multiple variable logic product term |
| NLFPE | - nonlinear Fabry-Perot etalon |
| NOTNF | - noncoherent optical tracking novelty filter |
| OHASS | - optical holographic associative symbolic substitution |
| OMF | - optical morphological filtering |
| OPLA | - optical programmable logic array |

ORTMOs - optical register transfer microoperations

ORTP - optical register transfer processor

O-SLM - optically addressed spatial modulator

PCRN - position coded residue number

PLA - programmable logic array

RN - residue number

RTL - register transfer language

SBP - space-bandwidth product

SEED - self-electrooptic effect device

SLM - spatial light modulator

SLN - sign-logarithm number

SNR - signal-to-noise ratio

SS - symbolic substitution

SSFLC - surface stabilized ferroelectric liquid crystal

TNF - tracking novelty filter

TR - triple-rail

## IX PUBLICATIONS RELATED TO THESIS

*- Journal Publications*

1. "Free-Space Folded-Path Optical Programmable Logic Array", (with Y. Li, A. Kostrzewski and G. Eichmann), Opt. Lett., Vol. 13, 895 (1988).
2. "A Liquid-Crystal-TV-Based White Light Optical Tracking Novelty Filter", (with Y. Li, A. Kostrzewski and G. Eichmann), Appl. Opt., Vol. 28, 4861 (1989).
3. "A Compact Parallel Real-Time Programmable Optical Morphological Image Processor", (with Y. Li, A. Kostrzewski and G. Eichmann), Opt. Lett., Vol. 14, 981 (1989).
4. "Optical Position Coded Residue Processor using Inexpensive LCTV Devices", (with A. Kostrzewski, Y. Li, B. Ha and G. Eichmann), Appl. Opt., Vol. 28, 415 (1989).
5. "Optical Position-Coded Multiple-Valued Logic and Arithmetic using Liquid-Crystal TVs and Holograms", (with Y. Li, B. Ha, A. Kostrzewski and G. Eichmann), Opt. Comm., Vol. 70, 379 (1989).
6. "Optical Parallel Register Transfer Microoperations using a Holographic Associative Symbolic Substitution", (with G. Eichmann, A. Kostrzewski and Y. Li), Appl. Opt., Vol. 28, 3860 (1989).
7. "Content Addressable Memory Based Single-Stage Optical Modified Signed Digit Arithmetic", (with Y. Li, A. Kostrzewski and G. Eichmann), Opt. Lett., Vol. 14, 1254, (1989).
8. "Optical Higher-Order Symbolic Recognition", (with G. Eichmann, A. Kostrzewski and Y. Li), Appl. Opt., Vol. 29, 2135 (1990).
9. "Fast Hybrid Parallel Carry Look-Ahead Adder", (with A. Kostrzewski, Y. Li and G. Eichmann), Opt. Lett., Vol. 15, 915 (1990).

10. "Parallel Optical Content Addressable Memory (CAM) Arithmetic Multi-Processor", (with A. Kostrzewski, G. Eichmann and Y. Li), Int. J. of Optical Computing, Vol. 1, 5 (1990).
11. "Fast Optical Binary Multiplication using a Sign/Logarithm Number System", (with A. Kostrzewski, G. Eichmann and Y. Li), Opt. Lett., Vol. 16, 91 (1991).

*- Other Publications*

12. "Parallel Optical Pyramidal Image Processing", (with G. Eichmann, A. Kostrzewski and Y. Li), SPIE Vol. 939, Hybrid Image and Signal Processing, 93 (1988).
13. "Compact Free-Space Optical Programmable Logic Array", (with Y. Li, A Kostrzewski and G. Eichmann), Technical Digest of the 1988 OSA Annual Meeting, Vol. 11, 59 (1988).
14. "Optical Liquid Crystal TV and Hologram-based Position-Coded Multiple-Valued Logic and Arithmetic Operations", (with A. Kostrzewski, Y. Li, B. Ha and G. Eichmann), Technical Digest of the 1988 OSA Annual Meeting, Vol. 11, 65 (1988).
15. "Optoelectronic Content Addressable Memory-Based Modified Signed Digit Arithmetic", (with Y. Li, A. Kostrzewski and G. Eichmann), Technical Digest of the 1989 OSA Annual Meeting, Vol. 18, 118 (1989).
16. "Optical Pyramidal Processing Based-On Noncoherent Tracking Novelty Filter", (with Y. Li, A. Kostrzewski and G. Eichmann), SPIE Proceeding Vol. 1151, Optical Information Processing Systems and Architectures, 292 (1989).
17. "Real-Time Optical Morphological Image Processor Based-On Programmable Lenslet Array", (with Y. Li, A. Kostrzewski and G. Eichmann), Presented at Gordon Research Conference on Holography and Optical Information Processing (Plymouth, N.H., 1989).

18. "A Non-Coherent Optical Tracking Novelty Filter", (with Y. Li, A. Kostrzewski and G. Eichmann), Presented at Gordon Research Conference on Holography and Optical Information Processing (Plymouth, N.H., 1989).
19. "Real Time Programmable Optical Morphological Filter", (with Y. Li, A. Kostrzewski and G. Eichmann), Technical Digest of the 1989 OSA Annual Meeting, Vol. 18, 195 (1989).
20. "An Optical-Holographic-Associative-Memory-Based Parallel Register Transfer Processor", (With G. Eichmann, A. Kostrzewski and Y. Li), Optical Computing 1989 Technical Digest Series Vol. 9, 240 (1989).
21. "Hybrid Content Addressable Memory MSD Arithmetic", (with Y. Li, A. Kostrzewski and G. Eichmann), SPIE Proceeding Vol. 1215, Digital Optical Computing II, 34 (1989).
22. "Hybrid Higher Order Optical Symbolic Recognition", (with G. Eichmann, A. Kostrzewski and Y. Li), SPIE Proceeding Vol. 1215, Digital Optical Computing II, 51 (1989).
23. "Non-Holographic Content Addressable Memory Based Arithmetic Processor", (with A. Kostrzewski, Y. Li and G. Eichmann), SPIE proceeding Vol. 1230, 725 (1990).
24. "Fast Optical Digital Arithmetic Processors", (with Y. Li, A. Kostrzewski, B. Ha and G. Eichmann), SPIE Proceeding Vol. 1296, Advanced in Optical Information Processing IV, (1990).
25. "A Sign/Logarithm Number System-based Fast Optical Multiplier", (with A. Kostrzewski, Y. Li and G. Eichmann), Tehnical Digest of the 1990 OSA Annual Meeting, Vol. 15, 124 (1990).
26. "An Optical Carry Look-Ahead Adder Based On a Content Addressable Memory", (with A. Kostrzewski, Y. Li and G. Eichmann), Tehnical Digest of the 1990 OSA Annual Meeting, Vol. 15, 123 (1990).

27. "Optical Higher-Order Symbolic Substitution", (with G. Eichmann, A. Kostrzewski and Y. Li), Tehnical Digest of the 1990 OSA Annual Meeting, Vol. 15, 124 (1990).

28. "Optical Binary Multiplication based on A Non-Holographic Content Addressable Memory", (with A. Kostrzewski, Y. Li and G. Eichmann), Optical Computing 1991 Technical Digest Series, Vol. 5, 18 (1991).

## X BIBLIOGRAPHY


Anderson, D. Z., Lininger, D. M., and Feinberg, J., "Optical tracking novelty filter," Opt. Lett. 12, 123 (1987).

Arrathoon, R., "Logic based spatial light modulators," Proc. SPIE, 881 230-239 (1988).

Arrathoon, R., and Kozaitis, S., Proc. SPIE, 752, 34 (1987).

Arrathoon, R., and Kozaitis, S., "Architectural and Performance Consideration for $10^7$-Instruction/sec Optoelectronic Central Processing Units," Opt. Lett. 12, 956 (1987).

Avizienis, A., "Signed-Digit Number Representations for Fast Parallel Aruthmetic," IRE Trans, Electronic Computers, EC-10,389 (1961).

Bocker, R. P., Drake, B. L., Lasher, M. E., and Henderson, T. B., " Modified-Signed Digit Addition and Subtraction using Symbolic Substitution," Appl. Opt. 25, 2456-2457 (1986).

Boivin, L. P., "Multiple imaging using various types of simple phase gratings," Appl. Opt. 11, 1782-1792 (1972).

Brenner, K-H., "Programmable Optical Processor based on Symbolic Substitution," Appl. Opt, 27 1687-1691 (1988).

Brenner, K-H., Huang, A., and Streibl, N., "Digital optical computing with symbolic substitutions," Appl. Opt. 25, 3054-3060 (1986).

Brenner, K-H., Lohmann, A. W., and Merklein, T. M., "Symbolic Substitution Implemented by Spatial Filtering Logic," Opt. Eng. 28, 390-395 (1989).

Brenner, K-H. and Sauer, F., "Diffractive-Refractive Optical Interconnects," Appl. Opt. 27, 4251-4254 (1988).

Brubaker, T. A. and Becker, J. C., "Multiplication using Logarithms Implemented with Read-Only Memory," IEEE Trans. Comput.,24, 761, (1974).

Burt, P. J., "The pyramid as a structure for efficient computation," in *Multiresolution Image Processing and Analysis*, A. Rosenfeld, ed. (Springer-Verlag, Berlin, 1984) Ch. 2.

Capps, C. D., Falk, R. A., and Hook, T. L., "Optical Arithmetic/Logic Unit based on Residue Arithmetic and Symbolic Substitution," Appl. Opt. 27, 1682-1686 (1988).

Cavanagh, J. J., *Digital Computer Arithmetic.* New York: McGraw-hill, 1984.

Casasent, D. and Botha, E., "Optical Symbolic Substitution for Morphological Transformations," Appl. Opt. 27, 3806-3810 (1988).

Casasent, D. and Botha, E., "Optical Symbolic Substitution for Morphological Transformations," Appl. Opt. 27, 3806 (1988).

Casasent, D. and Botha, E., "Multifunctional Optical Processor based on Symbolic Substitution," Opt. Eng. 28, 425-433 (1989).

Casasent, D. and Xia, S. F., "Phase correction of light modulators," Opt. Lett. 11, 398 (1986).

Chiou, A. E. and Yeh, P., "Parallel image subtraction using a phase-conjugation Michelson interferometer," Opt. Lett. 11, 306 (1986).

Combet, M., Van Zonneveld, H., and Verbeek, L., "Computation of the base two logarithm of binary numbers," IEEE Trans, Electronic Computers, vol. EC-14, 863, (1965).

Dashiell, S. R., Lohmann, A. W., and Michaelson, J. D., "Real-time coherent optical-electronic image subtraction," Opt. Comm. 8, 105 (1973).

Drake, B. L., Bocker, R. P., Lasher, M. E., Patterson, R. H., and Miceli, W. J., Opt. Eng. 25, 38 (1986).

Davio, M., Deschamps, J-P., and Thayse, A., *Digital Systems with Algorithm Implementation*, (John Wiley, New York, 1983), ch.3.

Eichmann, G. and Basu, S., "Parallel Optical Syntactic Pattern Recognizer," Appl. Opt. 26, 1859-1865 (1987).

Eichmann, G., Kostrzewski, A., Ha, B., and Li, Y., "Parallel optical pyramidal image processing," Opt. Lett. 13, 431 (1988).

Eichmann, G., Kostrzewski, Kim, D. H., and Li, Y., "Optical Parallel Register Transfer Microoperations using Holographic Symbolic Substitution," Appl. Opt. 28, 3860-3863 (1989).

Eichmann, G., Lu, C., Zhu, J., and Li, Y., "Pyramidal Image Processing Using Mathematical Morphology," Proc. Soc. Photo-Opt. Instrum. 974, (1988).

Eichmann, G., Zhu, J., and Li, Y., "Optical Parallel Image Skeletonization using Content-addressable Memory-based Symbolic Substitution," Appl. Opt. 27, 2905-2911 (1988).

Feinberg, J., "Interferometer with a self-pumped phase conjugation mirror," Opt. Lett. 8, 569 (1983).

Feldman, M. R., Esener, S. C., Guest, C. C., and Lee, S. H., "Comparison between optical and electronical interconnects based on power and speed considerations," Appl. Opt. 27, 1742-1751 (1988).

Flores, I., *The Logic of Computer Arithmetic.* New York: Van Nostrsand, 1955.

Ford, J. E., Fainman Y., and Lee, S. H., "Time integrating interferometry using photorefractive fanout," Opt. Lett. 13, 856 (1988).

Goodman, S. D. and Rhodes, W. T., "Symbolic Substitution Applications to Image Processing," Appl. Opt. 27, 1708-1714 (1988).

Goutzoulis, A. P., "Complexity of residue position-coded lookup table array processor," Appl. Opt. 26, 4823 (1987).

Goutzoulis, A. P., Davis, D. K., and Malarkey, E. C., "Prototype position-coded look-up table using laser diodes," Opt. Comm. 61, 302 (1987).

Guest, C. C. and Gaylord, T. K., "Truth-table look-up optical processing utilizing binary and residue arithmetic," Appl. Opt. 19, 1201 (1980).

Guilfoyle, P. S. and Wiley, W. J., "Combinatorial logic based digital optical computing," Appl. Opt. 27, 1661-1673 (1988).

Habiby, S. F. and Collins, S. A., Jr., "Implementation of a fast digital optical matrix-vector multiplier using a holographic lookup table and residue arithmetic," Appl. Opt. 26, 4639-4651 (1987).

Haralik, R. M., Sternberg, S. R., and Zhuang, X., "Morphological Skeleton Representation and Coding of Binary Images," IEEE Trans. Acoust. Speech Signal Process. ASSP-34, 1228 (1986).

Harata, Y., Nakamura, Y., Nagase, H., Takigawa M., and Takagi, N., Proc. ICCD'84, Oct. 1984.

Henkel, H., "Improved Addition for the Logaithmic Number System," IEEE Trans. ASSP, 37, 301 (1989).

Huang, A., "Parallel Algorithms for Optical Digital Computers," Proceeding of the Tenth International Optical Computing Conference, 13-17 (IEEE Computer Society, Los Angeles, 1983).

Huang, A., Tsunida, Y., Goodman, J., and Ishihara, S., "Optical computation using residue arithmetic," Appl. Opt. 18, 149 (1979).

Huang, K. S., Jenkins, B. K., and Sawchuk, A. A., Proc. IEEE Computer Society Workshop on Computer Architecture for Pattern Analysis and Machine Intelligence, Seattle, Washington, Oct. (1987).

Hughes, K. D., Rogers, S. K., Mills, J. P., and Kabrisky, M., "Optical preprocessing using liquid crystal televisions," Appl. Opt. 26, 1042 (1987).

Hwang, K. H., and Louri, A., "Optical Multiplication and Division using Modified-Signed-Digit Symbolic Substitution," Opt. Eng. 28, 364-372 (1989).

Ichioka, Y. and Tanida, J., "Optical Parallel Logic Gates using A Shadow-Casting System for Optical Digital Computing," IEEE Proc. 72, 787 (1984).

Jahns, J. and Huang, A., "Planar Integration of Free-space Optical Components," Appl. Opt. 28, 1602-1605 (1989).

Jang, J. S., Shin, S. Y., and Lee, S. Y., "Adaptive Two-Dimensional Quadratic Associative Memory using Holographic Lenslet Arrays," Optical Computing in 1989 the Technical Digest Series, 40-43 (OSA, Salt Lake City, 1989).

Johnson, K. M., Surette, M. R., and Shamir, T., "Optical interconnection network using polarization-based ferroelectric liquid crystal gates," Appl. Opt. 27, 1727 (1988).

Kiamilev, F., Esener, S. C., Fainman, Y., Guest, C. C., and Lee, S. H., "Programmable Optoelectronic Multiprocessor and their Comparison with Symbolic Substitution for Digital Optical Computing," Opt. Enf. 28, 396-409 (1989).

Kohonen, T., *Self-Organization and Associative Memory* (Springer-Verlag, New York, 1984) Ch.4.

Kostuk, R. K., Kato, M., and Huang, Y-T., "Substrate Mode Holograms for Optical Interconnect," Technical Digest of OSA Topical Meeting on Optical computing, Vol. 9, 168-171 (1989).

Kozaitis, S. P., "Higher-Ordered Rules for Symbolic Substitution," Opt. Comm. 65, 339-342 (1988).

Kwong, S., Rakuljic, G. A., and Yariv, A., "Real-time image subtraction and "exclusive or" operation using a self-pumped phase conjugation mirror," Appl. Phys. Lett. 48, 201 (1986).

Lee, W. H., "High efficiency multiple beam gratings," Appl. Opt. 18, 2152-2158 (1979).

Leith, E. N., "Complex spatial filters for image deconvolution", Proceedings of the IEEE 65 (1), 18-28, (1977)

Li, Y. and Eichmann, G., "Multipass Counterrotaing Wave-Plate Frequency Shifts for Hetrodyne Interferometry," Opt. Lett. 11, 718-720 (1986).

Li, Y. and Eichmann, G., "Conditional Symbolic Modified Signed-Digit Arithmetic using Optical Conten-Addressable Memory Logic Elements," Appl. Opt. 26, 2328-2333 (1987).

Li, Y. and Eichmann, G., Dorsinville, R., and Alfano, R. R., "An AND operation-based symbolic pattern recognizer," Opt. Comm. 63, 375-379 (1987).

Li, Y. and Eichmann, G., Dorsinville, R., and Alfano, R. R., "Parallel Digital and Symbolic Optical Computation via Optical Phase Conjugation," Appl. Opt. 27, 2025-2032 (1988).

Li, Y. and Eichmann, G., Dorsinville, R., and Alfano, R. R., "Demonstration of a picosecond optical residue computation," Opt. Lett. 13, 178 (1988).

Li, Y., Kostrzewski, A., Kim, D. H., and Eichmann, G., "A Compact Real-Time Programmable Optical Morphological Image Processor," Opt. Lett. 14, 981-983 (1989).

Liu, H. K., Davis, J. A., and Lilly, R. A., "Optical data processing properties of a liquid-crystal TV spatial light modulator," Opt. Lett. 10, 635 (1985).

Livescu, G., Miller, D. A. B., Henry, J. E., Gossard, A. C., and English, J. H., "Spatial light modulator and optical dynamic memory using a 6 times 6 array of self electro-optic-effect devices," Opt. Lett. 13, 297-299 (1988).

Lu, C., Eichmann, G., Zhu, J., and Li, Y., "Pyramidal image processing using mathematical morphology," Proc. SPIE, 974, 30 (1988).

Mait, J, N., "Design of Dammann Gratings for Optical Symbolic Substitution," Proceeding SPIE 963, 646-652 (1988).

Mait, J. N. and Brenner, K-H.,"Optical Symbolic Substitution: System Design using Phase-only Holograms," Appl. Opt. 27, 1692-1700 (1988).

Mano, M. M., *Computer System Architecture*, (Prentice-Hall, NJ, 1982) ch.4.

Maragos, P., Opt. Eng. 26, 623 (1987).

Matthijsse, P., "Multiple imaging with thin phase filters: a signal processing approach," J. Opt. Soc. Am. 68, 733-738 (1978).

McDonald, R. I., "Optoelectronic switch matrix as look-up table for residue arithmetic," Opt. Lett. 12, 787 (1987).

McEwan, J. A., Fisher, A. D., Rolsma, P. B., and Lee, J. N., J.Opt.Soc.Am. A2, 8 (1985).

McManus, J. B., Putnam, R. S., and Caulfield, H. J., "Swithed Holograms for Reconfigurable Optical Interconnection: Demonstartion of a Prototype Device," Appl. Opt. 27, 4244-4250 (1988).

Michell, J. N., IRE Trans. Electron. Comput., pp 512-517, Aug. (1962).

Miller, D. A. B., "Quantum Wells for Optical Information Processing," Opt. Eng. 26, 2059-2069 (1987).

Miller, D. A. B., Chemla, D. S., Damen, T. C., Gossard, A. C., Wiegmann, W., Wood, T. H., and Burrus, C. A., "Novel Hybrid Optically Bistable Switch: The Quantum Well Self Electro-optic Effect Device," Appl. Phys. Lett. 45, 13-15 (1984).

Miller, D. A. B., Chemla, D. S., Damen, T. C., W., Wood, T. H., Burrus, C. A., Gossard, A. C., and Wiegmann, W., "The Quantum Well Self Electro-optic Effect Device: Optoelectronic bistablility and Oscilation, and Self-lineared Modulation," IEEE J. Quantum Electronic QE-21, 1462-1476 (1985).

Mirsalehi, M. M. and Gaylord, T. K., "Truth-Table Look-up Parallel Data Processing using on Optical Content-Addressable Memory," Appl. Opt. 17, 2277-2283 (1986).

Mirsalehi, M. M., Gaylord, T. K., Fielder, D. C., and Guest, C. C., "Number Representation Effects in Truth-Table Look-Up Processing: 8-Bit Addition Example," Appl. Opt. 28, 1931-1939 (1989).

Mok, F., Diep, J., Liu, H-K., and Psaltis, D., "Real-time computer-generated hologram by means of liquid-crystal television spatial light modulator," Opt. Lett. 11, 748 (1986).

Murdocca, M. J., "Digital Optical Computing with One-Rule Cellular Automata," Appl. Opt. 26, 682-688 (1987).

Murdocca, M. J., "Theory and Applications of Free-space Digital Optical Computing," Ph.D. Dissertation, (The State University of New Jersey at Rutgers, 1988). Ch.6.

Ogura, T., Yamada, S-I., and Nikaido, T., IEEE J. Solid State Circuits SC-20, 1277 (1985).

O'Neill, K. S. and Rhodes, W. T., Proc. Soc. Photo-Opt. Instrum. Eng. 638, 41 (1986).

Peyghambarian, N. and Gibbs, H. M., "Optical Bistability for Optical Signal Processing and Computing," Opt. Eng. 24, 68-73 (1985).

Preston,K. Jr., *Coherent optical computers*, McGraw-Hill, 1972

Ramamoorthy, P. A. and Anthony, S., Opt. Eng. 26, 1169 (1987).

Ramamoorthy, P. A., Anthony, S., and Grogan, T. A., "Symbolic-Substitution-based Median Filters," Opt. Eng. 27, 409-412 (1988).

Sakaguchi, M., Nishida, N., and Nemoto, T., "A New Associative Memory Systems Utilizing Holograpy," IEEE Trans. Comput. C-19, 1174 (1970).

Serra, J., *Image Analysis and Mathematical Morphology*, (Academic, New York, 1982).

Sicuranza, G. L., "On Efficient Implementations of 2-D Digital Filters using Logarithmic Number Systems," IEEE Trans. ASSP, 31, 877 (1983).

Smith, S. D., Walker, A. C., Wherrett, B. S., Tooley, F. A. P., Mathew, J. G. H., Taghizadeh, M. R., and Janossy, I., "Cascadable Digital Optical Logic Circuit Elements in the Visible and Infared: Demonstration of Some First All-optiical Circuits," Appl. Opt. 25, 1586-1564 (1986).

Suzuki, Y., Hara, T., Ooi, Y., and Wu, M. H., "Optical Transfer Characteristics of Microchannel Spatial Light Modulator," Proc. SPIE, 881 (1988).

Szabo, N. S. and Tanada, R., *Residue Arithmetic and Its Application to Computer Technology*. New York: McGraw-Hill, 1967.

Tai, A. M., Cindrich, I., Fienup, J. R., and Alexsoff, C. C., "Optical residue arithmetic computer with programmable computation modules," Appl. Opt. 18, 2182 (1979).

Tanida, J. and Ichioka, Y., "Programming of Optical Array Logic. 1: Image Data Processing," Appl. Opt. 27, 2926-2930 (1988).

Thalmann, R., Pedrini, G., Acklin, B., and Dandliker, R., "Optical Symbolic Substitution Using Diffraction Gratings," Proceeding SPIE 963, 635-641 (1988).

Tsao, M. T., Wang, L., Jin, R., Sprague, R. W., Gigioli, G., Kulcke, H. M., Li, Y. D., Gibbs, H. M., and Peyghambarian, N., "Symbolic Substitution using ZnS Interference Filters," Opt. Eng. 26, 41-44 (1987).

Tzou, K-H., "Progressive image transmission: a review and comparison of techniques," Opt. Eng. 26, 581 (1987).

Vainos, N. A., "Real-time optical Winer-Kolmogorov and novelty filtering with phase conjugation," Opt. Lett. 14, 128 (1989).

Wuthrich, A. and Lukosz, W., "Holographic with Guided Optical Waves," Appl. Phys. Lett. 21, 55-58 (1980).

Yoon, J. S. and Lee, S. S., "Multiple-Reflection Laser Doppler Interferometer," Appl. Opt. 24, 3429 (1985).

Young, M., "Low-cost LCD video display for optical processing," Appl. Opt. 25, 1024 (1986).

Yu, F. T. S. and Jutamulia, S., "Implementation of symbolic substitution logic using optical associative memories," Appl. Opt. 26, 2293-2294 (1987).

Yu, F. T. S., Jutamulia, S., and Gregory, D. A., "Optical parallel logic gates using inexpensive liquid-crystal televisions," Opt. Lett. 12, 1050 (1987).

Yu, F. T. S., Jutamulia, S., and Gregory, D. A., "Real-time liquid crystal TV XOR- and XNOR-gate binary image subtraction technique," Appl. Opt. 26, 2738 (1987).

Yu, F. T. S., Zhang, C., and Jutamulia, S., "Applications of one-step holographic associative memory to symbolic substitution," Opt. Eng. 27, 399-402 (1988).

Zhao, D. and Liu, H-K., "Real-time optical interferometric image subtraction by wave polarization," Appl. Opt. 21, 3864 (1982).